NTNU
Norwegian University of
Science and Technology

Development of the Market's Lightest Backcountry Ski Binding

A Study on Structural Optimization

David Tollnes Flem

Master of Science in Mechanical Engineering
Submission date: June 2018
Supervisor: Martin Steinert, MTP

Norwegian University of Science and Technology
Department of Mechanical and Industrial Engineering

Abstract

The aim of this thesis *Development of the Market's Lightest Backcountry Ski Binding* is to see how topology optimization can be used to create a light weight and stiff ski binding. Sports equipment is getting lighter and lighter, making it increasingly important to use material as effectively as possible. Topology optimization is not a new technology, but the rapid development of constraint free production methods, like additive manufacturing, creates new possibilities which now makes topology optimization more relevant in mechanical engineering than ever.

This thesis firstly examines the mountain ski binding market, user scenarios and relevant design variables. In the second stage, a set of optimizations are done to gain knowledge and experience, to define the test setup and to ensure that the optimized results will be as realistic as possible. Further, a set of models with different combinations of design variables (boundary conditions and design space dimensions) are topology optimized. The results are tested for both static and cyclic loading and redesigned to reduce von Mises stresses and increase the fatigue life. Prototypes are then manufactured and tested to verify the design. The result is a binding with a weight of 26.70 grams, which is lower than the current market leader. Including the design variables in the optimization halved the strain energy, thus making the binding stiffer, from the initial topology optimizations.

Several topology optimization cases are studied and in many of these a fixed setup is topology optimized, leaving boundary conditions and design space dimensions unchanged in the analysis although there is a huge potential in optimizing these as well. These discoveries result in the categorization of three different approaches and the identification of several limitations which are discussed in the paper *State of the Art of Generative Design and Topology Optimization and Potential Research Needs (Tyflopoulos, Flem, Steinert, & Olsen, 2018)*. This paper was accepted at the NORDESIGN 2018 conference.

Sammendrag

Målet med denne oppgaven *Utvikling av markedets letteste fjellskibinding* er å se hvordan topologioptimalisering kan brukes til å lage en lett og stiv skibinding. Sportsutstyr blir lettere og lettere, noe som gjør det stadig viktigere å utnytte materiale så effektivt som mulig. Topologioptimalisering er ikke en ny teknologi, men den raske utviklingen av begrensningsfrie produksjonsmetoder, som additiv tilvirkning, skaper nye muligheter innen utvikling av fysiske produkter, som nå gjør topologioptimalisering mer relevant enn noensinne.

Denne oppgaven undersøker først markedet for fjellskibindinger, brukerscenarier og relevante designvariabler. Deretter blir det gjort flere optimaliseringer for å få kunnskap og erfaring, for å definere testoppsettet og for å sikre at de optimaliserte resultatene skal bli så realistiske som mulig. Videre blir et sett med modeller, med forskjellige kombinasjoner av designvariabler (grensebetingelser og mål av designrommet), topologioptimalisert. Resultatet blir testet for både statisk og syklisk belastning og deretter redesignet for å redusere von Mises-spenning og for å øke levetiden. Prototyper blir deretter produsert og verifisert gjennom testing. Resultatet er en binding som veier 26,70 gram, en vekt som er lavere enn markedets letteste. Ved å inkludere designvariablene i optimaliseringen blir tøyningsenergien halvert, og dermed bindingen stivere, i forhold til de første topologioptimaliseringene.

Flere topologioptimaliseringstilfeller blir studert, og i mange av disse blir et fast oppsett optimalisert, altså er grensebetingelsene og målene av designrommet uendret gjennom analysen selv om det ligger et stort potensial i å optimalisere disse også. Disse funnene resulterer i kategoriseringen av tre forskjellige tilnærminger og identifikasjon av flere begrensninger, disse diskuteres videre i artikkelen *State of the Art of Generative Design and Topology Optimization and Potential Research Needs* (Tyflopoulos et al., 2018). Denne artikkelen ble akseptert på konferansen NORDESIGN 2018.

Acknowledgement

I would like to thank;

Øyvar Svendsen for giving me this opportunity, backing me up and including me in Rottefella's R&D team. I would also like to thank the rest of the team; Magnus, Jørn and Thomas.

Professor Martin Steinert for his guidance and supervision throughout the project and the master thesis. I would also like to thank all the master students and all the Ph.Ds. at TrollLabs for inputs and ideas.

Associate Professor Jan Torgersen for helping me with topology optimization and sharing his knowledge on the topic.

Even Hovik for printing prototypes at IPK, for always being helpful and for taking an interest in the project.

Pål Erik Endrerud for printing bindings in Gjøvik and using time on my project.

Evangelos Tyflopoulos for including me in the paper *State of the Art of Generative Design and Topology Optimization and Potential Research Needs*.

Table of Contents

List of Figures

List of Tables

Abbreviations

CAD Computer-Aided Design

CAE Computer-Aided Engineering

FE Finite Element

FEA Finite Element Analysis

IST Integrated Shape and Topology

SBD Simulation-based Design

STL Stereolithography

TO Topology Optimization

1 Introduction

1.1 Problem Description

The research and development team at Rottefella is in the process of developing a new norm to complement their backcountry ski bindings. The innovation in this new binding system is that the moving parts are moved from the binding to the shoe, which means that only a simple bracket is needed on the ski (see section 4.1.2). The challenge from Rottefella has been to make this bracket as light as possible, and in doing so, developing the lightest backcountry ski binding on the market. The lightest mountain ski binding[1] on the market today is the Dynafit DNA at 62 grams (see section 4.1.3) which is made in carbon-fibre with an extreme focus on weight. The question is, can an even lighter ski binding be made by introducing topology optimization into the ski binding segment?

The aim in this master thesis is to study how topology optimization can be used to develop the lightest backcountry ski binding on the market.

1.2 Previous Work and Motivation

The project work in the course *TMM4560 - Engineering Design and Materials* fall 2017 was a preliminary study to this master thesis. Some of the theory presented in the sections Topology Optimization and Understanding the Problem, are based on the project report. The aim was to find a way to make the lightest backcountry ski binding on the market and test out different approaches to achieve this. Topology optimization was selected as the most promising technology and it was decided to systematically test how this could be used to design the lightest backcountry ski binding, in the master thesis.

The result of the project work was a prototype; see Figure 1-1 and Figure 1-2. This model was both lighter and stiffer than a non-topology optimized reference model which was provided by Rottefella (see Figure 1-3). This gave an indication of this technology's potential, but it also revealed some of the challenges. Firstly, topology optimization is time demanding; a full optimization cycle can take between 2-24 hours. This limits the number of cycles that are possible to run and makes the process of learning slow. Learning is key to make an optimization

[1] Backcountry-, alpine touring- and telemark-ski bindings

setup which accurately represents reality. Secondly, the analysis is very sensitive to which forces and boundary conditions that are put into it. Because the optimization returns the very optimal structure to the load scenarios you have defined, it is important to define these carefully. Specific challenges which were encountered in the project work are discussed in detail in section 3.1.

The topic was chosen because of the author's interest in skiing and because the author found the challenge of trying to make the market's lightest ski binding interesting. A limited use of topology optimization in the design of sports equipment, motivated the author to test how far this technology could be pushed in this segment.

Figure 1-1:The result of the project work.

Figure 1-2: The binding mounted on a ski.

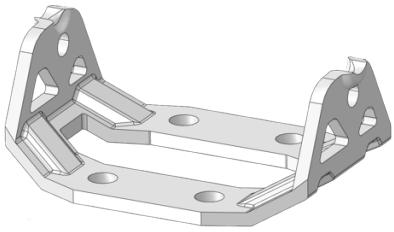

Figure 1-3: Early prototype from Rottefella.

1.3 Objectives

To achieve the aim a set of objectives was defined on the start of the semester in cooperation with the supervisor.

- Study how topology optimization can be used in a product development process.
- Continue the work from the project work in Abaqus CAE; refining the simulation parameters and the model setup.
- Find, evaluate and discuss the topology optimization input-values (optimization task parameters, loads and design variables)
- Study how the design variables (boundary conditions and design space dimensions) can be optimized
- Find the optimal (stiffness vs. weight) component structure of the ski binding
- Verify the optimized design with finite element analysis and physical testing

1.4 Limitations

The focus of the thesis has been on a new ski binding system in the backcountry skiing segment; the ski binding system is presented in section 4.1.2. The binding is still in the early development phase which means that it is not fully developed. Therefore, the focus has been to optimize the bracket in Figure 4-6 and only consider features which are implemented in the prototype presented in section 4.1.2; a flex (see Figure B-1 and Figure B-2).

Since the aim has been to develop the lightest ski binding, elements like visual design, usability, user group and production costs have not been considered.

1.5 Structure of the Thesis

In the second section, topology optimization is described, and the terminology defined here is used throughout the thesis. It is discussed how it works and what kind of problem the ski binding optimization is. The word 'optimal' is used many places in this thesis to describe the one, best solution to a problem. What can be defined as optimal is discussed. Further, the software that was used to conduct topology optimization is described.

In the third section, the development framework which was used in this thesis is described. The aim was to find a way to systematically optimize both the design variables and the topology in a physical product development project while making sure the output was realistic. From studying literature, three different approaches to the topology optimization step in a product development setting were identified and are here described. These approaches were later presented in a paper which is described in section 7. The framework used in this thesis was put together from already defined workflows, experience from the preliminary project work and the master thesis.

In the fourth section, a background study is presented. To design a superlight ski binding it is important to understand the limitations and opportunities of the mountain skiing segment. First, the mountain ski binding segment with Rottefella's new norm and state of the art bindings are presented. Then relevant materials and manufacturing processes are described. The first phase in the framework presented in section 3.3 is *Understanding the Problem*, and the points

described in this section are further discussed; the load scenarios, design variables, restrictions and the starting point of the optimization.

The fifth section addresses the remaining topics presented in the development framework (section 3.3). First, the elements within the *Design Variable and Topology Optimization* sub-section are presented and an overview over the optimization tests is given. Then, how the finite element analysis was conducted. Finally, manufacturing and physical testing are described.

In the sixth section, the results from completing one full cycle of the optimization framework are presented. The final design (topology and design variables) is presented, and the redesign cycles that were necessary to achieve a realistic design are discussed.

In the seventh section limitations with topology optimization and approach 3 (section 3.2.2) are discussed with references to the paper *State of the Art of Generative Design and Topology Optimization and Potential Research Needs* (Tyflopoulos et al., 2018). The framework which was used in this thesis is also discussed and suggestions are made for future research.

Finally, a conclusion summarizing what has been done, with comments on what could be studied further.

2 Topology Optimization

2.1 How It Works

Efficient use of materials has become increasingly important in many applications; designing structures that are stiffer and stronger and at the same time remain light. Topology optimization is not a new technology, many industries have applied methods to reduce weight and volume of structural and mechanical components before. However, due to limitations in the manufacturing process, it is not until later years the full potential of such optimization algorithms has been utilized. Additive manufacturing (see section 4.2.1) makes it possible to produce more complex geometries than e.g. moulding, casting and machining.

Topology optimization is essentially finding the optimal (see section 2.2) material structure based on a set of requirements. Simply put, you start by discretizing the initial design into small pieces, a mesh. The algorithm then calculates which of these pieces that contribute the most and which pieces that contribute the least, to fulfil the objective(s) that has been defined by the user. The pieces that are favoured are kept and the others are removed, what percentage of the material that is removed in each cycle is defined in the beginning. This cyclic process of adding favourable and removing unfavourable material is repeated either to a set maximum of cycles or a criterion is fulfilled. “The purpose of topology optimization is to find the optimal lay-out of a structure within a specified region.” (Bendsøe & Sigmund, 2004, p. 1). E.g. to find the stiffest structure of a beam at a defined volume percentage. In other words, you design a model and apply forces, boundary conditions and other requirements relevant to your problem. Then you set the volume to be reduced to e.g. 25% of its original size. The algorithm then finds the stiffest structure at 25 % reduced volume, see Figure 2-1.

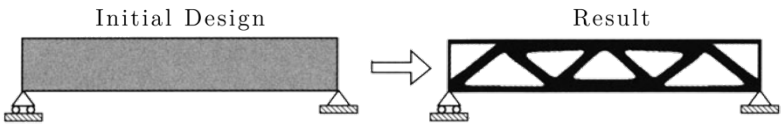

Figure 2-1:Topology optimization (Bendsøe & Sigmund, 2004).

The benefit of this approach is that you don’t have to make a lot of different models to find the optimal structure; the best design in the case you study might even be something you could not have thought of. “In the most general terms, optimization theory is a body of mathematical results and numerical methods for finding and identifying the best candidate from a collection

of alternatives without having to explicitly enumerate and evaluate all possible alternatives" (Ravindran, Ragsdell, & Reklaitis, 2006, p. 1).

2.2 What is Optimal?

The word optimal means the best or the most favourable (Oxford, n.d.). In other words, to decide if a design is optimal will vary with what the aim is; a solution that may be optimal in one situation might be poor in another. The aim in this thesis is to design the lightest ski binding on the market. Therefore, the optimal solution would be a binding that fulfils the criteria for being a ski binding and being the lightest one. Although there are many different ski bindings, the purpose of a binding remains mainly the same; to keep the ski boot connected to the ski, and in some applications, release the ski boot if the excessive loads become too high (Senner, Michel, Lehner, & Brügger, 2013). This means transferring the three force components and the three moment components from the shoe to the ski. So, if the binding can connect the shoe to the ski, release the shoe when needed and withstand the loads applied to it, it can be called a ski binding. Therefore, the optimal solution to this problem will come at the expense of usability, durability, visual design, user preferences, etc.

A typical optimization problem is to optimize the stiffness of a structure and minimize the mass or volume, called a minimum compliance design. The optimal result in a minimum compliance design, is a structure that is compliant to the loads and criteria you define, but if higher loads are applied, it will fail. In other words, a ski binding that cannot be made lighter.

2.3 Minimum Compliance Design

In a minimum compliance design, the model is initially divided into a set of small finite elements. The purpose is to see which elements are going to be kept and which should be discarded, when an optimization objective is maximized or minimized, while a set of constraints are fulfilled. "We are interested in the determination of the optimal placement of a given isotropic material in space, i.e., we should determine which points of space should be material points and which points should remain void (no material)" (Bendsøe & Sigmund, 2004, p. 4).

Abaqus, which is the software used in this thesis, use an approach called SIMP (Solid Isotropic Microstructure with Penalization) (Fiebig et al., 2015). The algorithm minimizes the strain

energy in the model by scaling the element densities. The Strain energy (the energy that is stored when the model deforms) is a global measure of the displacement in the model, i.e. lower strain energy results in a higher stiffness. Figure 2-2 shows an example from the Abaqus 6.13 documentation (Simulia, 2013). The strain energy for the different elements is calculated in each cycle, the algorithm then tries to minimize the maximum values for the strain energy. The density of the elements which do not contribute to the stiffness are then scaled down, as if they were removed. However, if the algorithm at a later cycle sees that these elements will contribute, they are scaled up again. In this way, the model will continue to decrease and increase at different places until the volume constraint is met. The analysis will either stop when the maximum number of cycles are reached (defined by the user), or when the convergence criteria are met (related to changes in density and strain-energy).

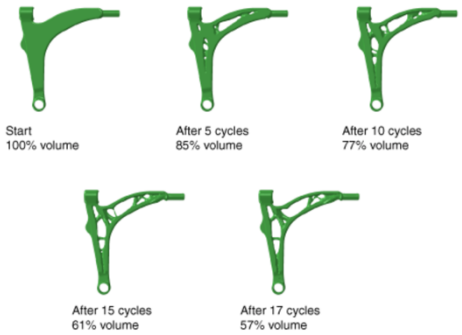

Figure 2-2: Topology Optimization of an automotive control arm (Simulia, 2013).

Abaqus has two algorithms for optimization; the condition-based and the sensitivity-based algorithm, see Figure 2-3. The condition-based algorithm allows only strain energy and volume as design responses. In the sensitivity-based approach you can have multiple constraints and multiple design responses, but it takes more cycles to compute, usually 50 - 150 cycles instead of 15-30 cycles. Another difference is that the sensitivity based approach starts by scaling the entire model to meet the volume constraint, and then tries to optimize the objectives. The condition based approach on the other hand, starts with the original design space and then slowly decrease the model until the volume constraint is met.

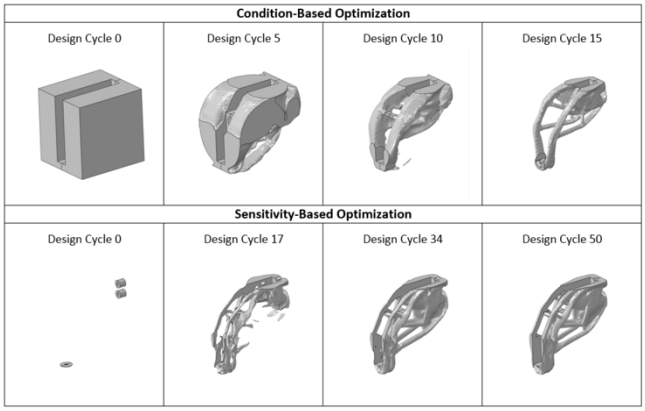

Figure 2-3: Condition-based and sensitivity-based optimization (McKee & Porter, 2017).

In this thesis, the condition-based optimization algorithm was used in most of the optimizations; because it was easiest to use in this problem and gave the best results. When using the sensitivity-based algorithm, both volume and strain energy can be used as objectives. To tell the algorithm which of the objectives it should prioritize, a weighting number must be defined, the challenge is then; how much stiffness is one gram worth? In the condition-based algorithm only strain energy can be set as the objective and volume is used as a constraint. The challenge is to set the lowest volume constraint that still results in a compliant model. This turned out to be easier than selecting a weighting number.

2.4 Optimization Software

In the preliminary project work, Autodesk Fusion 360 was used. This is a simple CAD program with a built-in optimization algorithm. A disadvantage with this software is that it offers a limited amount of options for applying mesh, loads, boundary conditions, contacts, etc. There are also less options when defining an optimization job. The benefit is that it is simple to understand and gives the user insight into some of the challenges of conducting an optimization.

Abaqus CAE is a software for doing computer-aided engineering and finite element analysis while Tosca is an optimization suite, which use input from Abaqus FE-simulations to conduct optimizations. In the 2017 version of Abaqus, which was used in this thesis, the Tosca Software is implemented in Abaqus. This means you can choose to access it directly in the Abaqus modelling environment or run it separately. Both approaches were tested out; the advantage of using Tosca separately is that you can que multiple optimization jobs, but because it was easier to monitor the progress of the optimization, the Abaqus environment was used. This software

was recommended from Associate Professor Jan Torgersen and former master student Jørgen Kjær Eliassen. Jørgen wrote his master thesis on topology optimization for Revolve in the spring of 2017; designing the uprights for a race car. Abaqus is a complex program which gives the user full freedom to change every parameter in the model and in the analysis.

When working with topology optimization it became evident how computational expensive these analyses are. An optimization could take all from 2 to 24 hours depending on number of mesh elements, number of cycles, how many steps that were included in the analysis, etc., and of course the computer. The computer that was used to run most of the experiments was a private computer with an Intel i7 processor (3,40 GHz) with four cores and 8 GB RAM. Efforts to acquire a faster computer were unsuccessful which greatly reduced the number of cycles that could be completed.

3 Development Framework

3.1 Limitations in Previous Work

Through the project work in the course TMM4560 fall 2017 the process of using topology optimization in product development was tested out briefly as one of the approaches to design a light ski binding. The work was mainly conducted like the flowchart presented in Figure 3-1. First the input values (loads, boundary conditions and the dimensions of the design space) for the topology optimization were found, then the topology optimization was completed before the optimized model was validated with finite element analysis and mechanical testing.

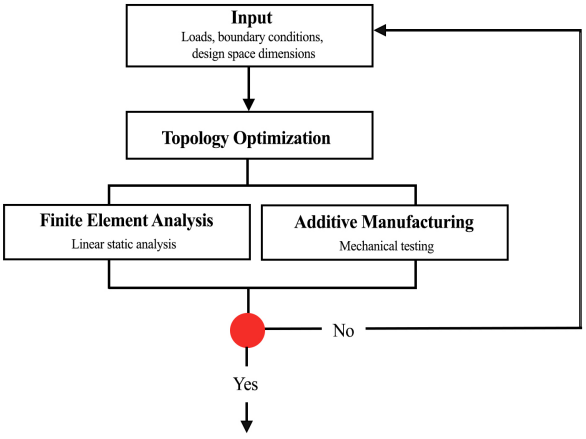

Figure 3-1: Flowchart used in the preliminary project work.

Several limitations were discovered which needed to be addressed in further works. Because the structure of the optimized results was highly organic, it was difficult to do small changes to the geometry. This meant that if the FEA revealed stress peaks in the model, e.g. a sharp edge, the whole process needed to be repeated even though the problem might have been solved with a small refinement, e.g. a fillet. A comment from Rottefella was that the model in Figure 1-1 might be a theoretically optimal result, but in real life, when the load scenarios were more complex, the part could fail. They referred to the sharp edges between the sides where the pin-holes are and the screws are fastened. The workflow was time-consuming since each cycle included the process of FEA and 3D-printing. If a larger set of cases was to be studied it would be essential to reduce all unnecessary time. A few designs were tested throughout the project, but to do this more systematically, clear criteria were needed to select the optimal design and to verify that it withstands its intended use.

3.2 Literature Review

3.2.1 Simulation-Based Design

The use of CAD (Computer-aided design) and CAE (Computer-aided engineering) in product development can be categorized as simulation-based design (SBD). Several SBD workflows which include topology optimization were studied and the most interesting findings are described below.

The ATOM Workflow

The ATOM (Abaqus Topology Optimization Module) workflow show how topology optimization and shape optimization can be used together and is described in an article at Simulia's web page (Simulia, 2011). As Figure 3-2 shows, the initial geometry is first meshed and converted into a finite element model where loads and boundary conditions can be defined. In the next step the optimization model is created, and the criteria for the optimization, restrictions, algorithm, etc., are set. After this the model is topology optimized through several cycles. The optimized model is then extracted before a shape optimization is performed. Shape optimization adjusts the outer boundaries of the model, e.g. to remove high stress peaks. It is different from topology optimization since it uses the already defined topology and changes only the shape of the model, see Figure A-1. This workflow presents the very basic steps of an optimization process, from the input of CAD geometry to recovering the results. The difference from some of the other workflows is the use of shape optimization.

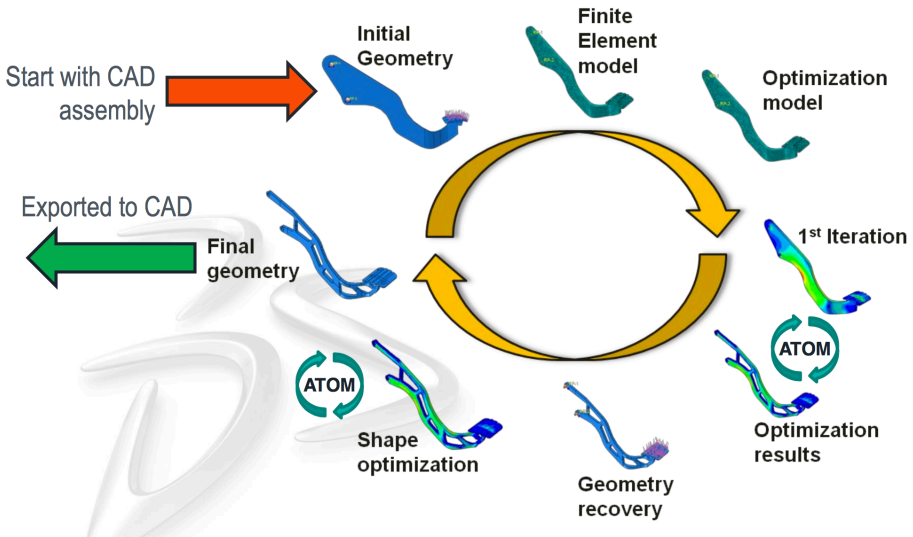

Figure 3-2: ATOM workflow (Simulia, n.d.-b).

Workflow Presented by Haley J. McKee and John G. Porter

This is presented as a first step towards a workflow where topology optimization can be used as a design method. The workflow was created to be able to effectively design, manufacture and qualify topology optimized parts (McKee & Porter, 2017). A chart of the complete process can be seen in Figure A-2.

It begins one step before the ATOM workflow in the early phase where the optimization is defined. The aim in this stage is to find all the critical requirements. Here the authors propose a set of questions that needs to be asked to identify the normal use of the part, find the low-likelihood conditions, consider human factors (wrong use, misunderstandings), define the goals for the optimization and prioritize them, and set the design space and its restrictions. The idea is to optimize the part for high-likelihood conditions while the part should be tested afterwards for the low-likelihood conditions; "Including low probability loading or boundary conditions in the optimization setup can be inefficient, adding hours or even days to computation time with little added value. It can also skew the design process by disproportionately weighting the significance of low likelihood conditions instead of design critical, high likelihood conditions. Later in the design process, validation simulations will be completed to ensure acceptable safety factors under other known abnormal conditions" (McKee & Porter, 2017, p. 56).

The next step is to define the finite element analysis model and the topology optimized model. The focus is to capture the correct stress-state which is an important step since; "the quality put into a topology optimization analysis directly correlates to the quality of analysis results" (McKee & Porter, 2017, p. 58). Further, the optimization algorithm, design responses, objective functions and geometric restrictions are defined. After the optimization, in the design feedback phase, the results are analysed by prototypes, 3D-models, images, etc. "While there is still considerable work to be completed, it is a good time to determine whether the optimized solution and shape adequately satisfy the requirements" (McKee & Porter, 2017, p. 64). A further step is verification by simulations and additive manufacturing before part validation by light-scanning or CT-scanning.

3.2.2 The Topology Optimization Step

The process of conducting topology optimization can be approached in several different ways. However, in most of the articles that were studied these differences were not described explicitly, but to know the limitations and advantages of these different approaches is important.

Many use topology optimization as a term for finding the optimal solution to a problem, but it is important to differentiate between finding the solution to an already defined CAD model, a local optimum, and trying to find the optimal solution to the problem itself, the global optimum. Through studying literature, the work conducted in the project work and the master thesis, three distinct ways that the topology optimization step was conducted in early stage product development were identified. Table 3-1 summarize the strengths and weaknesses with these approaches, and was later used in the paper *State of the Art of Generative Design and Topology Optimization and Potential Research Needs* (Tyflopoulos et al., 2018).

The first approach is when topology optimization is used to improve an existing design and where this design is used directly as the design space. An examples of this was found in the optimization of an upper carriage of a naval gun (Wang & Ma, 2014), see Appendix A.2. The advantages are that the design fits easier into an assembly or that it can keep some of the initial visual design like the upper carriage of the naval gun. The disadvantage is that the optimization is limited by the restricted design space, because the algorithm cannot add material outside the defined design space. This approach was tested out on a prototype made by Rottefella, see Figure 3-3.

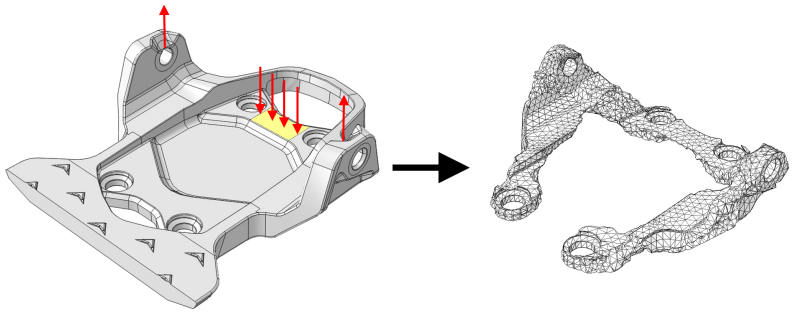

Figure 3-3: Approach 1: *Predefined Design Space*.
The design space on the left, the optimized result on the right.

In the second approach, which seems to be the most common, a larger design space is defined in the beginning. It is made as big as possible within the restrictions given by the problem, this could be with respect to an assembly or other interacting features. The boundary conditions, design space dimensions and loads are based on previous experience, optimizations and FEA. Examples were found in the development of a laser-remote-scanner (Emmelmann, Kirchhoff, & Beckmann, 2011), the optimization of a compressor bracket (Chang & Lee, 2008), the design of a trailer chassis (Ma, Wang, Kikuchi, Pierre, & Raju, 2006) and the optimization of a hanger (McKee & Porter, 2017), see Appendix A.3. The approach was also tested on the same prototype from Rottefella, making the design space larger (see Figure 3-4). The advantage is

that the design space is larger, enforcing less restrictions on the algorithm. However, like approach 1, the boundary conditions (e.g. the screw holes in Figure 3-4) and the design space dimensions are fixed throughout the optimization. Although you might find the optimal material structure to that specific setup, it is likely that by iterating on the design variables (boundary conditions and the dimensions of the design space) a better result could be found.

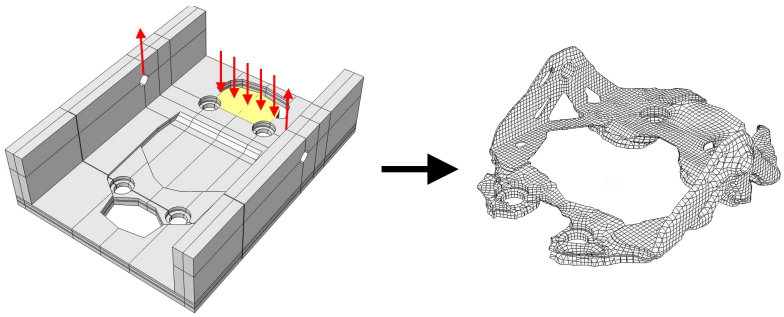

Figure 3-4: Approach 2: *Maximum Possible Design Space*.
The design space on the left, the optimized result on the right.

The third approach is to combine optimization of design variables and topology. By testing out different design variables a solution closer to a global optimum can be found. This is emphasized in the newly published article *Integrated Shape and Topology Optimization - Applications in Automotive Design and Manufacturing* (Fiedler, Rolfe, & De Souza, 2017). In one of the cases presented here, the bolt pattern used to fasten a bracket is optimized. This was done by topology optimizing over 290 designs, reducing the weight from the initial designs from ~ 1300 grams to ~380 grams, see Appendix A.4. Unfortunately, this is very time consuming; "The IST (Integrated Shape and Topology) optimization approach is computationally costly, since for each set of geometry design variables, a topology optimization run is performed. In one such iteration step, typically the geometry update and meshing is fast, while the topology optimization part requires 90% of the computing time." (Fiedler et al., 2017, p. 9). One of the tests cycles described in Appendix D.2 is visualized in Figure 3-5. Four different values for the distance d were tested out; d = 20.5 → 35.5 mm.

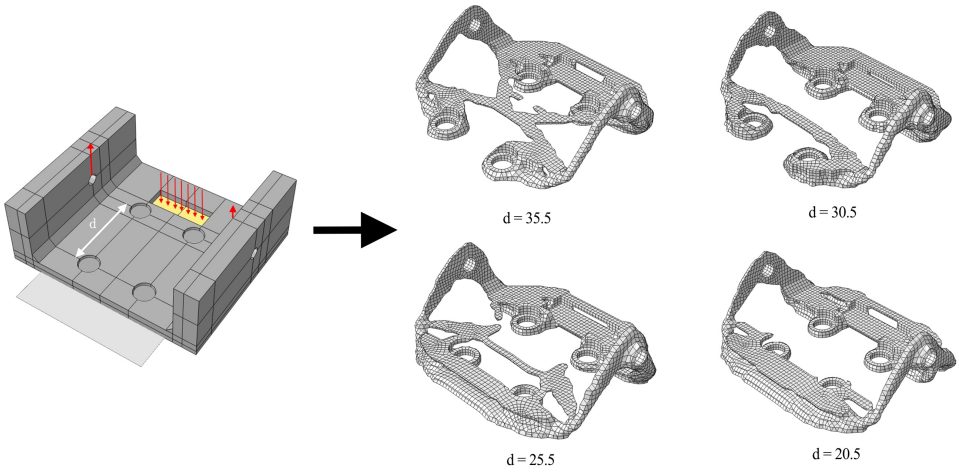

Figure 3-5: Approach 3: *Integrated Shape- and Topology Optimization*.

Practice	Examples	Strengths	Weaknesses	Recommended papers
Approach 1: *Predefined design space*	Upper carriage of a naval gun	Partially hold of the initial visual design	Restricted design space (fixed dimensions and boundary conditions)	(Wang & Ma, 2014)
Approach 2: *Maximum possible design space*	Laser-remote-scanner	Larger design space (less restrictions on the algorithm)	Restricted design space (fixed dimensions and boundary conditions)	(Emmelmann et al., 2011)
	Compressor bracket			(Chang & Lee, 2008)
	Trailer chassis			(Ma et al., 2006)
	Hanger			(McKee & Porter, 2017)
Approach 3: *Integrated shape-and topology optimization practice*	Automotive Design and Manufacturing	Optimization of boundary conditions	Computationally costly and time consuming	(Fiedler et al., 2017)

Table 3-1: The three approaches (Tyflopoulos et al., 2018).

3.3 The Framework

The most promising procedure when it comes to finding the lightest and stiffest design is approach 3; because of the large design space and possibilities to optimize the input values of the analyses as well. Since there to the authors knowledge was no workflow describing the process from the problem understanding phase to manufacturing and testing, which used this approach, a framework was developed to optimize both design variables and topology. The workflow is based on the figure presented in section 3.1, the literature presented in the previous sub-sections and experience gained in the early stages of working with this thesis. It served as a framework for the process. Each step is described in this section and an overview is presented in Figure 3-6.

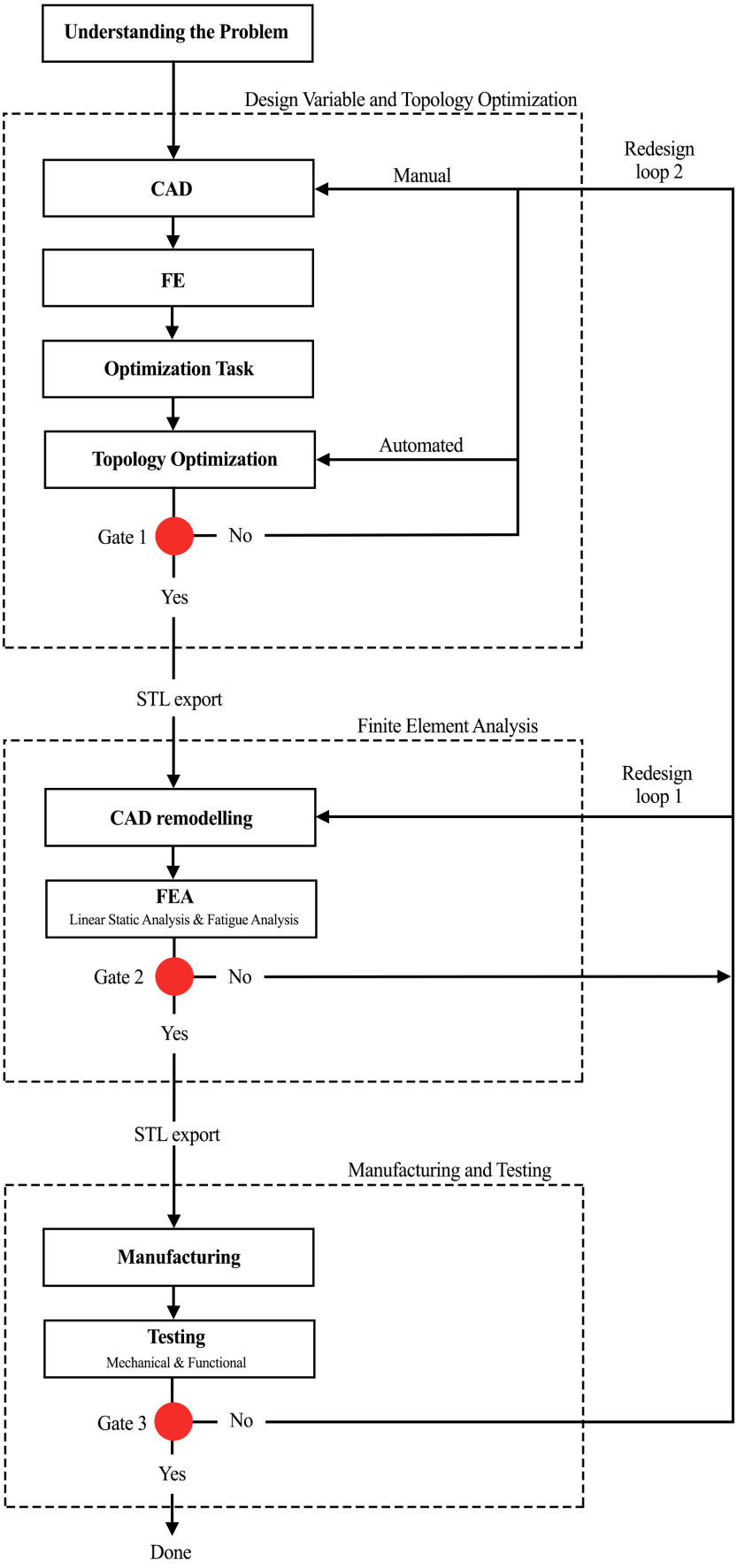

Figure 3-6: Flowchart of the framework used in this thesis.

Understanding the Problem

Before optimizing it is important to fully understand the problem. The amount of background study needed depends on the problem and level of previous knowledge, but the most important things to define are the goal for the optimization, the load scenarios and the design variables. The success of the outcome depends on how accurately the optimization model replicate reality and how little restrained the algorithm is; optimizing as many of the design variables as possible.

Initially, the goal with the optimization needs to be defined. This could be to find the lightest and stiffest design, optimizing to avoid certain eigenfrequencies, etc. The goal should be translated into a criterion, e.g. the stiffest design at a certain weight. To ensure that the optimized part satisfies the criteria, it is important to optimize the part for the right kind of load cases. As Haley J. McKee and John G. Porter explain in their article (McKee & Porter, 2017), loads can be categorized into low-likelihood and high-likelihood load scenarios. The critical high likelihood load cases are used in the topology optimization, then the result is tested for critical low-likelihood load cases. The part can then be fatigue tested for the 'normal' load cases; the less critical, but more repetitive, high-likelihood load cases.

When it comes to finding the optimal design, it lies a huge potential in including the design variables in the optimization, as seen in the case with the IST optimization of the solid bracket (Fiedler et al., 2017). Topology optimization can be used to improve the design greatly, but to reach its full potential the input must be optimal as well. The design variables can be separated into the fixed and the adjustable. The fixed ones are the variables which cannot be altered and they are not optimized. These are often defined by restrictions or by the engineer, e.g. contact surfaces to other parts in an assembly, manufacturing method, user-friendliness, visual design, etc. However, in this thesis it was necessary to set more restrictions due to time and computational limitations, which are further discussed in section 4.4.2. The adjustable variables can be optimized, i.e. should be changed between topology optimizations to see which gives the best result.

Design Variable and Topology Optimization

In this phase, the design space is defined, and the finite element model is created. This process happens in much of the same way as the ATOM workflow. Loads, boundary conditions, interactions and restrictions are defined before the optimization task is specified and the process

of optimizing the design variables and topology can begin. The topology optimization step in Figure 3-6 visualizes where the software runs the optimization job. If iSight or any other optimization software are not used to automatically iterate on different design variables, this must be done manually. The optimization phase was completed before any FEA to save time.

Gate 1

It is at gate 1 that the optimal design is selected based on the criteria that were defined in the beginning, e.g. selecting the best design out of a defined number of iterations or a script programmed to converge towards a solution. The gates were created to meet the need for a more systematic approach after the preliminary project work. If the optimal design is found, you may go to the next step, if not, the loop of changing the design variables is repeated.

CAD Remodelling

The optimized result can be extracted directly from Abaqus, but this will often be a rough model, as experienced during the project work. It was clear that working with a regenerated CAD model was much easier than working with the extracted surface mesh from the optimization. When a CAD model is regenerated, you get the whole tree of operations (sketches, extrusions, etc,), this means that making small changes to radiuses, distances, thicknesses, etc., are easy. This is important; "It is well understood that any density distribution returned by the topology optimization algorithm requires manual rework to reduce local stress concentrations and to create a final design for a manufacturable part" (Fiedler et al., 2017, p. 4).

Finite Element Analysis

Finite element analyses are conducted to make sure that the design is strong enough for the intended use, but also to check whether the design makes sense. The analyses indicate which regions of the part that are weakest when it comes to failure and fatigue, this provides knowledge to remove unrealistic features as the sharp edges seen in the previous project work. In this thesis, FEA was used to test the critical low-likelihood conditions, and the fatigue life was estimated with the normal load cases as input.

Gate 2

If the regenerated CAD model does not satisfy the criteria that have been set, small changes are either done in redesign loop 1 or larger changes in redesign loop 2. It is difficult to say in general if changes should be done through redesign loop 1 or 2. Small changes were here seen as smoothing out radiuses and sharp edges or increasing the thickness of some of the members; changes that did not significantly change the structure of the part. If changes to e.g. the placement of the screws or the height of the binding, were needed, the topology optimization cycle had to be done. The criteria at this gate can be that the maximum von Mises stress must be under a certain stress, that the fatigue life should be over a certain number of cycles, etc. The process of adjusting the model and running static and fatigue tests, i.e. redesign loop 1, are done until the model satisfies the criteria.

Manufacturing and Physical Testing

The part is then manufactured and tested. If the part should be casted or machined, manufacturing restrictions should be implemented in the topology optimization. The physical tests will work as an extra safety net; both to see that the model really withstands what it should and to see how accurate the FEA setup replicate reality.

Gate 3

These criteria are defined to verify the physical model. This could be criteria based on the part's performance; for instance, if it fits into an assembly, if screw holes are big enough, etc., or to verify the stiffness or strength of the part. E.g. that the part should deform less than a certain number of millimetres when subjected to a defined load. If the part fails to meet any of the criteria, it must be redesigned in loop 1 or 2, depending on how big the changes are.

4 Understanding the Problem

4.1 Bindings for Mountain Skiing

There are almost as many ski bindings as it is applications; cross country skiing (classic- and skate skiing), alpine skiing, alpine touring, telemark skiing, backcountry skiing, etc. The focus of this study has been on backcountry-, alpine-touring- and telemark-skiing, since these bindings include both diagonal striding in flat terrain and downhill skiing.

4.1.1 Backcountry, Alpine Touring & Telemark

Backcountry skiing is the segment which refers to skiing mainly outside groomed trails. The skis, bindings and shoes are developed to work in every condition from deep snow to icy slopes. Backcountry ski equipment is made to be easy to walk on (diagonally striding) and stiff enough for small slopes and difficult weather conditions; ideal for trips to a cabin with a light backpack or more heavy expeditions with a sled. Therefore, the focus in the backcountry segment (Figure 4-1) is different from alpine touring (Figure 4-2) and telemark (Figure 4-3), where downhill skiing performance is the most important part. The bullet points below are written with respect to backcountry skiing and describe some of these differences.

- The skis have smaller width and less carving for better walking performance.
- The shoes are more flexible, which make them better to stride with, but reduce the support needed for downhill skiing.
- The binding system includes a flex; either as a part of the binding (Figure B-1 and Figure B-2) or a part of the shoe (Figure B-3). It is made to dampen the rotational motion when walking; making the striding motion smoother. When the flex is compressed, it stores energy which in turn accelerate the ski forwards.
- The bindings are in general dimensioned to withstand lower forces.
- The heel is loose and not fastened like alpine touring bindings in ‘downhill mode’.
- The 75-mm backcountry binding has a cable like telemark bindings, but the Rottefella NNN bindings do not have this feature.

These differences are important to understand when building a simulation model and the knowledge is used when defining the load scenarios (section 4.3) and the design variables (section 4.4).

Figure 4-1: Backcountry ski binding.

Figure 4-2: Alpine Touring ski binding (Sport, 2018).

Figure 4-3: Telemark ski binding (Dostie, 2013).

4.1.2 The New Norm

The biggest change with the new norm is, as stated earlier, that the moving parts are moved from the binding to the shoe. Moving parts are the parts which form the mechanism that allows you to fasten and unfasten the shoe to the binding. As Figure 4-4, Figure 4-5 and Figure 4-6 show; the new system has only need for a simple bracket on the skis; a way to fasten the two pins to the ski.

Figure 4-4: The new norm.

Figure 4-5: The prototype mechanism in the shoe.

Figure 4-6: Prototype of a simple bracket.

You fasten or unfasten the shoes by moving the pins on the sides of the shoes, out or in. The two pins on either side of the shoe are controlled by a handle fitted on to the back of the shoe. The pins are through a mechanism connected to a wire, and the wire is connected to the device on the heel, see Figure 4-7. The focus of the new norm is on the backcountry segment, but because the wide binding give the skier a more rigid connection to the ski, it encourages more downhill skiing. If the binding system was to focus more on downhill skiing, the complete binding system may include different features like a heel riser, heel fastener or telemark cable, crampons, etc. However, Rottefella said that the focus should be on the backcountry segment as is today. Therefore, only the features included in Figure 4-4, Figure 4-5 and Figure 4-6 are considered.

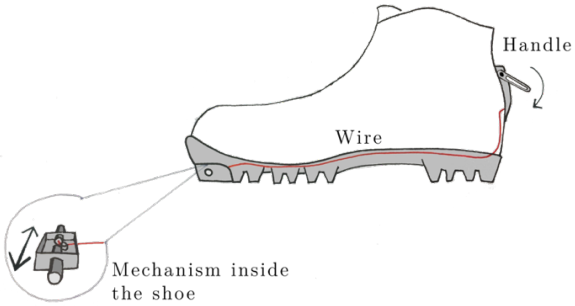

Figure 4-7: The mechanism in the shoe.

4.1.3 State of the Art

Since the goal was to make the lightest ski binding, it was interesting to find out what could be considered the state of the art in this segment. The weight is measured per one binding, including the heel piece, but without the screws. The lightest backcountry bindings are the Rottefella BC Auto at 222 grams and the Rottefella 75 mm at 185 grams (Rottefella, n.d.-g). The lightest bindings for alpine-touring are the Dynafit DNA (Figure 4-8) at 62 grams and the Dynafit P49 at 49 grams (Figure 4-9). P49 was presented autumn 2017 and is not yet for sale, therefore, it was not used as benchmark in this thesis. Table B-1 presents several other bindings that were studied. The lightest backcountry bindings are made with a focus on versatility, usability and durability, and do not have the same extreme focus on weight as the Dynafit DNA and P49, which are made for ski touring race. The Dynafit bindings are not backcountry bindings, but the fact that these bindings are made with an extreme focus on weight makes it interesting to see if their weight can be challenged. Therefore, the aim has been to make this backcountry ski binding lighter than the lightest binding in the mountain skiing segment (backcountry, alpine touring and telemark); 62 grams. The new binding system will most likely consist of a heel part, and the weight of the mechanism in the shoe could also be added to be conservative, but the focus for now has been on the bracket connecting the shoe to the ski.

Figure 4-8: Dynafit DNA (Dynafit, n.d.-a).

Figure 4-9: Dynafit P49 (Dynafit, 2017).

4.2 Manufacturing and Materials

4.2.1 Additive Manufacturing

Additive manufacturing is simply a way of producing by adding material layer by layer. The general step-by-step process is described in Figure 4-10, while the printing processes used in the thesis are described in the next paragraph. Because of the highly complex shapes generated by the optimization all the prototypes were made with additive manufacturing. It is possible to add manufacturing constraints in Abaqus, e.g. to make parts castable, but as discussed, it was desirable to give the algorithm full freedom.

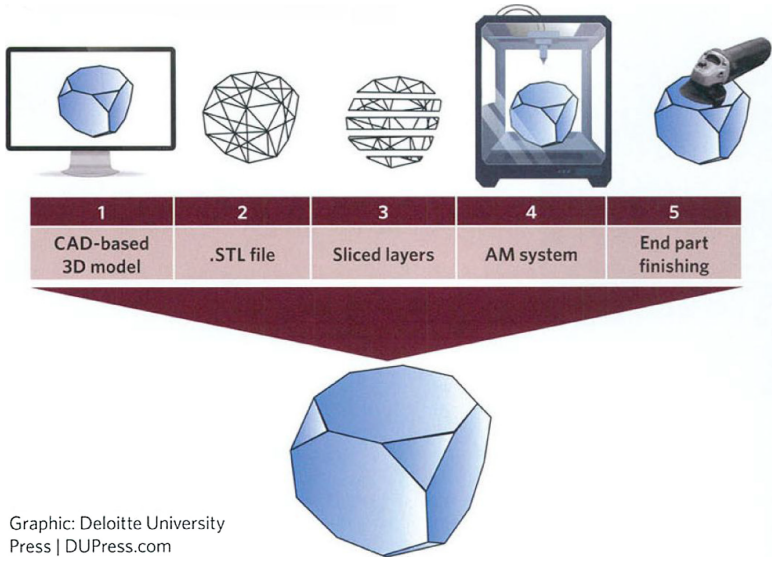

Figure 4-10: Additive manufacturing (Dizon, Espera, Chen, & Advincula, 2018).

Prototypes were made cheap and fast in the materials; PLA (Polylactic Acid), Tough Resin and PA2200 (Polyamide). PLA was printed using FDM (Fused Deposition Modelling) technology. The material is fed through a nozzle head which builds the model in the horizontal plane, then the height is adjusted, before the next layer is build, see Figure B-5. The advantages with this process are that it is cheap and relatively fast. The disadvantage is that it prints with low accuracy, and because of the layer-by-layer adding of material, the part will be anisotropic (weaker in the vertical direction). SLA (Stereolithography Apparatus) was used to print Tough Resin. This is more expensive, but SLA prints with a much higher degree of accuracy. In this process, liquid resin is cured using a UV-laser producing a hardened plastic part, see Figure B-6. This process creates isotropic parts because of the chemical bonding between the layers, which results in much better material properties. PA2200 was printed using SLS (Selective

Laser Sintering), material powder is sintered by a laser, layer by layer, into a solid structure, see Figure B-7.

In the beginning, most parts were printed with FDM, but the prints were too weak to be tested with a shoe because of the thin structures. However, SLA and SLS prints were much stronger and could be used for functional testing. SLS prints were also used for mechanical testing. Printing in metal is also relatively fast since you don't have to make any moulds or tools to make the parts, but it is more expensive. The plan is to print the final model in titanium using an EBM printer at NTNU Gjøvik. The parts are built in vacuum melting material layer by layer using an electron beam, see Figure B-8.

4.2.2 Material Selection

Since 3D-printing was the favoured way of manufacturing the final prototype, a material that could be used in this process was selected. The available materials are listed in Table 4-1; Ti-6Al-4V grade 5 (Titanium), 316L (CL 20ES, Stainless steel) and AlSi10Mg (CL 31AL, Aluminium). These could be printed at NTNU in Trondheim and Gjøvik. The key features for this optimization problem are high stiffness and low weight. The stiffness and weight were compared by calculating the specific stiffness for each material, see Equation 4-1. Titanium was selected due to the high specific stiffness and the extremely high yield point; it can withstand much higher stresses than the two other materials before any permanent deformation.

$$\kappa = \frac{E}{\rho}$$

Equation 4-1: Specific stiffness (κ = specific stiffness, E = Young's Modulus and ρ = density).

Material	E $[GPa]$	Density $[g/cm^3]$	Specific stiffness	Yield Point $[MPa]$
Ti-6Al-4V	110 - 120	4.41	24.94 - 27.2	1010 - 1110
316l	200	7.72	25.9	369 - 379
AlSi19Mg	50 - 70	2.68	18.66 - 26.1	215 - 245

Table 4-1: Properties of relevant materials.
Titanium: (Stirling, 2014), Stainless steel: (GmbH, n.d.) (Karma, 2008) and Aluminium: (Materialise, n.d.).

4.3 The Load Scenarios

To run an optimization using all the forces and moments in every skiing scenario as input is of course impossible. To narrow it down, the load scenarios were separated into three types as described in section 3.3; the normal, the critical high-likelihood and the critical low-likelihood. These are described further in this section and Figure 4-11 shows the coordinate system which is used to describe forces and moments in this thesis. After several optimizations, the importance of optimizing the part for the 'right' load scenarios was emphasized, because of the optimization algorithms sensitivity to the size of and how loads were applied. One of many examples can be seen in Figure B-9 and Figure B-10; the effect of including the load to the flex-area dramatically changed the optimized result. This is one of the major challenges with topology optimization; small changes in how loads are applied can result in totally different models. In this case, the shoe and the flex was predefined. So, defining the forces was more about making a setup which replicated reality in the most accurate way, than trying to find the 'optimal' placement of the forces.

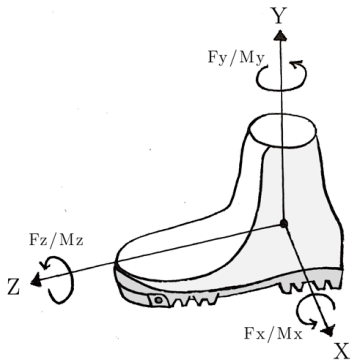

Figure 4-11: Coordinate system used throughout the thesis.

4.3.1 The Critical High-Likelihood Load Scenarios

The critical load scenarios are defined as the movements, when skiing, which generate the highest forces which in turn can lead to either fracture, the screws getting ripped out of the ski, a deformed binding (stress over yield point), etc. In other words, the maximum loads the binding should withstand. Load scenarios that were identified as critical and highly likely, are when the skier is falling forwards (Figure 4-12) and when the skier twists the ski when skiing downhill or falling (Figure 4-13). There are many other load-scenarios to consider, but these were the ones that are believed to be the most common and generate the highest peak forces, which was confirmed by Rottefella (Ø. Svendsen, personal communication, February 16,

2018). Alpine ski bindings are built to release the skier when the moments which are generated in the two cases discussed here, Mx and My, are above a certain value, see ISO 8061 *Alpine ski-bindings* (Standardization, 2015).

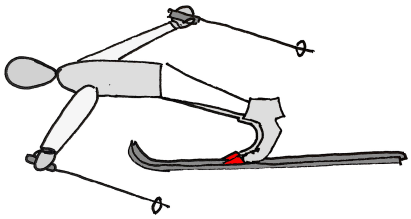

Figure 4-12: The skier falling forwards generating a forward lean moment Mx.

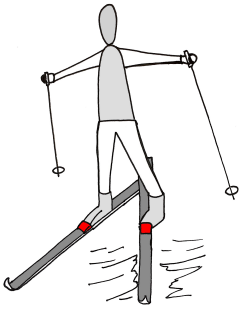

Figure 4-13: The skier twisting the ski generating a torsional moment My.

Forward Lean Moment: Mx

When the skier is falling forwards, the shoe is rotated, and the flex is compressed, see Figure 4-14. This results in the positive moment Mx generated by the shoe-pins pushing the binding up while the flex pushes it down. To find out how the force between the shoe-pins and the binding worked, a steel-thread was inserted in the shoe. The steel-thread was rotated in the test. This indicated that the shoe-pin generates a force straight up, see Figure 4-14. At first, the binding was optimized for the upwards force only, ignoring any effects from the force into the flex. After studying it closer, it became clear that it was important to include these effects as well. If this force does not go through the binding, i.e. the flex is in direct contact with the ski, the pressure from the skier will constantly work to separate the binding from the ski. However, if this force goes through the binding, it will contribute to the force needed to hold the binding fastened, relieving the screws. This was confirmed by Rottefella (Ø. Svendsen, personal communication, February 12, 2018).

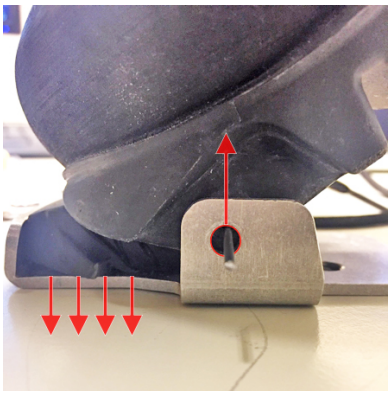

Figure 4-14: Mx generated by the compressed flex and the forces in shoe-pin holes.

Two tests were done to find out how much force that goes into the flex when a skier falls. In the first setup (Figure 4-15), a load cell was mounted in front of the shoe at a 35° angle. This angle was found by pushing a shoe as hard as possible forwards on a ski binding, see Figure B-11. The load cell was connected to a computer using an Arduino microcontroller, making it possible to record the measurements. A person then stepped into the shoe and pushed it forwards as hard as possible (until the knee hit the ground because of the flexible shoe). The first tests were conducted with a load cell composed of aluminium plates (Figure B-12), which gave peak forces of 1040 N and 1290 N, but the plates bent over. In the last test, the plates were changed to steel plates, which gave a peak force of 1480 N. To verify the measurements, a second test was done at Rottefella, see Figure 4-16. Here the load cell was mounted under the front of the binding; the idea was to get a more realistic measurement because the flex in the new prototype from Rottefella compressed more than 35°. According to Øyvar Svendsen (personal communication, February 12, 2018) the ideal angle was 20-22°. This increased flexibility resulted in lower forces, the highest force from the test was 458 N. Therefore, the load was defined to 1 000 N; between the first and the second measured value.

Figure 4-15: The first setup.

Figure 4-16: The second setup.

The upwards force was set to Fy = 2 000 N which is higher than the retention strength of the screws (section 4.4.1) and the maximum load the shoe can take. Shoe soles should withstand a force perpendicular to the sole of 1500 N - 2000 N (J. Danielsen, personal communication, October 3, 2017) before the sole is ripped from the rest of the shoe. This was a criterion from Rottefella.

Twist Moment: My

The second critical load scenario that was considered, is when the skier twists the shoe boot in the ski binding. To measure the twist moment My a test rig was built, see Figure 4-17 and

Figure B-13. The bracket which the shoe was mounted into could rotate freely around the y-axis and when the shoe rotated, it compressed a load cell. The moment was found by multiplying the measured force by the distance (105 mm) from the load cell to the rotation centre. A person put on the shoe, and several tests were done by twisting the shoe so hard that it caused pain in the knee, the peak force that was measured was 300 N, which results in a torque equal to 31.5 Nm. This is lower than the release moment in alpine ski bindings which lies between 50-80 Nm. The size of this force will vary with the skier, how stiff the shoes are, how much support the heel has (Figure B-14), etc. The force was set to 50 Nm, which is higher than the measured force and the same as a low release value for alpine skis.

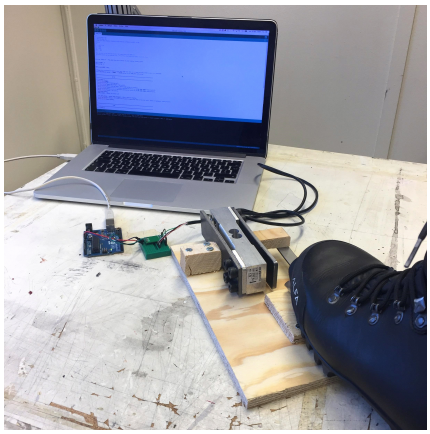

Figure 4-17: Measuring the moment My.

4.3.2 The Critical Low-Likelihood Conditions

These are scenarios that can occasionally happen, but is not seen as common or a part of the intended usage. A case that was considered here was if someone stepped on the ski binding while not skiing, resulting in a high sideway force that might break the binding. The force Fx was set to 1000 N, which simulates the weight of a person of 100 kg stepping on the binding. This force was decided in cooperation with Rottefella during the project work. Another criterion from Rottefella was that the binding should withstand a force of 2 000 N straight up with no permanent deformation. This was to ensure the binding was both stronger than the shoe and the screw ripping force out of the skis, as described in the previous section.

4.3.3 Normal Use

These load scenarios are considered the most common and are much lower than the critical load scenarios. Since the topology optimization does not consider effects from cyclic loading, the result was fatigue tested. The fatigue analysis was done to locate ‘hot-spots’ for crack initiation

and failure and to calculate the fatigue life (N_f). The Fatigue Life is the number of cycles until a material fails when subjected to fluctuating stress below the yield stress.

The first scenario simulates the forces applied to the binding while diagonally striding. When striding, the skier glides with one ski while pushing the other ski down and backwards, generating speed. The shoe is rotated and starts compressing the flex while the shoe-pins lift the binding, two setups were built to measure the size of these forces. In Figure 4-18 the force into the flex was measured and in Figure 4-19 the force needed to hold the binding onto the ski was measured. The data was measured by a load cell and captured to a computer with an Arduino microcontroller. All the tests were performed in the workshop and several measurements were done to get usable data. There are several limitations with a setup like this and it is hard to capture the correct loads. The loads might also vary with the skier, skis that are used, skiing terrain, etc., but the tests gave an indication on the values.

Figure 4-18: Measuring the force when the flex is compressed.

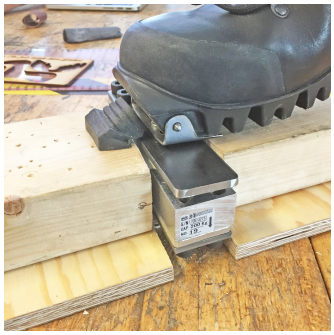

Figure 4-19: Measuring the force needed to ´hold´ the binding to the ski.

The other two scenarios simulate forces when skiing downhill. The first was meant to simulate a continuous up and down motion, which could be the case in an icy slope. The second simulates when a skier is ‘edging’ the ski, which happens when ploughing or steering. Figure 4-20 shows how the ‘up and down’ forces was measured and Figure 4-21 shows how the side force was measured.

Figure 4-20: Measuring the forces straight up and down.

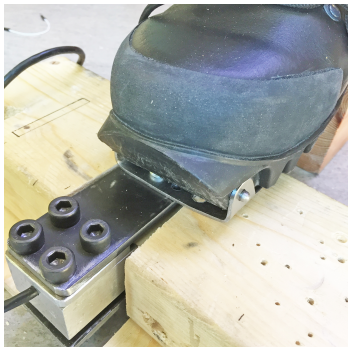

Figure 4-21: Measuring the force generated when the skier is ‘edging’ the skis.

4.3.4 Pre-Tension

In addition to the critical load scenarios, pre-tension in the screws was included in the topology optimization task, see Figure 5-5. When Rottefella mount ski bindings they first use a drill to insert the screws into the ski, but the final tightening of the screws is always done by hand. If the screws are fastened too hard it might destroy the core of the ski, which in many cases is wood. When tightening, a tension will develop in the screws, a so-called pre-tension. This pre-tension is important because the screws are not built to withstand shear forces, only tensile forces. In other words, it is the friction force between the ski binding and the ski which are meant to resist the shear forces, e.g. when the binding is rotated.

The force F (Equation 4-2) will work in the opposite direction of what would be the binding's motion if there are no friction. If a torque was applied to the ski binding, trying to rotate it, the force F would be equal to the force exerted on the binding. If the magnitude of the force F is overcome, i.e. a force higher than the friction coefficient multiplied with the normal force, the binding will rotate. The static friction can be increased by increasing the friction coefficient or the normal force. If pre-tension is left out of the optimization, the screws must resist the shear forces from the rotation of the binding which can be seen in Figure B-15. This might destroy the screws. In Figure B-16 the binding is optimized with pre-tension. The displacements in the two cases described in these figures were measured when a torque equal to 50 Nm was applied to the models. The model in Figure B-16, with a pre-tension equal to 1 500 N, was three times as stiff as the model in Figure B-16, which had no pre-tension.

$$F = \mu \ N$$

Equation 4-2: Static friction (F = force of static friction, μ = static friction coefficient, N = normal force).

To calculate pre-tension for screws in wood is very difficult and only equations for calculating this in bolted connections were found. A simple test was done by tightening the screws by hand as one would on a ski binding, see Figure 4-22. The peak force that was measured in the tests was ~ 1 000 N (2 screws). Therefore, a rough estimate of the pre-tension per screw was set to 550 N.

Figure 4-22: Measuring the force generated by pre-tension.

4.3.5 Summary and Gate Criteria

Table 4-2 summarizes the findings described in this sub-section. The experiments in these sub-sections are not fool-proof, but gave a good indication on what to use as input in the topology optimization, the linear static analysis and the fatigue calculations.

Load Scenarios	Description	Component	Size	Included in
Critical, high-likelihood	Stride	Fy	2 000 N	TO, Static FEA
		- Fy	1 000 N	TO, Static FEA
	Twist	+/- My	50 000 Nm	TO, Static FEA
Critical, low-likelihood	Side force	+/- Fx	1 000 N	Static FEA
	Straight up	Fy	2 000 N	Static FEA
Normal	Stride	Fy	0 → 250 N	Fatigue analysis
		- Fy	0 → 250 N	Fatigue analysis
	Up and down	+/- Fy	- 150 N → 50 N	Fatigue analysis
	'Edging'	+/- Mz	- 6.4 Nm → 6.4 Nm	Fatigue analysis
Other	Pre-tension	- Fy	550 N	TO

Table 4-2: Load scenarios (TO: Topology Optimization).

4.4 The Design Variables

The boundary conditions and the dimensions of the design space are described as the design variables (Fiedler et al., 2017). In this problem, the boundary conditions are the way the ski binding is fastened to the ski, and the dimensions of the design space is the parametric dimensions of the CAD model used in the topology optimization.

As explained in section 3.2 there are to this date no optimization software where the engineer can enter the problem description (loads, boundary conditions, maximum dimensions and restrictions) and automatically get the optimal boundary conditions and design space dimensions in return. So, even though approach 3 (section 3.2.2) is used to find the optimal design variables through cyclic iteration, some initial decisions must be made. Some of the design variables may be restricted by restrictions presented in the assignment, e.g. to fit in an assembly or that the part needs to be fastened in a specific way, these are referred to as fixed variables. The design variables which are not restricted in any way are called the adjustable variables. The fixed and adjustable variables in this problem are discussed in the next sub-sections.

4.4.1 Ski Binding Restrictions

Rottefella uses ISO standards when designing their ski bindings. All the skis and bindings that are manufactured in compliance with the different ISO standards are compatible. The *ISO 9119 Cross-country skis - Binding mounting area* (Standardization, 1990), defines that the minimum width of the binding mounting area is 33 mm for cross-country skis. This standard is used by Rottefella for backcountry ski bindings. It also states that the screw retention strength, the load it takes to pull two screws, mounted sideways (Figure 4-23), out of the ski, should be at least 1600 N.

The *ISO 7794 Cross-country skis - Ski binding screws - Requirements* (Standardization, 2011), describes the dimensions of the screws that are used, see Figure 4-24. The *ISO 13992 Alpine touring ski-bindings* (Standardization, 2014) states different release torque values for bindings with release functions (i.e. that the shoe is detached from the binding), and how to test if the bindings release at the correct values. *ISO 8061 Alpine ski-bindings* (Standardization, 2015), describes methods for calculating the release torques (My and Mx).

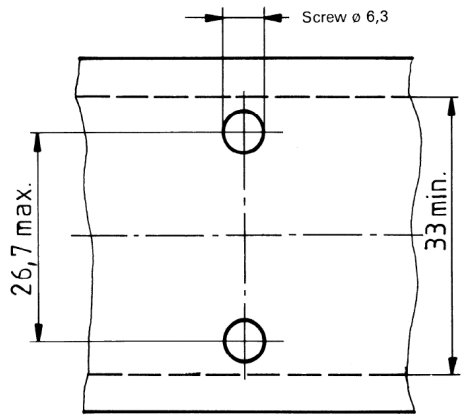

Figure 4-23: The binding mounting area (Standardization, 1990).

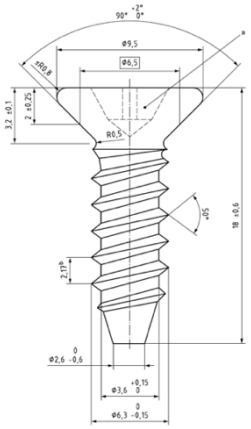

Figure 4-24: Dimension of thread, shank and head (Standardization, 2011).

The width of the ski-model in the setup was set to 58 mm, this is narrow for alpine touring and telemark skis, but a medium width for mountain skis. The shoe-pin holes were 5 mm in diameter and the distance vertically to the shoe-pin holes from the top surface of the binding was set to be 12 mm, this ensured that the current shoe made for this system could rotate freely and were values defined by Rottefella. The restrictions are summarized in Table B-2.

4.4.2 Additional Restrictions

The ideal case would be to optimize all the variables which were not restricted by the assignment, but due to time and computational limitations, additional restrictions had to be defined. This will probably be the case in many development projects; compromises must be made, and some initial decisions must be made by the engineer. The parameters that were restricted were; the screw hole pattern, the boundary conditions and the dimensions of the design space.

At the market today, bindings are fastened either by glue or screws. The advantage with glue is that the properties of the ski is not affected as it would be by screw holes, the disadvantage is that the binding is permanently stuck and removing it for using it on other skis may destroy the ski. Glue is used on some of Rottefella's cross country ski bindings. The glue used at Rottefella was tested out briefly in Abaqus using 'adhesive-elements' (Appendix B.4), but it made the model highly complex and increased computational time greatly. An idea was to use glue on the outer parts of the binding where the screws could not be placed. Because the analyses already were so time demanding, it was decided instead to focus on connecting the binding to the ski with screws.

To be able to simulate the force from the compressed flex, an area which a force could be applied to in the simulation needed to be defined. The red line in Figure 4-25 shows where this area was placed. It was set to be 9 x 26 mm at 12 mm from the shoe-pin centre line. The area was smaller than the flex, but when testing it, it seemed like most of the forces went into this area. Since this area had to be frozen in the optimization (section 5.1.3), the aim was to not make it too big. The restrictions described in this section are presented in Figure 4-26 and Table B-2 as fixed variables.

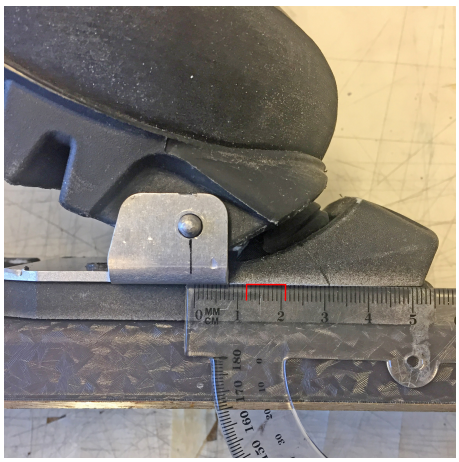

Figure 4-25: Defining the flex area.

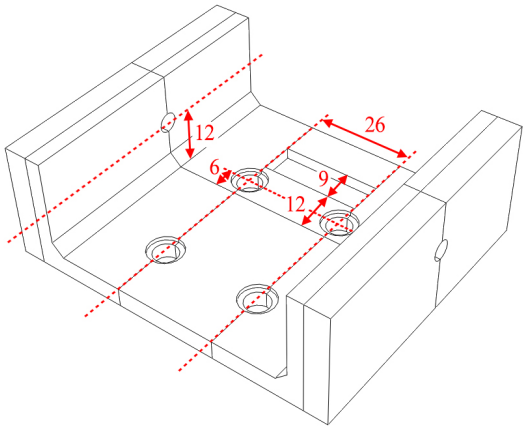

Figure 4-26: The fixed variables.

There are numerous screw hole patterns that could be tested by trying out different placements and number of screws, but because of the limited time a 'test-space' inspired by the article *Integrated Shape and Topology Optimization - Applications in Automotive Design and Manufacturing* (Fiedler et al., 2017) was defined. The idea was to test the parameters in Figure 4-27 / Table 4-3; the adjustable variables, in various combinations to see which gave the optimal design.

The screw hole pattern was restricted to four screws in a square pattern, which was based on the two lightest alpine touring ski bindings at the marked today, the Dynafit bindings described in section 4.1.3. It is likely that a better screw hole pattern, giving a stiffer and lighter structure, could be found by changing the number of screws or try out different screw hole patterns, but a starting point was needed to be defined. The screws were placed as far out on each side of the ski as possible (ISO-standard in Figure 4-23) to counteract the torsion moment My; this is described further in Appendix B.5. The front screws were fixed between the flex-area and where the shoe was fastened, like the Rottefella BC Auto binding in Figure 4-28. The rear screw

holes were fixed in the x-direction, but free in the z- and y-direction. The idea was to find the distance to the rear screws which was best in respect to both My and Mx, see Appendix B.6 .

Description	Direction	Parameter
Height of the binding	y	h (height)
Height of screw support structure	y	sh (screw height)
Height of flex support structure	y	fh (flex height)
Distance of rear screws from the front screws	z	d (distance)

Table 4-3: The adjustable variables.

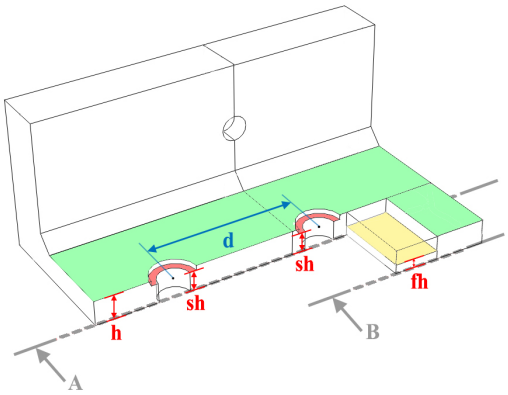

Figure 4-27: The adjustable variables. Cutting planes defined in Figure B-20.

Figure 4-28: Red dots show screws (Rottefella, n.d.-d).

5 Optimization Cycle and FEA

5.1 Design Variable and Topology Optimization

5.1.1 The Simulation Model

Abaqus was used to CAD the parts in the ski binding assembly and the focus was to create a realistic setup. Several different elements and features were tested and the most interesting discoveries are presented here.

A simple way to simulate interactions, e.g. between the binding and the screws, is to create constraints. A constraint couples the motion of a reference point to a surface; if the reference point is fixed or loaded, then the surface will be as well. An example of a model where the four screws, the shoe-pin and the flex were simulated with constraints can be seen in Figure 5-1. The green reference points were fixed, while loads were applied to the red and yellow reference points. The alternative is to CAD the screws and the shoe and include these in the assembly, see Figure 5-2. Contacts are then defined between the elements. These two approaches were tested out and the optimized models are displayed in Figure 5-3 and Figure 5-4.

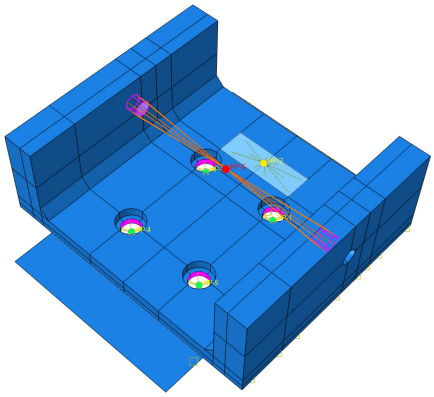

Figure 5-1: The setup with constraints.

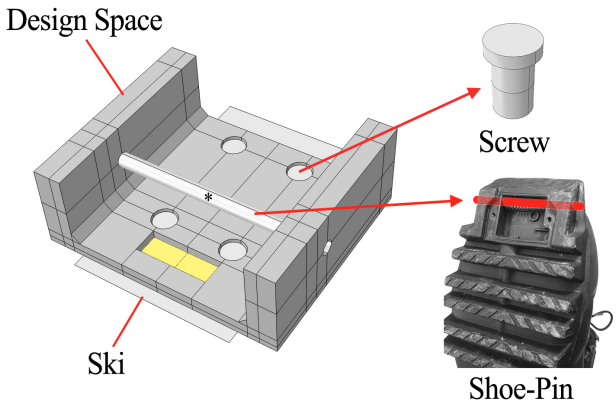

Figure 5-2: The assembly used in the thesis.

The setup displayed in Figure 5-2 was the one which gave the most promising results, i.e. the assembly that seemed to simulate reality in the most accurate way. There were mainly two reasons for this. The first was that constraints are rigid, i.e. they cannot be deformed. If an upwards force is applied to the shoe-pin, the binding will bend slightly around the z-axis. While the model in Figure 5-4 has connections between the rear screws that makes it stiffer, the model in Figure 5-3 does not. This indicates that these rigid constraints may be unnaturally stiff. Secondly, the constraints are connected to the entire surface that is selected, when the 'shoe-

pin' is pulled straight upwards, the nodes in the lower half of the pin-hole will be dragged just as much as the top surface is being pushed. This explains why the model in Figure 5-3 looks so thin at the upper half of the holes where the shoe-pin is connected and at the inner part of the screw holes. Including deformable screws in the optimization also made it possible to apply pre-tension, called a bolt-load in Abaqus (Figure 5-5). This will compress the screws and generate a pressure on the ski binding which pushes it down into the ski.

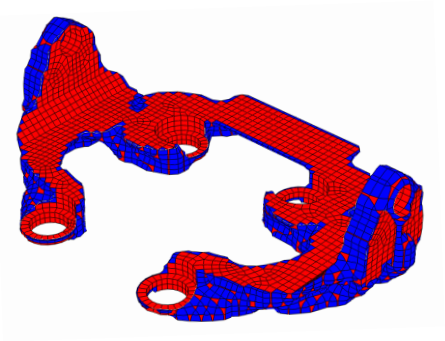

Figure 5-3: Using kinematic constraints as screws and shoe-pin.

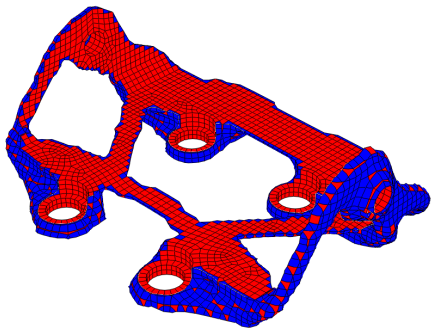

Figure 5-4: Including screws and a shoe-pin.

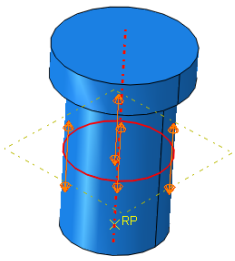

Figure 5-5: Bolt load in Abaqus.

The ski in Figure 5-2 is modelled as a 2D surface to reduce the number of mesh elements and thus computational time. Experiments were done with a larger, deformable ski as well, but it had little impact on the result. It was also experimented with a larger shoe, but the contacts between the shoe and the side walls made the analysis very complex. Therefore, it was decided to test the model for any forces to the sidewalls afterwards instead. Preliminary tests indicated that the algorithm favoured material on the edge between the top surface of the binding and the sides (Figure 5-6), which resulted in a very sharp edge that seemed exposed to fatigue and the low-likelihood load case presented first in section 4.3.2. Because of the algorithm's inability to add material outside the design space, a chamfer was added to these edges, see Figure 5-2. The design feature was inspired by Rottefella's prototype in Figure 5-7.

Figure 5-6: Prototype from the preliminary project work.

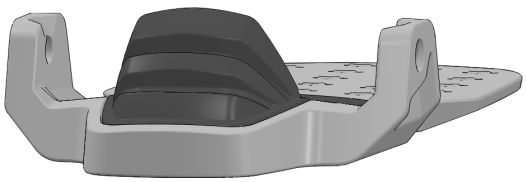

Figure 5-7: Rottefella prototype binding with chamfer on the side walls.

5.1.2 The Finite Element Model

Mesh

The parts were meshed with hexahedral elements to create a finite element model (Figure 5-8). To get an ideal mesh it is important to partition the model in a smart way, so that the mesh fits the contours of the model (see Appendix C.1). The mesh was checked for errors and warnings and refined until there were none. The hexahedral elements (C3D8R-elements) were chosen because of the simplicity of the model and because these elements can give just as good solutions as a tetrahedral mesh, but demands less computational time. For more complex geometries, where the hexagonal shape has a poor fit, tetrahedral works better. Therefore, tetrahedral mesh was used on the optimized models.

When considering the number of mesh elements; "a typical good rule of thumb is to apply a three elements minimum for any small feature being modelled with FEA" (McKee & Porter, 2017, p. 59). To follow this 'rule' it was necessary with a mesh seed = 0.5 (seeds controls the density of the mesh) which results in 550 000 mesh elements. When this mesh was used, Abaqus predicted a computational time of more than a week. Therefore, the mesh seed was set to 1.2; this was a relatively fine mesh with a manageable computational time of around 10 hours per optimization (30 cycles).

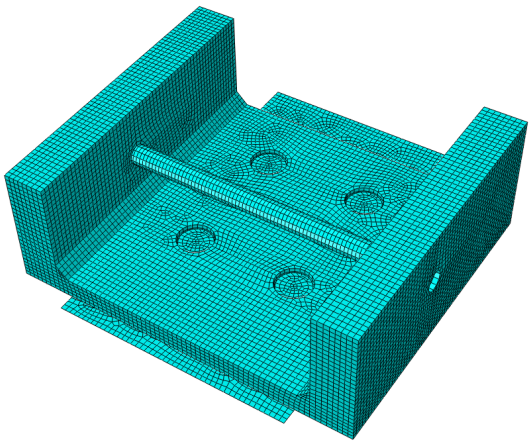

Figure 5-8: The meshed assembly.

Loads and Boundary Conditions

The loads were applied to the centre of the shoe-pin and to the reference point which was constrained to the flex area, see Figure 5-2. In hindsight, it seems that this constraint may have led to unnatural high stiffness in the flex-area, leading the algorithm to remove too much material. The ski and the lower end of each screw were fixed through the whole analysis, see Figure 5-9.

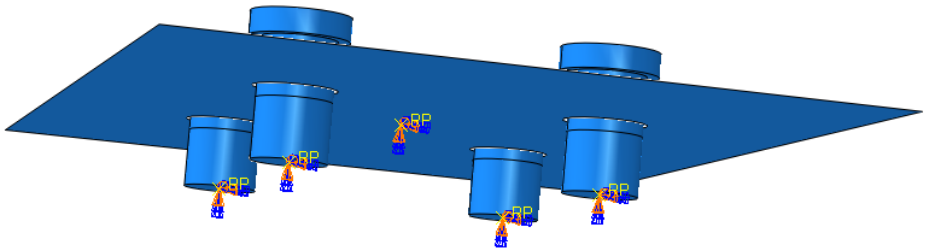

Figure 5-9: Fixed parts.

Steps and Interactions

The load cases were applied over separate static steps which together formed one optimization cycle. Static means that the load scenarios were not time-dependent. Contact was defined between the binding, the screws, the ski and the shoe-pin. Between the ski and the binding a friction coefficient $\mu = 0.3$ was defined and between the binding and the screws $\mu = 0.4$ was used (TeachEngineering, n.d.).

5.1.3 Optimization Task

After the FE-model had been created, it was time to prepare an optimization task and run it with Tosca. The condition-based optimization algorithm was selected (section 2.3) and the number of optimization cycles was defined.

Design Space

The design space is the elements the algorithm is free to change, i.e. where the topology is optimized. This was defined to be the bracket, with some restrictions which are mentioned below. The bracket may seem much bigger than the optimized result, but since material cannot be added outside the defined space, it is important to make sure that the optimization is not limited. Therefore, the key is to make this large enough within the restrictions. However, there is no point in having an unnecessary big design space, since a large design space means more mesh elements which results in longer computational times.

Design Responses

The design responses are the input values in the analysis; e.g. displacements, stiffness, volume, eigenfrequencies and stress. In a minimum compliance design, strain energy and volume are defined as the design responses; strain energy to be minimized and volume to be constrained.

Constraints

The design response called volume is here constrained. The volume which is defined here, 8 % in Figure 5-10, will be the volume the algorithm seeks to reduce the model into in the given number of cycles. In other words, the volume will be reduced by 92 %. The challenge was to set the lowest volume constraint which still resulted in a compliant model.

Objective Functions

This is the objective you want to accomplish. The target was set to minimize the design response values, see Figure 5-11. The conditions-based algorithm allows only the design response Strain-energy to be added here.

Geometric Restrictions

There are several geometric restrictions which can be applied to ensure symmetry, to keep regions of the model from being altered or ensure manufacturability. It is important to have in mind that applying too many restrictions will limit the algorithm. The surfaces where the screw heads and the shoe-pins interact with the binding and the flex area were frozen (Figure 5-12). When they were not frozen, the optimization task failed because it removed elements at these surfaces resulting in poor contact surfaces. The screws, the shoe-pin and the ski were also frozen. To ensure that the binding was symmetric around the longitudinal direction, a symmetric restriction was added. If material was added to one of the sides because of the positive moment My, it would be added to the other side as well, meaning it was not necessary to include a negative moment My.

Optimization Process

This is the last step, here the maximum number of cycles is defined. It is important to set this number equal or higher than the one defined in the optimization task, otherwise the optimization will quit before it is finished which may result in many intermediate elements. The computational time can be reduced by using multiple processors and GPU acceleration.

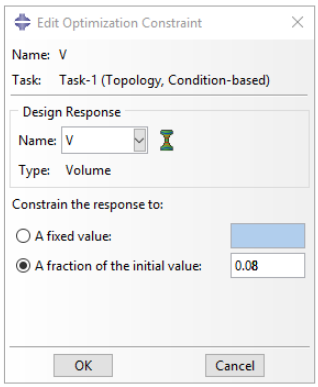

Figure 5-10: Optimization constraint.

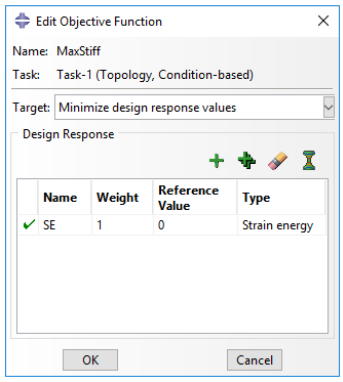

Figure 5-11: Objective function.

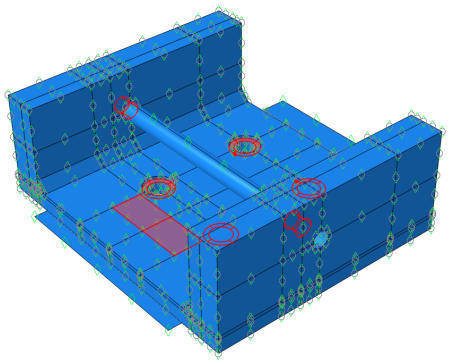

Figure 5-12: Red surfaces are frozen.

5.1.4 Criteria Gate 1

The optimal design was selected based on volume and strain energy. Models were tested requesting the same volume fraction and the result with the lowest strain energy was in this case the optimal. This criterion could be used to select the best design out of a defined number of tests, e.g. testing 20 designs and selecting the best. It could also be used in an automated process where an algorithm is programmed to converge towards the optimal solution; e.g. be scripted to stop when the decrease in strain energy between a set of models were below 2 %. How it was done in this thesis is described in the next section.

5.1.5 Optimization Cycle

When the finite element model, the optimization task and the gate criteria were defined, it was time to search for the optimal solution, i.e. the design variables and topology which in the best way satisfy the criteria. As mentioned, this could either be done automatically or manually. The process could be automated by making a script or using an optimization software like iSight. In iSight the test parameters (the adjustable variables) are first defined, e.g. the height of the binding with a minimum value of 1 mm and maximum value of 5 mm, and a step size of 0.5 mm. Between each topology optimization iSight compares the results and decides which parameters to test in the next cycle, converging to a solution (Figure 5-13). The finite element model is automatically changed between each cycle.

The initial idea was to use iSight for the design variable and topology optimization loop, but it was discovered that bottle neck in this optimization problem was the topology optimization step (~ 10 → 12 hours per optimization). To change the design space, e.g. the distance between the screw holes, update the FE-model and then the optimization task went relatively faster (~15

minuets). Therefore, this was done manually following the 'manual' loop in Figure 3-6. However, if sufficient computational power was available the favoured approach would be to automate the process.

The initial optimizations, the first eleven iterations in Figure 6-7, laid the foundation for the final tests. Through these tests the volume constraint, mesh size, the number of cycles and a set of adjustable variables were defined, see Table 5-1 and Figure 5-14. The volume constraint was set to 8 %; below this the models did not seem to be complaint. Optimizing over 30 cycles gave good results and an increase or decrease in the number of cycles did not give noticeable better results. The minimum- and maximum-values in Figure 5-14 / Table C-1 were defined after testing different adjustable variables to find the extremes (see Appendix D.1). Since every combination of the adjustable variables would not be tested, it was likely that the result would be a local optimum which is further discussed in section 7.2.1. However, the aim was still to see if it was possible to make the market's lightest backcountry ski binding using topology optimization.

Test parameters	
Mesh size	1.2 seeds
Optimization Cycles	30 cycles
Requested Volume	8 % of initial volume

Table 5-1: Test parameters.

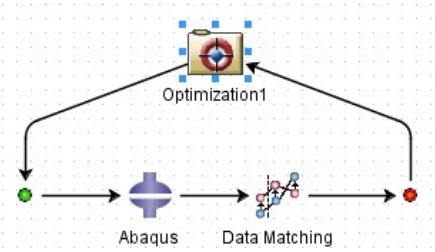

Figure 5-13: Screenshot from iSight 2017.

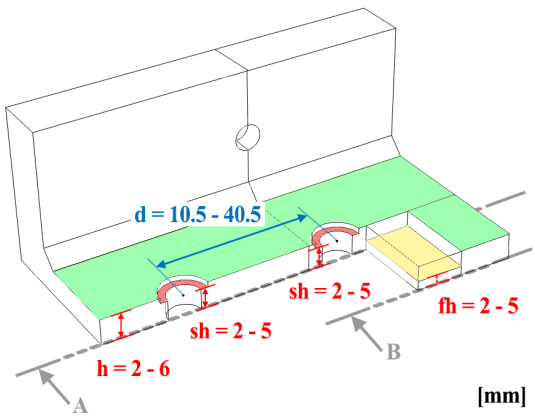

Figure 5-14: The chosen adjustable variables. Cutting planes defined in Figure B 19.

5.2 Finite Element Analysis

5.2.1 Post-Processing in Abaqus

The result from the topology optimization can be displayed as an isosurface in the post processing module in Abaqus. The isosurface visualize if mesh elements should be kept or discarded by assigning them colours. The red elements in Figure 5-15 and Figure 5-16 are those which contribute to the stiffness of the binding, while the blue do not. A successful optimization results in only blue and red elements, with no intermediate elements. The intermediate elements are those the algorithm could not decide if should be kept or not, these are visualized by colours from red to blue, see Figure 5-17. If the optimization result contains many intermediate elements it may help with a finer mesh or an increased number of cycles. An example of a poor optimization results can be seen in Figure C-8.

The isosurface can be extracted as a STL file or an Abaqus-input file. When exporting the model, an isosurface value must be defined. It is important to define a value which does not cut any red elements, but at the same time removes most of the blue elements. Figure 5-15 displays a model with a low isosurface value with many blue elements, while in Figure 5-16 a high isosurface value is selected, cutting some of the red elements. An isosurface value equal to 0.3 is used in the Abaqus Tosca learning material (Simulia, n.d.-a) and was selected in all the optimizations in this thesis.

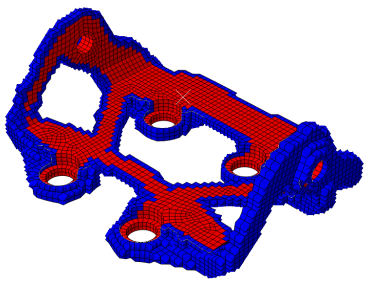

Figure 5-15: Isosurface value = 0.01.

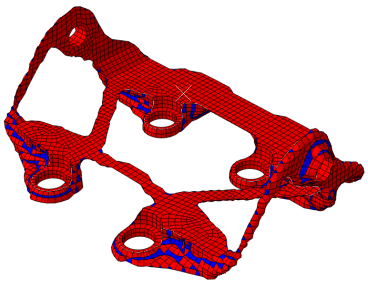

Figure 5-16: Isosurface value = 0.7.

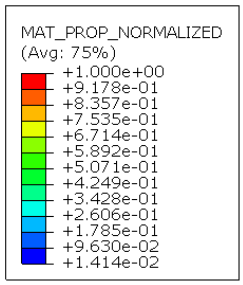

Figure 5-17: The colours that are assigned to the elements.

5.2.2 CAD Remodelling

The process of remodelling the optimized geometry can be done in many ways. The procedure presented here was used in this thesis. First, the STL file was imported as a ‘surface body’ into Solidworks (CAD/CAE software) where it was used as a reference-model. As Figure 5-18 shows, the new model was designed to fit the optimized result as accurately as possible. To save time it is important to use symmetry; in this problem half of the binding was modelled and then mirrored.

A set of datum-planes were created across the model; the planes were placed at strategic places where the model topology changes (Figure C-9). Then a set of 'intersection curves' were created between the reference-model and the datum-planes (Figure C-10). These intersection-curves were then used to create lofted sections along a set of guided curves (Figure C-11). The benefit with this approach is that both the intersection-curves and the guided curves can easily be altered later, making it simple to adjust the design in accordance with the redesign loop 1 changes.

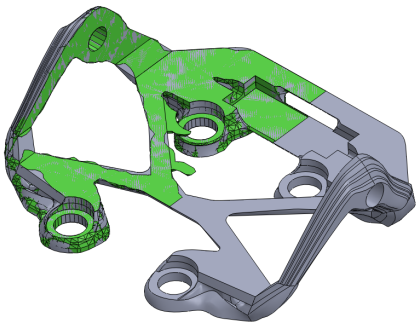

Figure 5-18: The green geometry is the reference model - the grey is the final design.

5.2.3 Static and Fatigue Finite Element Analysis

Abaqus was used to run the static finite element analysis and because of the complex geometry a tetrahedral mesh was used, see Figure C-12. The screws, the shoe-pin and the flex were simulated with constraints, even though these were found to be less realistic in section 5.1.1. The reason for this was that the solver in Abaqus crashed when the analysis contained interactions between elements with a tetrahedral mesh and not a hexahedral mesh. The red points were fixed, the critical high-likelihood load cases were applied to the green and orange reference points and the low-likelihood load case was applied to the yellow point, pushing the purple side wall outwards, see Figure 5-19.

The von Mises stress was then measured in each load case to check if the model satisfied the criterion. The von Mises stress is a measure of stress when the loading is uniaxial and complex and can be used to measure the stress at any place point in the model. If the von Mises stress is higher than the material's yield strength, the material will yield (Equation 5-1). This means that the part will be permanently deformed and in this case destroyed.

$$\sigma_v \geq \sigma_y$$

Equation 5-1: Material yields if the von Mises stress is higher than the yield stress.
σ_v: The von Mises stress. σ_y: The yield stress.

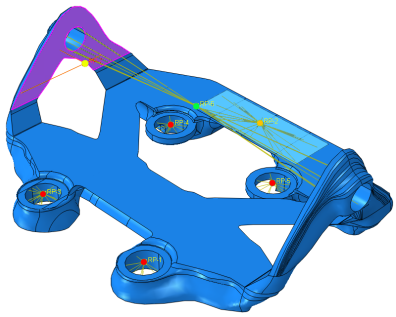

Figure 5-19: The FEA setup in Abaqus.

The fatigue analysis was done in FEDEM (Finite Element Dynamics in Elastic Mechanisms) which is a software for simulating dynamic systems. The focus was to find 'hot-spots' for crack-initiation and fracture, and to calculate the predicted fatigue life. The model was first imported into Siemens NX (CAD/CAE software) where it was meshed and 1-D connections were created to simulate the shoe-pin, the screws and the flex (the black lines in Figure 5-20). Siemens NX had to be used because these operations cannot be done in FEDEM. The model was then imported into FEDEM, where boundary conditions and loads were applied. The 1-D connections inside the screw-holes were fixed. The three normal load cases which are described in section 4.3.3 were applied using functions in separate analyses. The functions were created to simulate diagonally striding (Function 1 and 2, based on Figure C-13), downhill-skiing (Function 3) and 'edging' the skis (Function 4, when ploughing or turning on the skis); see Figure C-14, Figure C-15, Figure C-16 and Figure C-17 respectively.

FEDEM could then estimate how many times each function could be repeated before the part failed. The load cases and functions were empirically found, so the fatigue analyses are by no means definite. The model was covered with a 'strain-coat' to find the hot-spots for fatigue. The hot-spots were located by creating a contour on the model which showed the parts of the construction which had the lowest fatigue life (Figure 5-21). When these were located, a set of 3-directional strain rosettes were placed at these spots (Figure 5-22). The rosettes measure the stress and the strain in the x-, y- and 45°-direction. The analysis was then repeated and the data from the rosettes were recovered.

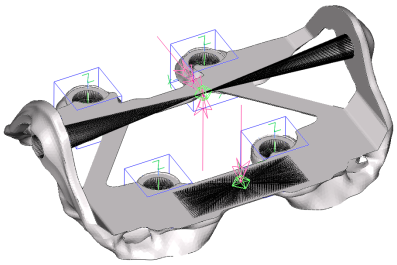

Figure 5-20: Setup in FEDEM.

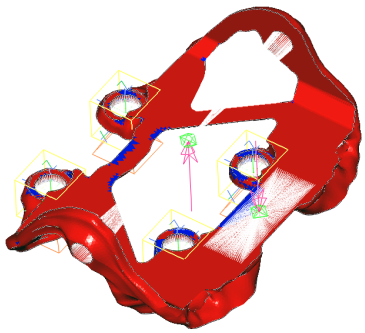

Figure 5-21: The blue regions show where the part fails first.

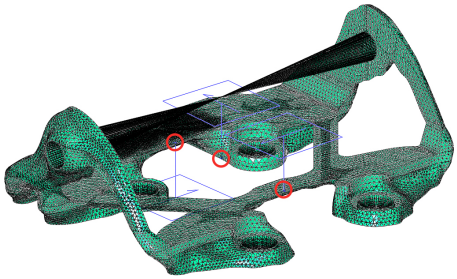

Figure 5-22: Strain rosettes placed at critical spots, here encircled in red.

5.2.4 Criteria Gate 2

These criteria were defined to ensure that the binding would withstand it's intended use; i.e. no permanent deformation in any of the load cases, and that it would have a sufficient service life. The first criterion was set after the material properties of titanium and the second after an estimated number of cycles until failure, see Table 5-2. Since what seems to be the most critical load case, Fy = 2 000 N, is higher than the force that could rip the screws out of the ski and destroy the shoe, a relatively low safety factor of 1.25 was used. The yield strength for titanium is given in Table 4-1, the criterion was therefore set to $\sigma_v < 800\ MPa$, see Equation 5-2. The aim is to make the lightest ski binding, this will of course comprise with service life and durability; the minimum service life criterion was set to 20 years (see Appendix C.4). First, a static analysis was run, if the von Mises stress was higher than the criterion, the binding was remodelled in Solidworks before it was tested again, following redesign loop 1. When it satisfied the static criterion a fatigue analysis was conducted. This followed the same procedure; if some of the members had too low fatigue life, it was remodelled and then retested. However, if larger changes were necessary, a new optimization cycle should be run, following redesign loop 2. This could mean that you must re-test all the adjustable variables.

$$\sigma_v < \frac{\sigma_y}{SF} = \frac{1000}{1.25} = 800$$

Equation 5-2: Safety factor.

Criteria	
Static analysis	$\sigma_v < 800\ MPa$
Fatigue life	$N_f > 1\ 000\ 000\ cycles$

Table 5-2: Criteria at gate 2.

5.3 Manufacturing and Physical Testing

5.3.1 3D Printing

After FEA the CAD models were exported and 3D-printed. For fast prototypes the FDM printers at IPM were used. To get more detailed prototypes they were sent to Even Hovik at NTNU Valgrinda who printed in Tough Resin, Aluminium and Steel, or to Pål Erik Endrerud at NTNU Gjøvik who printed in PA2200 and Titanium.

5.3.2 Functional Testing

There were two goals with these tests; to see the CAD model in real life and to see that the binding really fits into the binding assembly. When making physical prototypes you will gain knowledge that is hard to get by looking at the part in a 3D-modelling program. E.g. the model in Figure 5-23 had extremely thin side walls; the reason for the thin walls was the 'smoothening' option you may select when the model is extracted after the optimization. This option was turned off. The most important thing is that the shoe fit into the binding without causing too much wear on the sides of the shoe when it is rotating. The shoe-pins should be able to be extended or retracted easily and it should be possible to mount a flex on the binding. These criteria are summarized in Table 5-3.

The Tough Resin and metal prints were the best to test the function of the binding system because of their strength. Figure 5-24 shows a binding printed in Resin Tough where striding motion was tested out. Figure 5-25 shows a metal binding that was tested in the winter to see how the flex could be included. Different plastic parts were made to hold the flex, just to test the system, see appendix C.5.

Figure 5-23: Thin wall.

Figure 5-24: Tough Resin printed with SLA.

Figure 5-25: Field testing.

5.3.3 Mechanical Testing

The tensile testing machine in Figure 5-26 and Figure 5-27 was used to test prototypes and the test rig is more closely described in Appendix C.6. The setup is like the one that was used in the preliminary project work and is based on the machine Rottefella uses to test their bindings, see Figure C-21. The pinches in the test machine; the upper and lower claw holding the binding setup, were programmed to be moved apart from each other by 1 mm/min and in that way, stretch the binding. The binding is fastened and stretched until failure; this is defined as a certain drop in the applied force which happens when something in the test specimen fails. The rollers and the aluminium profile in the setup were originally unrestrained, to ensure that the force was correctly applied to the binding, but when testing more flexible materials like PA 2200, some modifications had to be done. The aluminium profile was fastened to the rollers, which again were fastened to the lower beam, see Figure 5-28. In this way, the binding did not have to carry the weight of the aluminium profile and the rollers when it was tested.

These tests were mainly conducted to verify the simulation model and the static FEA. By comparing where the bindings failed and how large the deformations were, it was possible to see how accurate the simulation model replicated reality. The setup was constructed to test the low-likelihood condition which is described lastly in section 4.3.2; a vertical force (Fy) applied to the centre of the shoe pin. When testing the titanium binding, it should be possible to apply this low-likelihood condition, Fy = 2 000 N, without any permanent deformation.

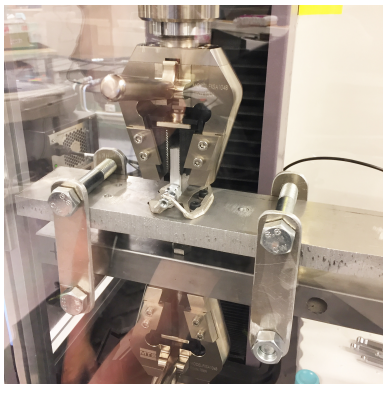

Figure 5-26: The tensile testing machine.

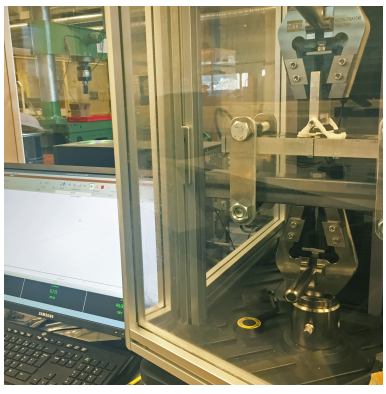

Figure 5-27: Time, force and displacement measured by a computer.

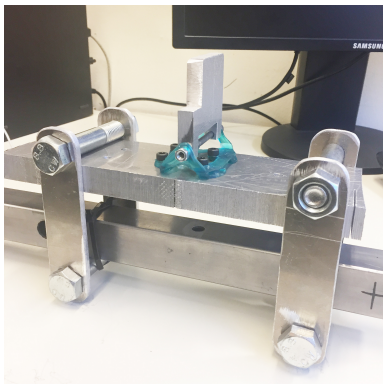

Figure 5-28: The setup for testing PA 2200 and Tough Resin.

5.3.4 Criteria Gate 3

The functional testing and the mechanical testing were completed to verify the simulation model and to ensure that the physical model satisfied the criteria, see Table 5-3. If these criteria were met, the cycle (flowchart in Figure 3-1) would be completed.

Functional Criteria	**Mechanical Criteria**
Fit into the binding with little resistance to the side walls	Measure and compare with the Abaqus simulation: the deformations under loading and where the bindings fail.
Extract and retract the shoe pins	
Mount and use a flex	Titanium print: $\sigma_v \leq \sigma_{yield}$ at Fy = 2 000 N

Table 5-3: Gate 3 criteria.

6 The Result of the Optimization Cycle

6.1 The Optimal Design

The binding displayed in Figure 6-1, Figure 6-2, Figure 6-3, Figure 6-4, Figure 6-5 and Figure 6-6 is the result of completing one full cycle of the workflow presented in section 3.3; design variable optimization, topology optimization, regenerating the CAD geometry, using FEA to redesign for stress peaks and fatigue life, and physical testing. The binding weighs 26.70 grams (Titanium) and FEA indicates that it is strong enough for its intended use. It was one of the stiffest structures that was generated in this process, even though it was one of the lightest. Iterating on the design variables halved the strain energy from the initial optimizations where theses parameters had been placed based on research and previous bindings; from 710 mJ to 346 mJ (see Figure 6-7).

The binding is 158.30 grams lighter than the Rottefella 75 mm (backcountry binding) and 35.30 grams lighter than the Dynafit DNA (alpine touring binding), without a flex and a heel part. The flex in Figure B-1 and the heel part of a Rottefella 75 mm binding weight ~ 10 grams each, and adding these features to the binding system will give a total weight of 46.70 grams. The flex and the heel part are not optimized for weight, but by adding them it gives an indication of what the weight of the whole binding system could be.

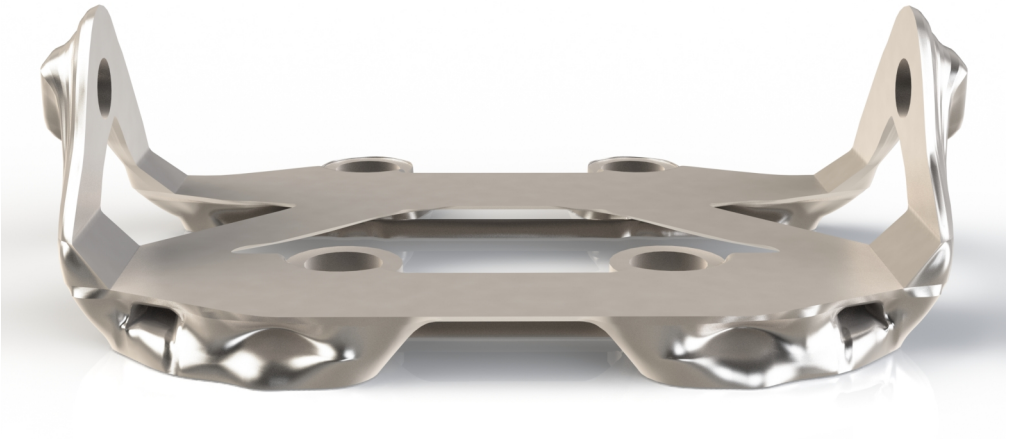

Figure 6-1: The final design.

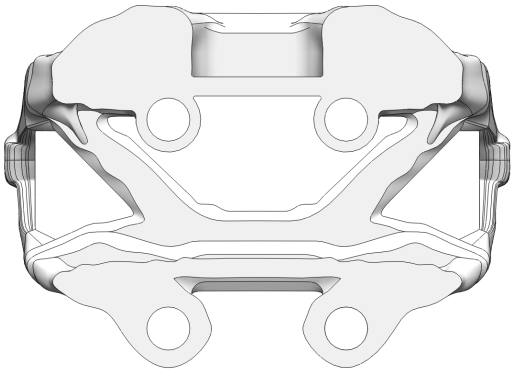

Figure 6-2: Bottom view.

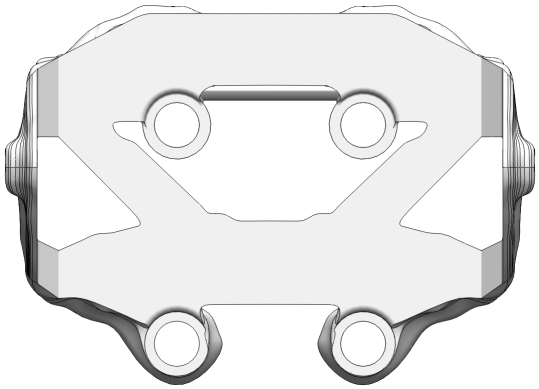

Figure 6-3: Top view.

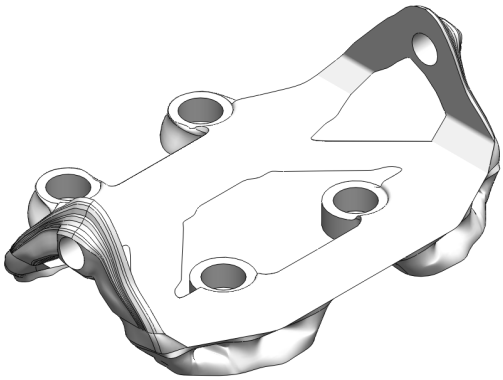

Figure 6-4: Side view.

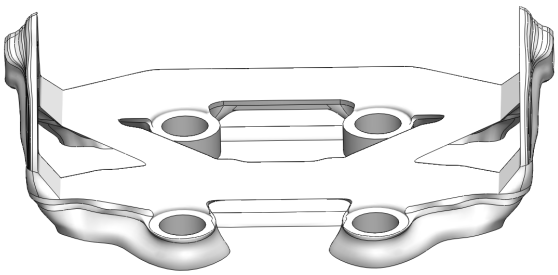

Figure 6-5: Back view.

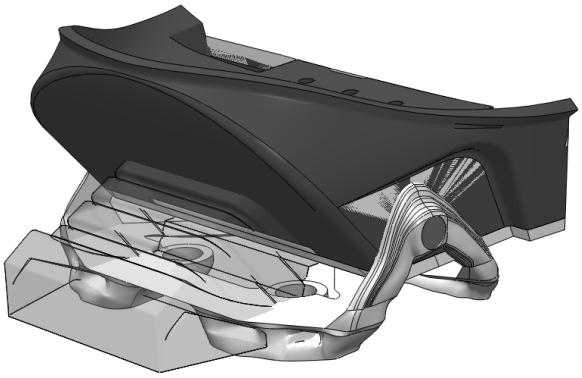

Figure 6-6: The binding with the front part of the shoe and a flex.

6.2 Design Variable and Topology Optimization

6.2.1 The Design Variables

The graph in Figure 6-7 shows the 29 iterations that were completed before a design was selected; strain energy on the left axis (blue) and volume on the right axis (yellow). The first 11 iterations were done to define the test parameters, as discussed in section 5.1.5, and are further described in section D.1.

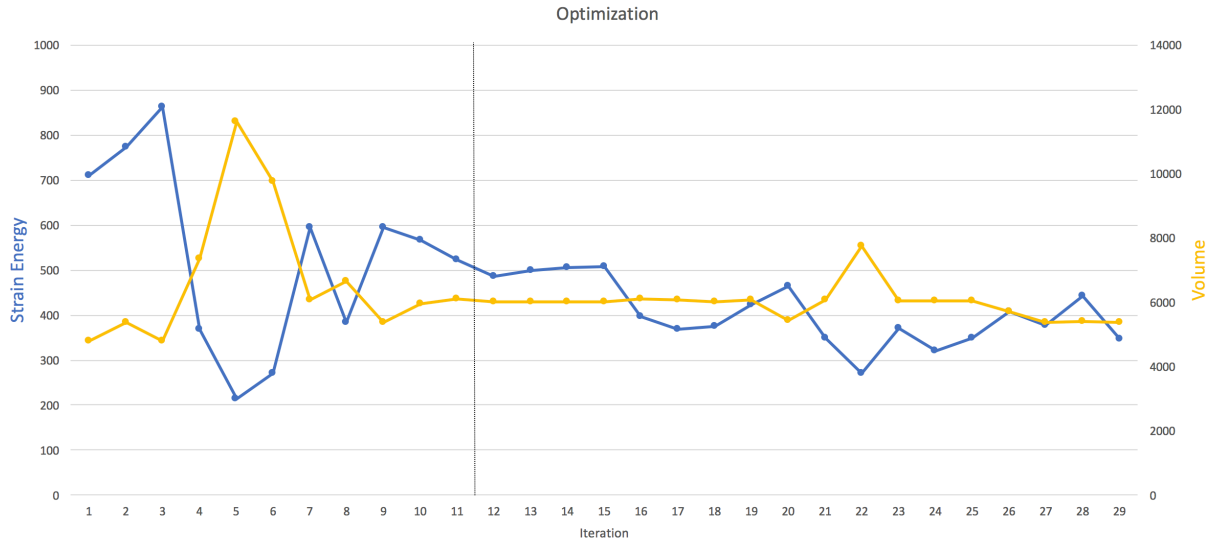

Figure 6-7: Design variable and topology optimization cycles.
The dotted line separates the initial tests from the more systematic tests.

In the remaining 18 iterations, different combinations of the design variables defined in section 5.1.5 were tested out. The results from these tests are presented in Appendix D.2 and a summary can be found in Table D-7. In the first two tests, iteration 12 - 19, different screw hole patterns (d) were tested at two different flex support heights (fh). The model with the lowest strain energy was then tested at various heights (h). Further, different values for the screw support height (sh) were tested in iteration 23-25, before the best design, iteration 24, was retested at various heights (h). The design in iteration 24 was still best after retesting, and all the design variables were locked. When *fh* was changed to 5 mm and *sh* to 4 mm the stiffness increased; a distinct drop in strain energy can be seen in iteration 16 and iteration 23 respectively. In iteration 27 - 29 the design was retested with a finer mesh, an increased number of cycles and a lower volume constraint. The best design was found in iteration 29; at 30 optimization cycles and a mesh seed equal to 1. In this way the testing converged, as seen in Figure 6-7, towards the stiffest and lightest model. The 'optimal' design variables are visualized in Figure 6-8.

Figure 6-10 and Figure 6-11 display the 'load path' for the two load cases, i.e. the von Mises stress from the simulation. These were useful to understand which part of the construction that was significant in the different load cases. E.g. the small member encircled in Figure 6-10 made the construction stiff between the rear screws when it was bent around the z-axis, and the member encircled in Figure 6-11 was important to counteract the torsion moment My.

The design, found in iteration 29, had almost the lowest volume and strain energy, making it a clear choice. Fatigue tests and FEA (section 6.3.1 and 6.3.2) indicated that it would be difficult to make this design lighter by requesting an even lower volume constraint. However, this is most likely a local optimum and a still lighter and stiffer binding could be found by testing more design variables. One of the major limitations with the experiment was that due to lack of time few designs could be tested. E.g. the distance between the screws was locked after iteration 19, but when the screw hole support structure was changed from 2 mm to 4 mm, it was not time to retest this distance. If it had been retested, it would have been necessary to test the height (h) and flex support structure (fh) as well. This emphasize how complex a problem like this is, even with all the restrictions.

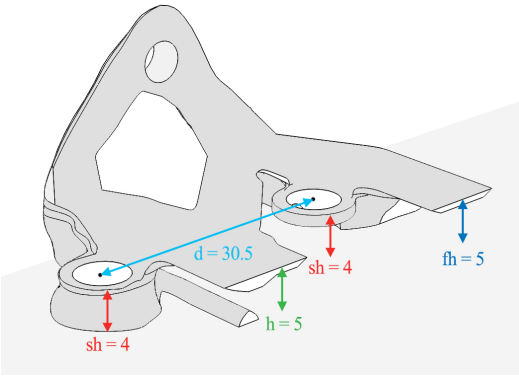

Figure 6-8: The regenerated CAD model with the optimal design variables.

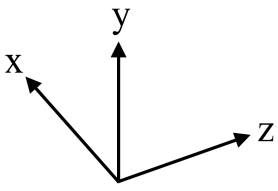

Figure 6-9: Coordinate system.

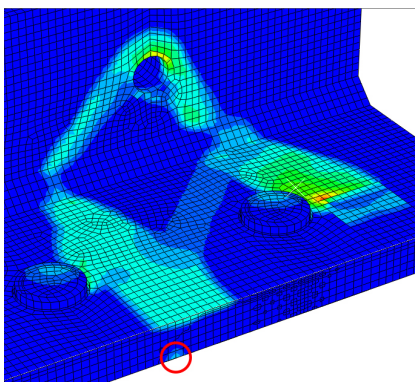

Figure 6-10: The model is cut in two, coordinate system in Figure 6-9. Load case: Mx.

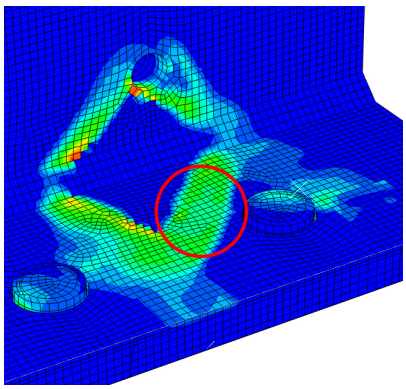

Figure 6-11: Load case: My.

6.2.2 Topology Optimization

The topology optimization was completed after 30 cycles resulting in a model at ~ 8 % of the initial volume. The optimization resulted in only red and blue elements (Figure 6-12) indicating that the algorithm was successful. As Figure 6-13 shows, the algorithm reduced the volume in each cycle while trying to keep the strain energy as low as possible.

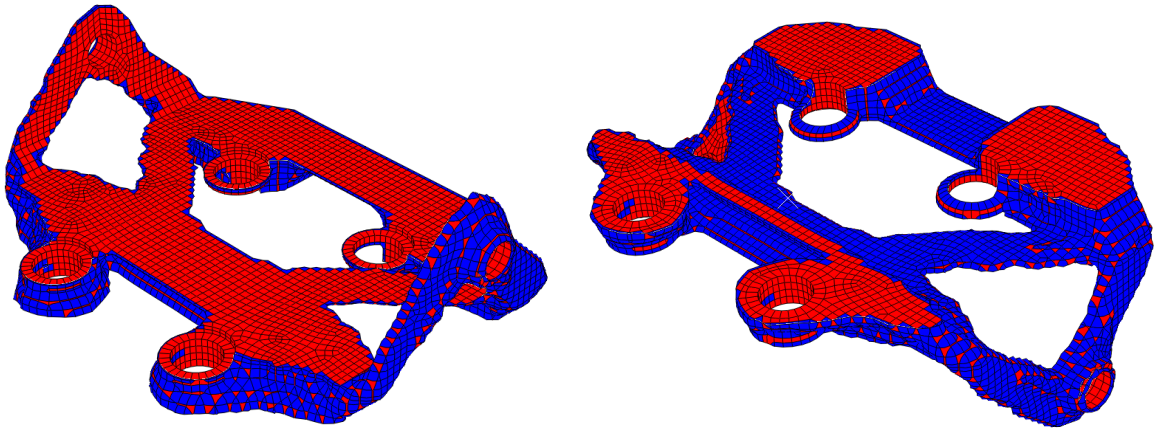

Figure 6-12: Optimized models at isosurface value = 0.3.

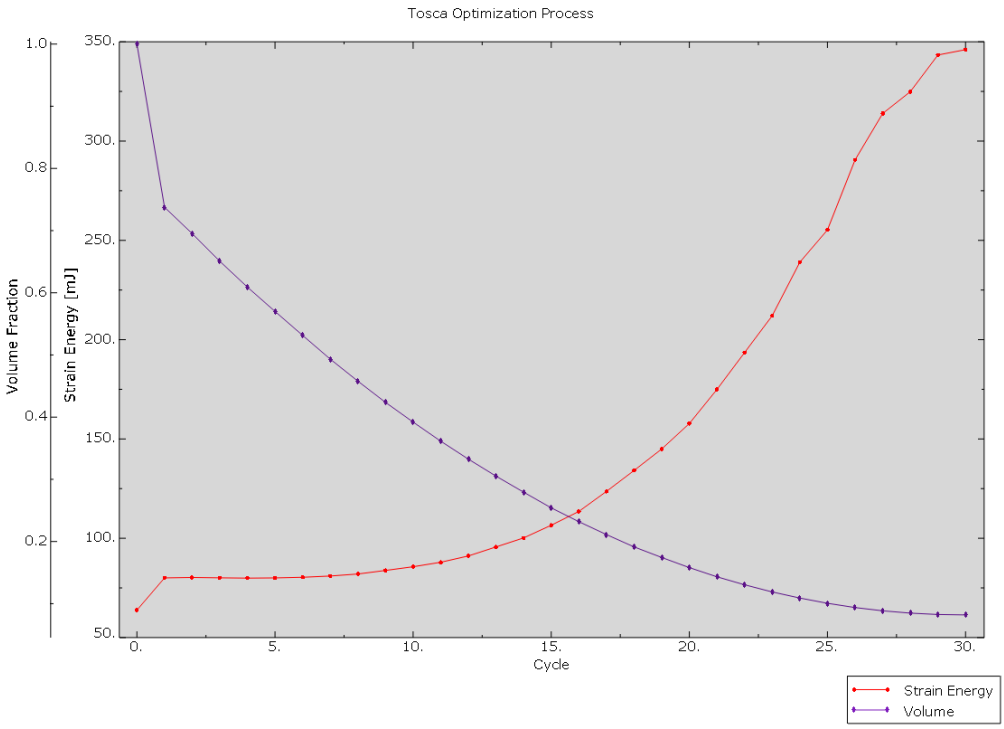

Figure 6-13: Volume fraction and strain energy vs. number of cycles.

6.2.3 The First Gate

The design was selected after different combinations of the adjustable variables had been tested out. It could have been easier with a more definite criterion, e.g. the lightest design which had less deformations than ‘x’ mm in any direction. However, this was a brand-new binding system and it was difficult to find appropriate bindings to use as benchmarks. Therefore, strain energy was used to compare the stiffness of the results.

6.3 Finite Element Analysis

6.3.1 Static Finite Element Analysis

The regenerated CAD model is displayed in Figure 6-14 and was modelled to fit the reference model as accurately as possible. The weight of the extracted isosurface (called Model A) was 24.27 grams (Titanium) while the regenerated model (Model B) weighed 25.46 grams. They were tested in Abaqus for the critical high- and low-likelihood load cases and the initial geometry had lower von Mises stresses than the regenerated model in all load scenarios. This shows how difficult it is to successfully replicate the organic shapes produced by the optimization, see Table 6-1. After iterating on the design, the highest stress peaks were removed (e.g. in Figure 6-15) and the model (Model C) satisfied the static FEA criterion. The FEA results of each load case for this model are included in Appendix D.3. The results from the FEA of the designs which are presented in section 6.3.2 (Model D) and 6.4.1 (Model E) are also included in the in Table 6-1.

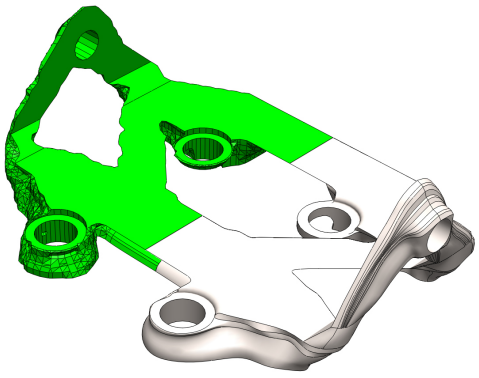

Figure 6-14: Green: the STL file extracted from the isosurface - grey: the regenerated model.

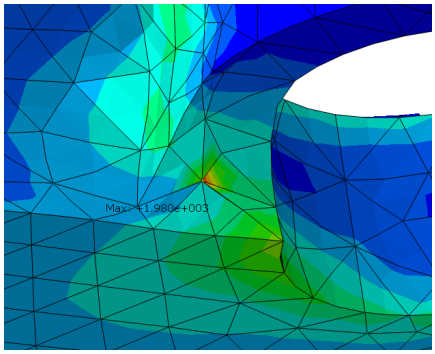

Figure 6-15: One of the stress peaks due to a sharp edge; σ_v = 1980 MPa.

3D-Model	Von Mises stress [MPa]			
	Mx	My	Fy	Fx
Model A; extracted isosurface	475	403	498	483
Model B, regenerated CAD	1980	538	3066	1491
Model C, stress-peaks removed	769	522	746	672
Model D, redesign for fatigue	710	525	767	725
Model E, redesign physical tests	712	526	768	650

Table 6-1: The static FEA results.

6.3.2 Fatigue Analysis

The model was tested for the fatigue load cases (Table 4-2) and it revealed that the flex support area (0.7 mm thick) and the front screw hole support structure (1.5 mm thick) were too thin when subjected to a cyclic load, see 1 and 2 in Figure 6-19 respectively. If the load case where striding was simulated was repeated continuously, the part would last for 103 560 cycles before it would fail in the place encircled in Figure 6-17. Six redesign cycles had to be completed before the part (Model D) had a satisfying fatigue life. The fatigue analyses are summarized in Table D-8; listing the two lowest fatigue lives in each test. Figure D-14 indicates by the strain rosettes, where the lowest values were measured.

Figure 6-20 shows how the flex support area and the screw hole support structure had to be reinforced; smoothing out radiuses and increasing thicknesses. These were minor changes and were done through redesign loop 1. The fatigue life was increased to 1 328 720 cycles in the striding load scenario, which proved to be the worst of the three load cases. The weakest place was now the screw hole support structure, encircled in Figure 6-18. The changes increased the weight of the model to 26.21 grams (Titanium). As discussed, it is difficult to know if the three load cases used in the fatigue analyses were realistic. It seems like the load case which simulates the striding motion might be too conservative; skiing in flat terrain produces low forces. Regardless of this, the fatigue analysis indicated where the model was weakest in cyclic loading.

Figure 6-16: Scale from 0 to 10 million repetitions.

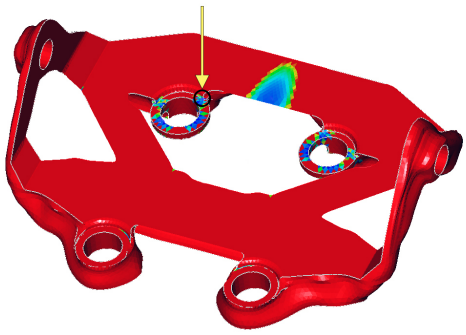

Figure 6-17: The initial fatigue analysis. Scale in Figure 6-16.

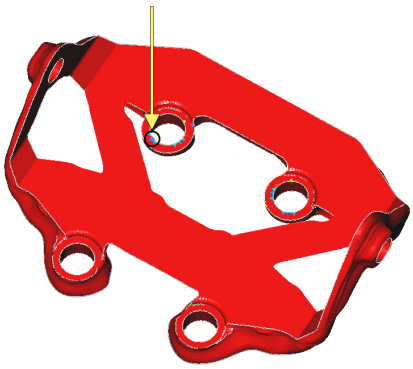

Figure 6-18: The final fatigue analysis. Scale in Figure 6-16.

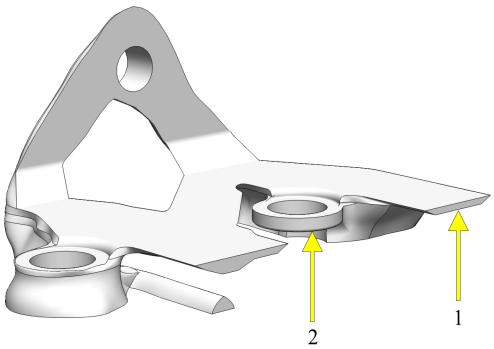

Figure 6-19: The initial regenerated CAD model.

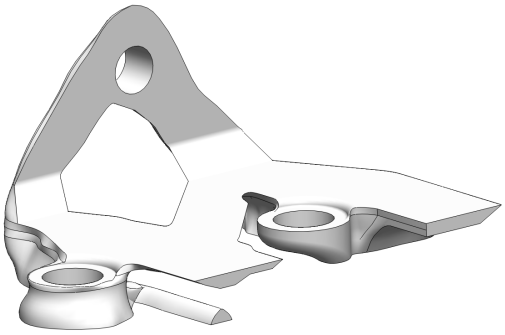

Figure 6-20: CAD model after 6 redesign cycles.

6.3.3 The Second Gate

Multiple redesign cycles were necessary before the model was accepted at this gate, the criteria are presented in Table 6-2. The reasons for this were difficulties when it came to accurately regenerate the CAD from the optimized result, and that Abaqus does not consider any dynamic load cases in the optimization. The fact that several redesigns were needed to satisfy the criteria shows how important this verification step was.

Criteria	
Von Mises stress	767.2 MPa < 800 MPa
Fatigue life	1 328 720 > 1 000 000 cycles

Table 6-2: Gate 2 criteria.

6.4 Physical Testing

6.4.1 Functional Testing

Several models were printed with Tough Resin, see Figure 6-21 and Figure 6-22. These (Model D) satisfied the functional criteria that had been set and revealed that the model was extremely stiff to bending between the rear screws, see Figure 6-23. This was because of the thin member, encircled in red; when the binding was subjected to an upwards force, the top surface of the binding got bent while this member was only exposed to an axial force, counteracting the deformation. However, the binding seemed to be flexible between the front screws. This was because of the constraint which was used in the simulation to apply the force to the flex area. By coupling the motion of this surface to a reference point, it may have caused this area to seem unnaturally stiff which led the algorithm to remove too much material here.

It was decided to conduct mechanical tests on two models. First, the model which had been redesigned for fatigue (Model D), then a new version of this which was designed to be stiffer between the front screws (Model E). The new version was inspired by the rear member in Figure 6-23 and the screw hole support structure was designed to go all the way down to the ski as well, see 1 and 2 in Figure 6-24 respectively. The weight was now 26.70 grams (Titanium). Figure 6-25 shows a prototype printed in PA 2200. The new design satisfied both the static FEA criterion (Table 6-1) and the fatigue life criterion (see Table D-9 and Figure D-15).

Figure 6-21: Tough Resin.

Figure 6-22: Tested on a backcountry ski.

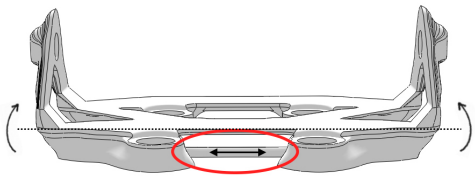

Figure 6-23: The thin member between the rear screws.

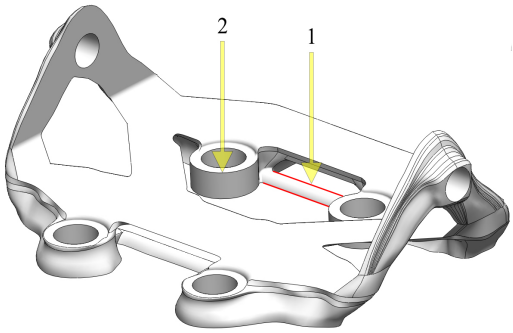

Figure 6-24: Redesigned for Fy.

Figure 6-25: Printed in PA 2200 with SLS-technology.

6.4.2 Mechanical Testing

Even though the bindings (Model D and E) were validated through FEA, the aim was to test printed versions of the bindings in titanium at NTNU. However, due to delays at IPM and NTNU Gjøvik the final print was not ready in time for the delivery of this thesis. Therefore, testing is scheduled in cooperation with Rottefella, later this year. In absence of the titanium print, Model D and Model E were printed in PA 2200[2] and tested. The results were compared to a simulation in Abaqus of the same models, where a load case like the one applied in the testing machine, was applied.

As Figure 6-26, Figure 6-27 and Figure 6-28 show, the bindings failed in the same way as the simulations indicated that they would; a crack formed in the side wall ripping outwards. Model D failed at 279 N while Model E failed at 333 N, see Figure D-17. The deformations were also compared and graphs from the Abaqus simulations and the tensile tests can be seen in Figure 6-29 and Figure 6-30. It looks like there was some slack in the setup resulting in an instant deformation of ~ 0.0175 mm in the first step, but after this, the slope of the test data corresponds accurately with Abaqus' predictions. At around ~ 20 N both graphs (the tensile tests) indicate a non-linear material behaviour, but since the simulations in Abaqus only considered linear behaviour, the increasing deviance was expected. PA 2200 is a much more flexible material than titanium and behaves differently under loading as described in Figure D-16; a more linear behaviour can be expected of titanium than of PA 2200. These tests show that in the linear elastic area, the structure is as stiff as Abaqus predicts it to be. This indicates that the structure is verified, since the maximum allowable stress in the titanium binding is ~ 200 MPa under the yield point (section 5.2.4).

[2] Material properties in Table D-10

The tests also indicated that the last redesign cycle made the model stiffer, see Figure 6-31 and Figure 6-32; Model D deforms more than Model E at a load of 200 N. Just before Model D failed, Model E was ~26 % stiffer, see the graph in Figure D-17. The conclusion was: the screw holes should go all the way down to the ski and the small member under the flex greatly increased the stiffness between the front screws. Model E was therefore the preferred design.

Figure 6-26: Test 1 fracture.

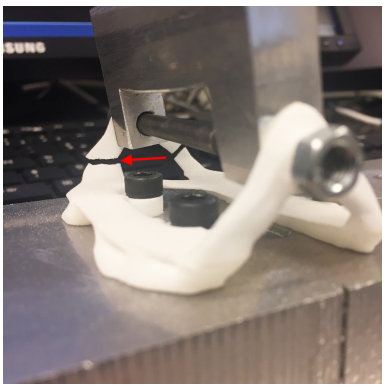

Figure 6-27: Test 2 fracture. Crack initiation where the red arrow points.

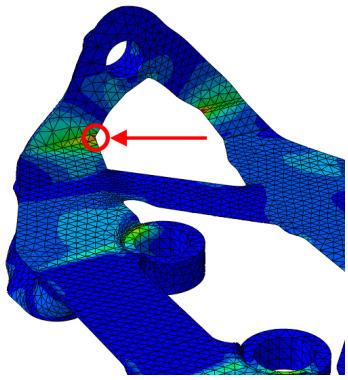

Figure 6-28: FEA, Fy = 2 000 N.

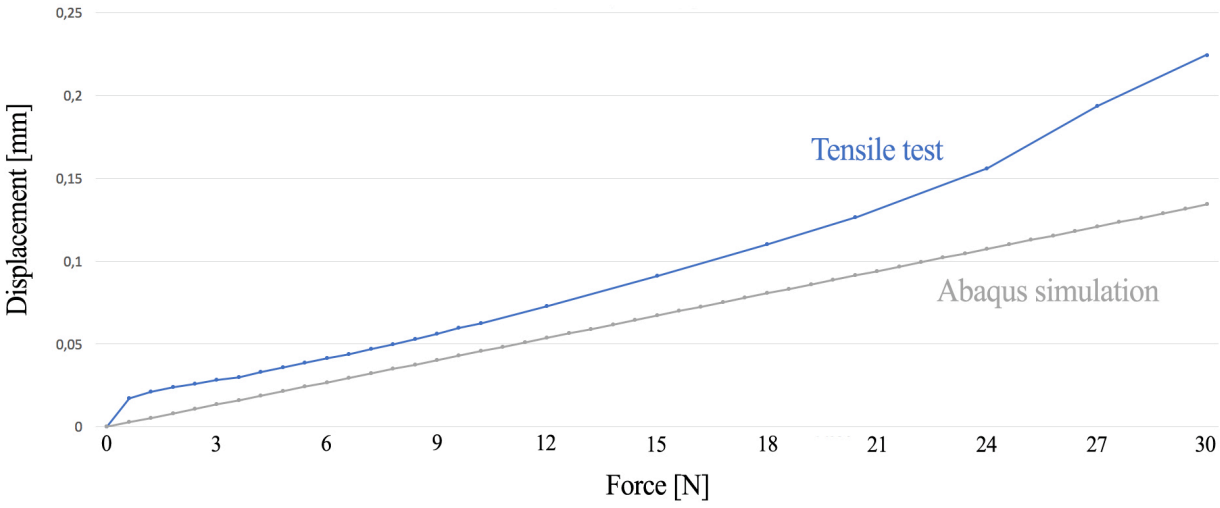

Figure 6-29: Test 1, Model D.

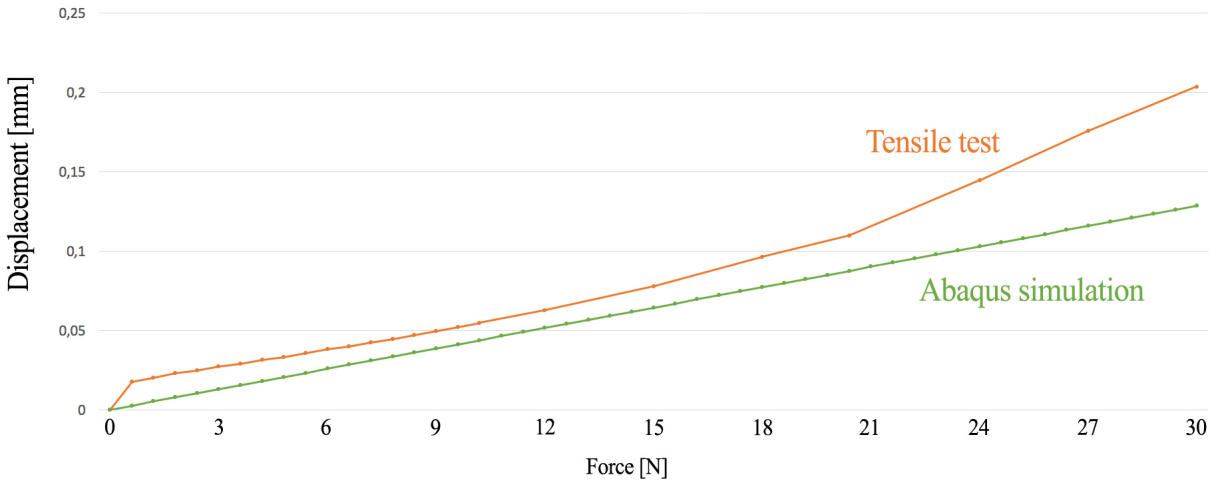

Figure 6-30: Test 2, Model E.

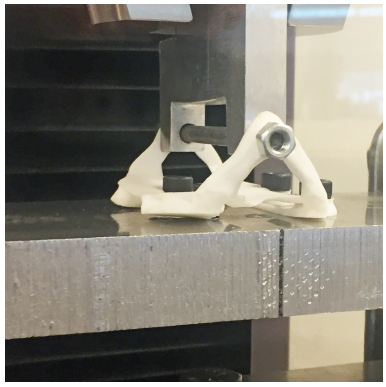

Figure 6-31: Test 1 at ~ 200 N.

Figure 6-32: Test 2 at ~ 200 N.

6.4.3 The Third Gate

The binding satisfied all the functional criteria, and physical tests indicated that it would hold for the mechanical test criteria as well, see Table 6-3.

Functional Criteria	**Mechanical Criteria**
Fits into the binding with little resistance to side walls	The tests indicate that the model in the Abaqus FEA accurately simulate reality.
Can easily extract and retract the shoe pins	
The flex can be mounted and used. However, the flex should be redesigned to work better with the new binding system.	$(\sigma_v \leq \sigma_{yield})$ at Fy = 2 000 N will be used to test the titanium bindings.

Table 6-3: Criteria gate 3.

7 Future Research Needs

Through the master thesis, several possibilities and limitations with topology optimization have been discovered. The lightweight, stiff ski binding that was produced indicates how extreme designs can be made by optimizing for the whole problem; both the design variables (input values) and the topology. However, there are several needs for further research. The main limitations with topology optimization and what has been defined as approach 3 are highlighted in the paper *State of the Art of Generative Design and Topology Optimization and Potential Research Needs (Tyflopoulos et al., 2018)*. The paper is included in Appendix F. The paper has been written by the author of this thesis, PhD Candidate Evangelos Tyflopoulos, Professor Martin Steinert and Associate Professor Anna Olsen, and has been accepted at the NORDDESIGN 2018 conference. It describes the present ways to conduct topology optimization and discusses key limitations. In this section, the framework used in this thesis is first evaluated, then the limitations with topology optimization and approach 3 are discussed with references to the paper, and finally some suggestions for further research are made.

7.1 Thesis Framework

The framework (section 3.3) used in this thesis was based on the principles in approach 3 (section 3.2.2) to search for both the optimal design variables and topology. One cycle of the flowchart (Figure 3-6) was completed; from understanding the problem to the presentation of a functional prototype. This flowchart is just one of many ways the work can be structured, thus can some of the decisions which have been made be adopted to any design variable and topology optimization case.

The first phase, Understanding the Problem, turned out to be one of the most challenging steps in the whole process. Skiing produces complex loads, and these are both hard to capture and to simulate correctly in a CAE software. The adjustable variables had to be defined at this step, and due to time and computational limitations they had to be more restricted than what was desired. These initial decisions, made by the designer/engineer, and the fact that the optimization task is extremely influenced by the selected loads, the design variables and how the simulation model is defined, makes the process of getting good, sensible results, a challenging task. This phase lays the foundation for the optimization and as discussed, the success of the outcome is extremely depended on how thorough this work is done. So, even

though it might seem like topology optimization results in organically shaped designs with little influence of an engineer, the whole optimization is in fact based on the assumptions of one.

The second phase, Design Variable and Topology Optimization, was the most time demanding. It is not visualized in the flowchart how much time that is needed to define a setup which accurately simulates reality; it does not help to measure the load scenarios precisely if they are simulated in the wrong way. E.g. compare the differences with and without constraints in Figure 5-3 and Figure 5-4. Something which also turned out to be a challenge was how complex the analyses got when trying to optimize all the design variables; there are numerous combinations of screw hole placements, design space dimensions, boundary conditions (glue, screws, etc.), etc.

The third and fourth phase, Finite Element Analysis and Manufacturing and Testing, turned out to work as a safety net in assuring that the optimized model would withstand its intended use. The reasons for all the redesign cycles (section 6.3.1, 6.3.2 and 6.4.1) were mainly because of difficulties when it comes to regenerating the optimized geometry, Abaqus' inability to include cyclic loading in the optimization and discrepancies between the simulation model and reality. 3D-printing was essential in discovering the latter; e.g. the unnatural stiffness of the constraint used to the flex was not discovered before the physical prototypes were inspected (section 6.4.1).

7.2 Limitations

7.2.1 Local Optimum

By changing the parameters which define the topology optimization setup, different results are produced. Some of these parameters can be better when it comes to solving a specific problem. So, to find the global optimal solution, the optimal input parameters must be found as well. The first and second optimization test in Appendix D.2 were used in the paper to emphasize this. Here the distance between the screw holes (d) and the height of the flex area support structure (fh) were changed (Figure 4-27). While the first test converged to a solution which looked optimal, the next test showed that by changing fh, a better solution could be found. "It is clear that these practices led to a local optimum and not to the best optimized solution of the ski binding. It is crucial to understand that the optimum solution to a defined setup might not be the ideal solution to the problem. In other words, the optimum material distribution is

influenced by the initial boundary conditions defined by the engineer. Therefore, it is not possible to find the real optimum of a structure, if its outer boundary conditions are not optimal and predefined. Then it is necessary to find first the optimum input (boundary conditions) for the topology optimization, and second the optimum material distribution." (Tyflopoulos et al., 2018, p. 11). This was also emphasized by the four last tests which were conducted in the thesis; when the adjustable variables defined in section 5.1.5 were changed, even better solutions were found.

7.2.2 Design Variable and Topology Optimization

The approach in the thesis, to find both the optimal input for the topology optimization and the optimal topology by testing and comparing every design in interest, turned out to be very computational expensive. This was because of the topology optimization step with running times of 10 - 12 hours per optimization. Even a relatively small design problem like this one, will become complex if every design variable should be evaluated. This would also include finding the optimal boundary conditions, i.e. how the binding should be fastened (glue, screws, etc.). "In this case (Ski binding optimization, see test 1 and 2 in section D.2), the identification of the real optimum has been carried out by comparing the different optimized design models in the conducted practices. However, this methodology has several limitations such as the requirement of a huge amount of time and computer capacity due to the analysis of big data (different sizes and placements of screws, variation of the support structure for the loads and boundary conditions, etc.)." (Tyflopoulos et al., 2018, p. 11).

As discussed in the previous section, several decisions must be made by the designer/engineer in the setup phase and it is likely that even more decisions and compromises must be made in other product development projects. E.g. Manufacturability, visual design, usability, etc., will influence the optimization. In many ways, it is these restrictions which define the test setup, e.g. in section 4.4.2 where the adjustable variables were defined. "This method also implies the need of all the setups to be defined by an engineer, making the final design more vulnerable to human error and his/her previous experience." (Tyflopoulos et al., 2018, p. 11).

7.2.3 Sensitivity to Changes in the Setup

Different design variables, mesh, numbers of optimization cycles and boundary conditions resulted in different topology optimized models. In other words, what you put into the

optimization will greatly affect what you get out; “Both SIMP and ESO are dependent on the design parameters (CAD), mesh and boundary conditions of the structures.” (Tyflopoulos et al., 2018, p. 12). Figure E-1 shows that by changing the number of optimization cycles and mesh seed, you end up with different designs even though the loads and design variables remain unchanged.

7.3 Summary Limitations

The following bullet points are used in the paper (Tyflopoulos et al., 2018, p. 12) to summarize the current limitations with topology optimization and the third approach.

- CAD is a limited design methodology due to its design parameters restrictions to known geometries.
- CAD encourages the re-usage of previously designed objects resulting in robust but nowhere near optimum designs.
- The main key limitation of the topology optimization is its sensitivity to the spatial placement of the involved components and the configuration of their supporting structure. For example, the local optimum of the ski binding will be completely different if we use three screws instead of four.
- Many topology optimization approaches are still dependent on starting guesses.
- All the existing topology optimization approaches and practices are time consuming and demand huge computational effort when they try to tackle big 3D construction models.

7.4 Future Research

Because the aim in approach 3 is to optimize the design variables and the topology, i.e. the whole problem, the future challenges are computational power and how to reduce influence of the engineer. The goal with a new approach should therefore be the same as in approach 3; optimizing design variables and topology. However, the new approach could differ from approach 3 by first finding the optimal design variables (the optimal input) before optimizing the topology. Since the topology optimizing step is time demanding, this will save time because you do not need to optimize every design. “The success of a topology optimization approach could be achieved through the identification of the evolutionary probing of the design boundaries. Hence, the topology optimization problem could be divided in two sub-problems

(levels); the optimization of the outer boundary conditions, and the optimization for the inner optimum." (Tyflopoulos et al., 2018, p. 11). A flowchart of the process is displayed in Figure 7-1. In the first iteration, the optimal input for the topology optimization is found; boundary conditions and dimensions of the design space. The next step is to optimize the topology. This approach is only, to the writer's knowledge, on a concept stage and is left as a future study. The process is also described through Figure 7-2; "The CAD-geometry of the structure could be replaced by a black box with the allowable design envelope (level 1). A topology optimization algorithm, based on NAND formulation, could be used for calculating the optimum adaptive (moving) boundaries of the structure with respect to outer design parameters (i.e. length, width, height, holes, etc.), constrains, loads and contact sets. The optimum boundary conditions could be used in their turn, as a starting point for a traditional topology optimization of the structure's interior (level 2)." (Tyflopoulos et al., 2018, p. 11). The idea with the black box is to reduce the influence of the designer/engineer. Only the contact surfaces, regions where loads are applied and maximum dimensions are defined, in other words; the design space is increased.

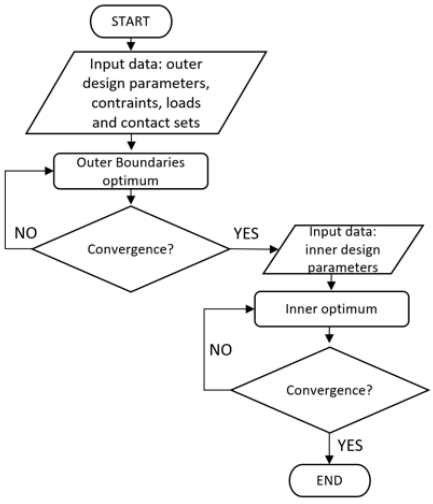

Figure 7-1: Flowchart of suggested approach (Tyflopoulos et al., 2018).

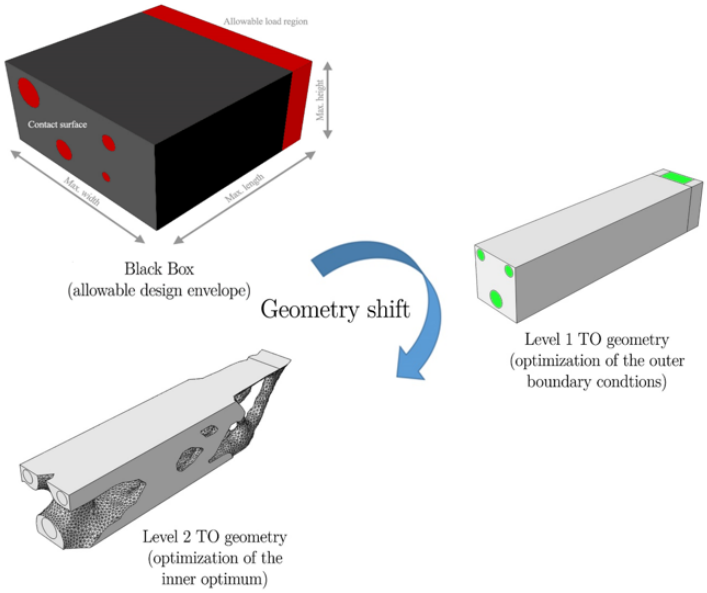

Figure 7-2: The suggested approach.

8 Conclusion

8.1 Summary and Conclusion

The study of different SBD workflows and topology optimization use cases, resulted in the categorization of three different approaches; approach 1 *Predefined Design Space*, approach 2 *Maximum Possible Design Space* and approach 3 *Integrated Shape- and Topology Optimization Practice*. The principles from the last approach were used to define a framework for the thesis, which structured the development and made it easier to verify if design variable and topology optimization could be used to make the market's lightest ski binding. Studying the mountain ski binding market gave a deeper understanding of the design restrictions and which parameters that could be optimized, and further research of the load scenarios and the design variables ensured a simulation model that more accurately replicated reality than the model in the preliminary project work did. This was in turn used as input values for the design variable optimization, the topology optimization, the static analysis and the fatigue analysis. The result was then redesigned to satisfy the von Mises criteria and the fatigue criteria, before it was manufactured, functional tested and tensile tested.

The binding bracket which was developed was lighter than the current market leader. In other words, topology optimization can clearly be used to develop an extremely light ski binding. To reach the full potential of topology optimization approach 3 should be used; one example of how this could be done is through the framework presented in section 3.3. By introducing deformable screws, pre-tension, chamfer on the side-walls and the flex force, the setup more accurately replicated reality. Finding the input values for the optimization was one of the most critical and difficult challenges. This was because of all the initial guesses that had to be made in this case, since it would be impossible to test out every combination of the design variables. Although the search for the optimal design variables was limited by time and computational capacity, it was evident that including the optimization of design variables in the topology optimization cycle, made the design much better. The binding was validated by FEA and physical testing, which indicated that the ski binding would withstand its intended use.

Topology optimization is popular right now, and the author thinks optimizing the design variables has a great future. Combining design variable and topology optimization in this case shows some of its potential; it can be used to reduce material usage and decrease weight in

many product development projects, with little compromise on strength and stiffness. By including the input values for the topology optimization in the optimization cycle, one step is taken towards optimizing the whole problem and not just a defined setup. However, several limitations were also revealed; the need for huge computational capacity, how sensitive the optimization result is to what is used as input and how many decisions an engineer actually must make in the early stages of this process.

8.2 Further Works

The binding is sent to NTNU in Gjøvik and will be printed in titanium. The next steps will be to test it in a real use case for a longer period and redesign the flex to work with the new system.

When it comes to using topology optimization in product development, the limitations mentioned in section 7.3 should be addressed and ways to reduce the need for computational power and the influence of the engineer should be explored. E.g. by studying ways to separate the design variable optimization from the topology optimization, as described in section 7.4.

Bibliography

Additively (Producer). (n.d., May 15, 2018). Electron Beam Melting (EBM). [Online image] Retrieved from https://www.additively.com/en/learn-about/electron-beam-melting - read-more

Alfa (Producer). (n.d., May 6, 2018). BC 75 Advance GTX M. [Online image] Retrieved from https://alfa.no/shop/skisko/backcountry/bc-75-advance-m

Andersson, E., Pellegrini, B., Sandbakk, Ø., Stöggl, T., & Holmberg, H.-C. (2014). The effects of skiing velocity on mechanical aspects of diagonal cross-country skiing. *Sports Biomechanics*, 1-18. doi:10.1080/14763141.2014.921236

Bendsøe, M. P., & Sigmund, O. (2004). *Topology Optimization Theory, Methods, and Applications* (2 ed.). Berlin: Springer.

Chang, J., & Lee, Y. (2008). Topology optimization of compressor bracket. *Journal of Mechanical Science and Technology, 22*(9), 1668-1676. doi:10.1007/s12206-008-0428-3

Dizon, J. R. C., Espera, A. H., Chen, Q., & Advincula, R. C. (2018). Mechanical characterization of 3D-printed polymers. *Additive Manufacturing, 20*, 44-67. doi:https://doi.org/10.1016/j.addma.2017.12.002

Dostie (Producer). (2013, May 9, 2018). Technique: Modifying TTS Heel Post. [Online image] Retrieved from http://www.earnyourturns.com/15568/technique-modifying-tts-heel-post/

Dynafit (Producer). (2017, April 4, 2018). DYNAFIT Race binding P49 [Online image] Retrieved from http://www.mountainblog.eu/product/dynafit-race-binding-p49-winter-2018-19-2/

Dynafit (Producer). (n.d.-a, December 12, 2017). DNA Binding. [Online image] Retrieved from https://www.dynafit.com/equipment/bindings/dna-binding

Dynafit. (n.d.-b). Dynafit RC1 Race. Retrieved from https://www.cripplecreekbc.com/products/dynafit-rc1-race-skimo-race-binding-by-pierre-gignoux

Dynafit. (n.d.-c). Low Tech Race 2.0 Manual Binding. Retrieved from https://www.dynafit.com/equipment/bindings/low-tech-race-2.0-manual-binding?number=08-0000048778_0000000001

Dynafit. (n.d.-d). ST Rotation 10 - 90MM binding. Retrieved from https://www.dynafit.com/equipment/bindings/st-rotation-10-90mm-binding?number=08-0000049100_0000000002

Emmelmann, C., Kirchhoff, M., & Beckmann, F. (2011). Systematic development of lightweight components for highly dynamic laser-remote-scanners using topology optimization. *Physics Procedia, 12*, 459-464. doi:10.1016/j.phpro.2011.03.157

Fadida, R., Rittel, D., & Shirizly, A. (2015). Dynamic Mechanical Behavior of Additively Manufactured Ti6Al4V With Controlled Voids. *Journal of Applied Mechanics, 82*(4), 041004-041004-041009. doi:10.1115/1.4029745

Fiebig, S., Sellschopp, J., Manz, H., Vietor, T., Axmann, K., & Schumacher, A. (2015). *Future challenges for topology optimization for the usage in automotive lightweight design technologies.* Paper presented at the Proc. of

11th World Congress on Structural and Multidisciplinary Optimization, Sydney, Australia.
Fiedler, K., Rolfe, B. F., & De Souza, T. (2017). Integrated Shape and Topology Optimization - Applications in Automotive Design and Manufacturing. *SAE International Journal of Materials and Manufacturing, 10*(3). doi:10.4271/2017-01-1344
Fischer. (n.d.). Fischer Tour Race Alpine Touring Binding. Retrieved from https://www.backcountry.com/fischer-tour-race-alpine-touring-binding
FormLabs (Producer). (n.d., May 10, 2018). The Ultimate Guide to Sterolithography (SLA) 3D Printing. [Online image] Retrieved from https://formlabs.com/blog/ultimate-guide-to-stereolithography-sla-3d-printing/
GmbH, C. L. (n.d.). CL 20ES Stainless steel. Retrieved from https://www.concept-laser.de/fileadmin/user_upload/Datasheet_CL_20ES.pdf
HaganSkiMountaineering. (n.d.). Ultra Binding. Retrieved from https://www.haganskimountaineering.com/collections/staff-picks/products/ultra-binding

Härkegård, G. (2014). *Dimensjonering av maskindeler* (3 ed.). Bergen, Norway: Fagbokforlaget.
Karma. (2008). Detailed report on Laser Cusing, SLA, SLS and Electrion Beam Melting. Retrieved from http://www.femeval.com/proyectos/karma/Documents/DL 1.1_Report on technologies_5_11.pdf
Ma, Z. D., Wang, H., Kikuchi, N., Pierre, C., & Raju, B. (2006). Experimental validation and prototyping of optimum designs obtained from topology optimization. *Computer-Aided Optimal Design of Stressed Solids and Multidisciplinary Systems, 31*(5), 333-343. doi:10.1007/s00158-005-0530-4
Materialise. (n.d.). Aluminum (AlSi10Mg). Retrieved from http://www.materialise.com/en/manufacturing/materials/aluminum
McKee, H. J., & Porter, J. G. (2017). Lessons Learned in Part Design from Topology Optimization through Qualification. *Science in the Age of Experience*.
Nehuen, A. (Producer). (2015, May 5, 2018). 3D Printing Technologies: SLS vs. SLA. [Online image] Retrieved from https://www.sculpteo.com/blog/2015/12/09/3d-printing-technologies-sls-sla/
OsloSportslager. (n.d.). 3-Pin Cable Telemark Binding 75 mm Retrieved from https://www.oslosportslager.no/produkt/voile-3-pin-cable-telemark-binding-75-mm-fjellskibinding-mvidje-20627.aspx
Oxford. (n.d.). Oxford Living Dictionary. Retrieved from https://en.oxforddictionaries.com/definition/optimal
Ravindran, A., Ragsdell, K. M., & Reklaitis, G. V. (2006). *Engineering Optimization: Methods and Applications* (2 Ed.): John Wiley & Sons.
Rottefella. (n.d.-a). Rottefella BC AUTO. Retrieved from https://www.rottefella.no/rottefella-bc-auto-singelpack
Rottefella (Producer). (n.d.-b, December 12, 2017). Rottefella BC Magnum Bindings Black. [Online image] Retrieved from https://cdn.skatepro.com/product/440/rottefella-bc-magnum-black-bindings-p7.jpg
Rottefella (Producer). (n.d.-c, May 9, 2018). Rottefella Flex fleks til BC-bindinger. [Online image] Retrieved from https://braasport.no/produkter/flex-40sh-fleks-til-bc-bindinger/10385/

Rottefella (Producer). (n.d.-d, May 15, 2018). Rottefella NNN BC Manual. [Online image] Retrieved from https://www.udenssport.se/product.html/rottefella-nnn-bc-manual

Rottefella. (n.d.-e). Rottefella NTN Freedom Binding. Retrieved from http://blistergearreview.com/gear-reviews/rottefella-ntn-freedom-binding

Rottefella (Producer). (n.d.-f, June 6, 2018). Super Telemark. [Online image] Retrieved from https://www.rottefella.no/bindinger/fjellski/back-country/super-telemark

Rottefella. (n.d.-g). Super Telemark 75mm Fjellskibinding. Retrieved from https://www.oslosportslager.no/produkt/rottefella-super-telemark-75-mm-fjellskibinding-5341.aspx

Senner, V., Michel, F., Lehner, S., & Brügger, O. (2013). Technical possibilities for optimising the ski-binding-boot functional unit to reduce knee injuries in recreational alpine skiing. *Sports Engineering, 16*(4), 211-228. doi:10.1007/s12283-013-0138-7

Simulia. (2011). Topology and Shape Optimiation with Abaqus. Retrieved from http://www.simulia.com/download/rum11/GL/Sandeep-Urankar-ATOM-SGL-RUM-2011.pdf

Simulia. (2013). Abaqus Analysis User's Guide: Abaqus 6.13. Retrieved from http://abaqus.software.polimi.it/v6.13/books/usb/default.htm?startat=pt04ch13s01abo16.html - usb-anl-aoptover-topo

Simulia. (n.d.-a). Non-Parametric Optimization with Abaqus. Retrieved from https://academy.3ds.com/en/learn/non-parametric-optimization-abaqus-0

Simulia (Producer). (n.d.-b, April 6, 2018). Topology and Shape Optimiation with Abaqus. [Online image] Retrieved from http://www.simulia.com/download/rum11/GL/Sandeep-Urankar-ATOM-SGL-RUM-2011.pdf

SolidFill (Producer). (n.d., May 10, 2018). Fused Deposition Modeling. [Online image] Retrieved from http://solidfill.com/en/Fused_Deposition_Modeling/

Sport, C. (Producer). (2018, May 9, 2018). Gear Review: the Dynafit TLT Speedfit Touring Boot. [Online image] Retrieved from https://www.sport-conrad.com/blog/en/testing-the-dynafit-tlt-speedfit-touring-boot/

Standardization, I. O. f. (1990). Cross-country skis - Binding mounting area - Requirements and test methods (ISO9119). In.

Standardization, I. O. f. (2011). Cross-country skis — Ski-binding screws — Requirements (ISO7794). In.

Standardization, I. O. f. (2014). Alpine touring ski-bindings — Requirements and test methods (ISO13992). In.

Standardization, I. O. f. (2015). Alpine ski-bindings — Selection of release torque values (ISO 8061). In.

Stirling, R. (2014). Material data sheet, EOS Titanium Ti64. Retrieved from http://www.rpplusm.com/assets/eos_titanium_ti64_en-(1).pdf

TeachEngineering. (n.d.). Coefficient of Friction. Retrieved from https://www.teachengineering.org/content/nyu_/activities/nyu_heavy/nyu_heavy_activity1_coftable.pdf

Tuan Rahim, T. N. A., Abdullah, A. M., Md Akil, H., Mohamad, D., & Rajion, Z. A. (2015). Preparation and characterization of a newly developed polyamide composite utilising an affordable 3D printer. *Journal of Reinforced Plastics and Composites, 34*(19), 1628-1638. doi:10.1177/0731684415594692

Tyflopoulos, E., Flem, D., Steinert, M., & Olsen, A. (2018). State of the Art of Generative Design and Topology Optimization and Potential Research Needs.
Wang, K., & Ma, D. (2014). Multi-Objective Structure Optimization Design on the Upper Carriage of a Naval Gun. *Applied Mechanics and Materials, 541-542*, 669-673. doi:10.4028/www.scientific.net/AMM.541-542.669

A Development Framework

A.1 Literature Study

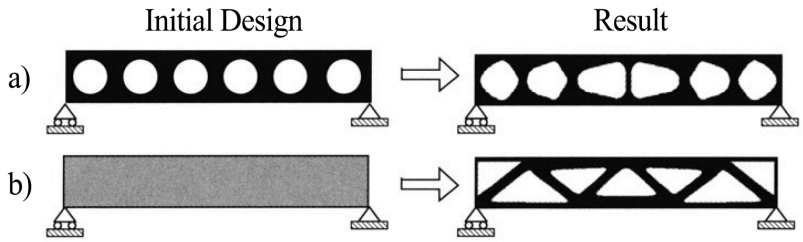

Figure A-1: a) Shape optimization - b) Topology optimization (Bendsøe & Sigmund, 2004).

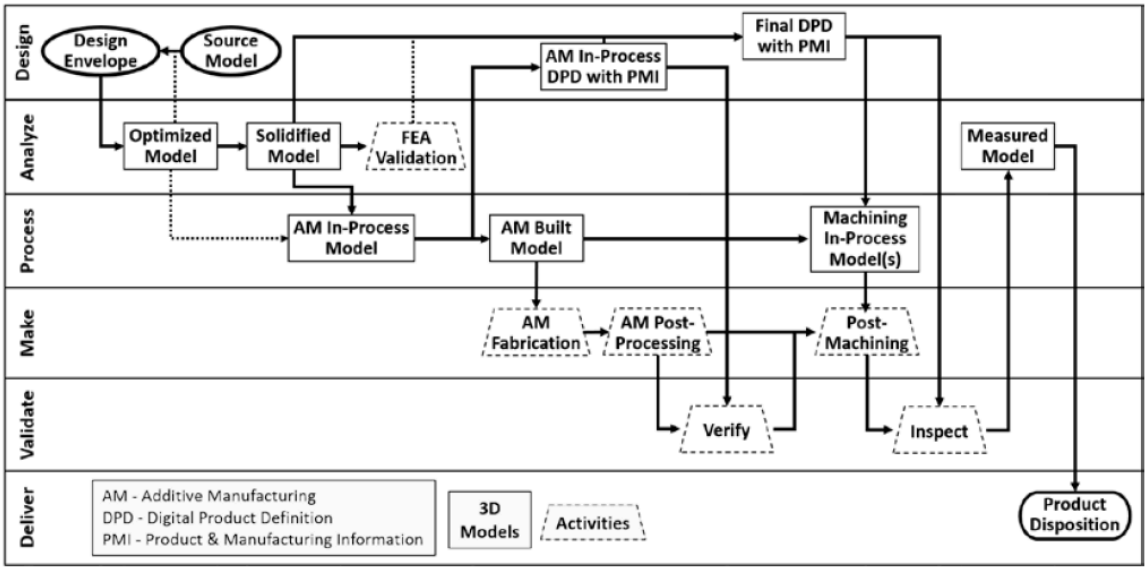

Figure A-2: Topology optimization workflow by Haley J. McKee and John G. Porter (McKee & Porter, 2017).

A.2 Approach 1: Predefined Design Space

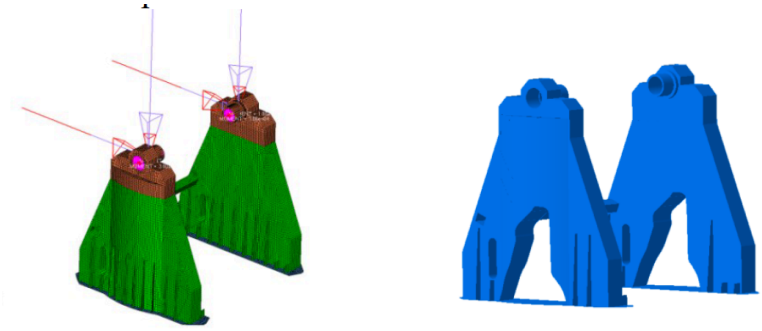

Figure A-3: The optimization of naval gun; the design space is on the left side and the optimized design is on the right (Wang & Ma, 2014).

A.3 Approach 2: Maximum Possible Design Space

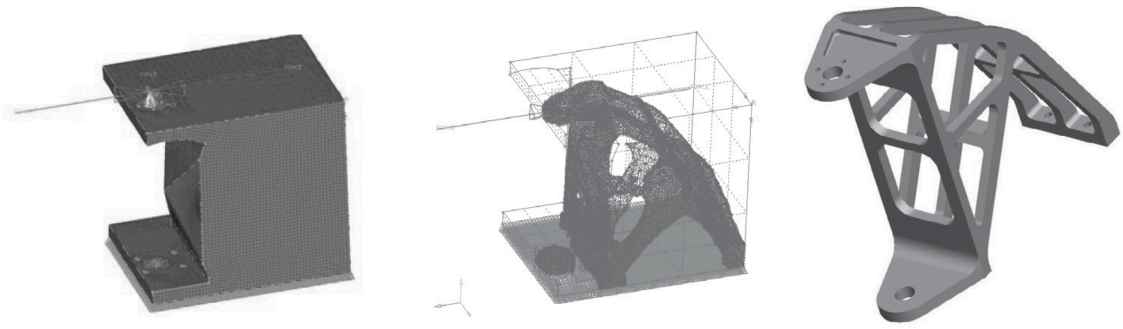

Figure A-4: Optimization of a laser-remote-scanner. The design space on the left side, in the middle is the isosurface showing the optimized result and to the right is the regenerated CAD (Emmelmann et al., 2011).

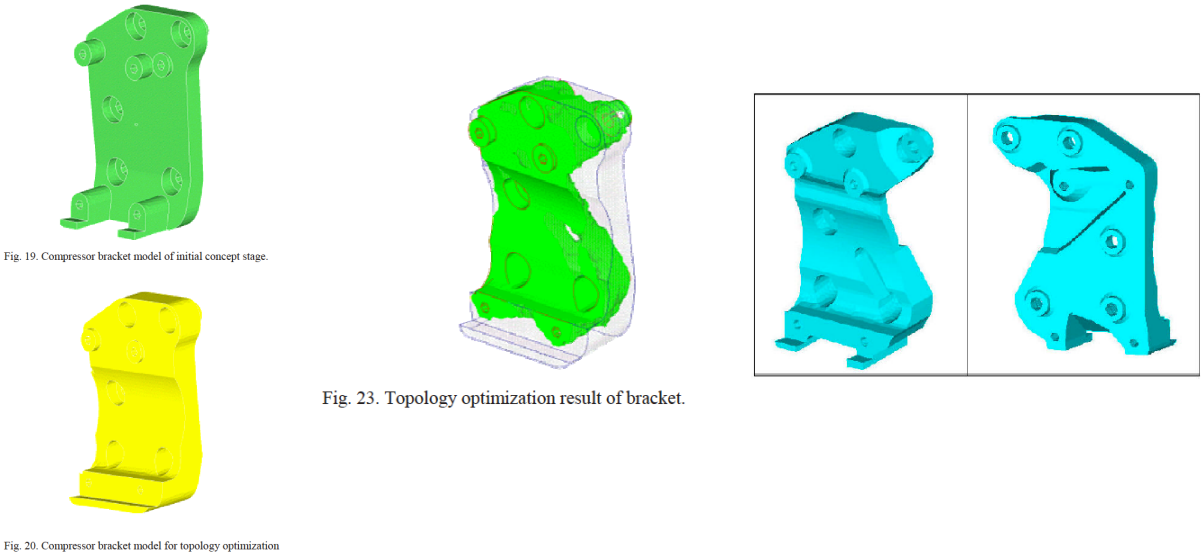

Figure A-5: Optimization of a compressor bracket. The upper left model shows the initial design, the lower left model shows the design space, the middle model shows the result from the topology optimization and the right model shows the regenerated CAD (Chang & Lee, 2008).

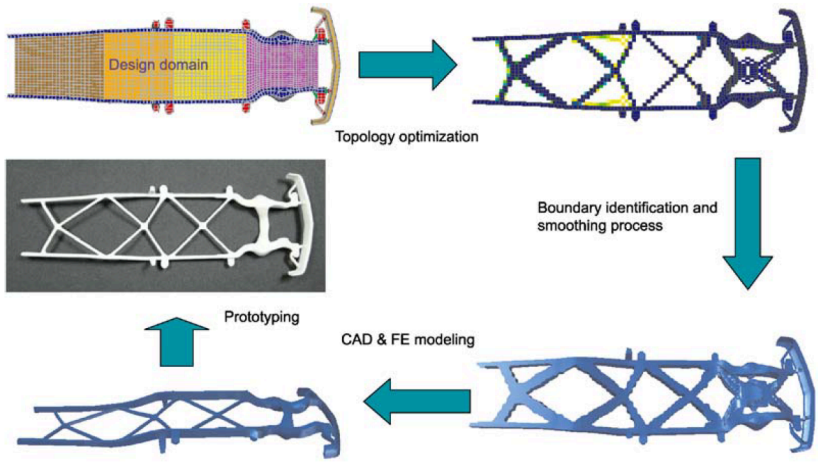

Figure A-6: Optimization of a trailer chassis (Ma et al., 2006).

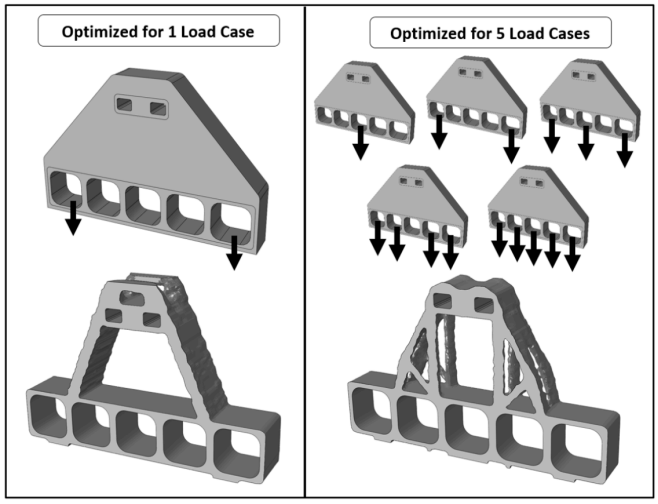

Figure A-7: Optimization of a hanger (McKee & Porter, 2017).

A.4 Approach 3: Integrated Shape- and Topology Optimization Practice

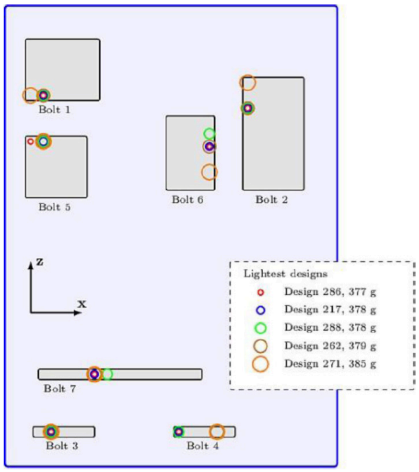

Figure 8. Schematic of the design space and optimal bolt positions. The outer blue rectangle corresponds to the topology design space of the bracket. The grey areas represent the geometrical parameter domains for each bolt. The bolt locations for the five lightest designs are displayed, showing distinct optimum positions for the 11 design parameters.

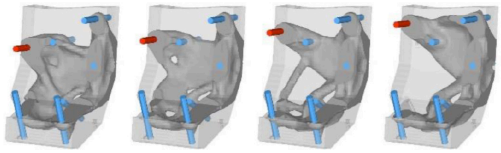

Figure 5. Topology optimization results of the bracket for different bolt locations. Here bolt 2 (shown in red) varies in z-direction between -10 mm and +20 mm. The resulting masses, from left to right, are 548g, 437g, 353g, 370g. The lightest design is found for dz = 10 mm.

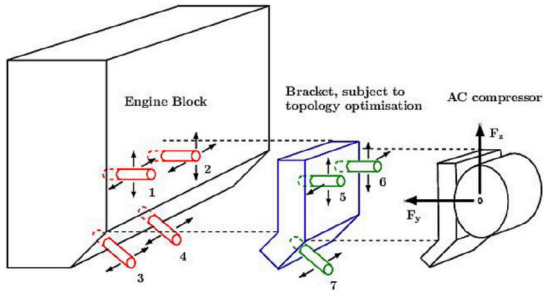

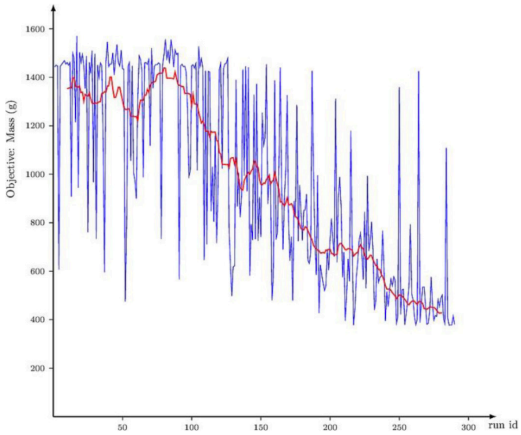

Figure A-8: Optimization of an engine block bracket. The figure on the upper left shows the design space for the placement of the bolts, the model on the lower left show the optimized models with different bolt placements, the figure on the upper right shows the design space (the blue box) and the model on the lower right show how the mass was reduced over 290 iterations (Fiedler et al., 2017).

B Understanding the Problem

B.1 Bindings for Mountain Skiing

Figure B-1: A flex, as the ones used in the NNN backcountry ski bindings (Rottefella, n.d.-c).

Figure B-2: Rottefella BC Magnum with a flex (Rottefella, n.d.-b).

Figure B-3: The flex is the front part of the shoe sole (Alfa, n.d.).

Figure B-4: Rottefella 75 mm binding (Rottefella, n.d.-f).

Manufacturer	Segment	Bindings	Weight
Dynafit	Alpine Touring	DNA. Lightest binding ISMF certified for ski touring race. (Dynafit, n.d.-a)	62 g
Dynafit	Alpine Touring	RC-1 (Dynafit, n.d.-b)	75 g
Dynafit	Alpine Touring	Low Tech race 2.0 manual (Dynafit, n.d.-c)	110 g
Hagan	Alpine Touring	Ultra Binding (HaganSkiMountaineering, n.d.)	110 g
Fischer	Alpine Touring	Tour Race (Fischer, n.d.)	108 g
Dynafit	Alpine Touring	TLT Superlight 2.0 (Rottefella, n.d.-g)	175 g
Rottefella	Backcountry	75 mm (Rottefella, n.d.-g)	185 g
Rottefella	Backcountry	BC Auto (Rottefella, n.d.-a)	222 g
Voile	Backcountry	75 mm - without cable (OsloSportslager, n.d.)	235 g
Dynafit	Alpine Touring	ST Rotation 10 (Dynafit, n.d.-d)	599 g
Rottefella	Telemark	NTN Freedom (Rottefella, n.d.-e)	750 g

Table B-1: The weight of some alpine-touring, telemark and backcountry ski bindings.

B.2 Manufacturing

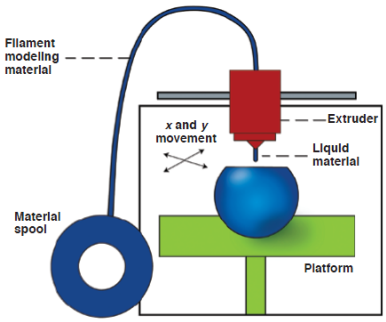

Figure B-5: The FDM 3D-printing process. Material is fed through the extruder which builds in the x-y direction, when one layer is complete the platform moves in the z-direction before a new layer is built (SolidFill, n.d.).

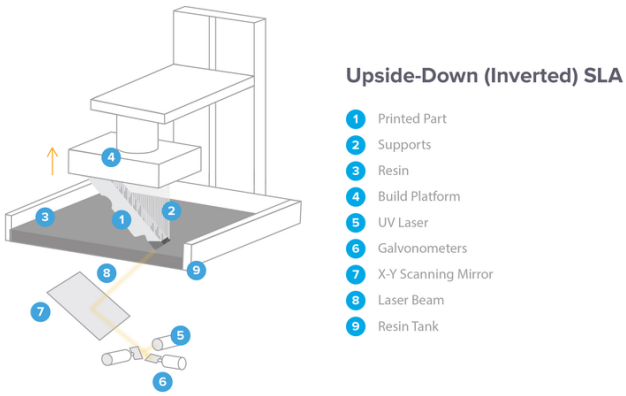

Figure B-6: There are two types of SLA; right-side and inverted. At IPK they use 'Form 2' which use the upside-down method. The UV-laser is directed through a set of mirrors and cures a layer of the resin at the bottom. Then the part is elevated and a fresh layer of resin is added, before the part is lowered into the resin one layer higher than the previous time. This process is repeated until the print is finished (FormLabs, n.d.).

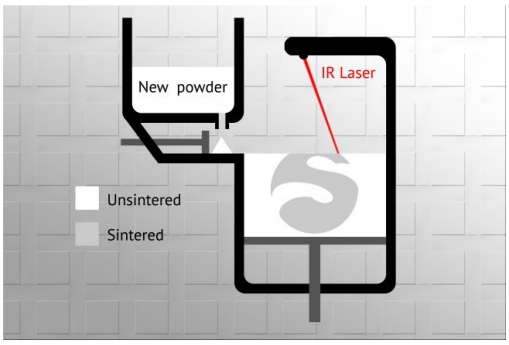

Figure B-7: The material powder is sintered layer by layer. The temperature in the printing chamber is just below the materials sintering temperature, so, when the laser heats the desired section the powder is sintered. Then a new layer is added and the process is repeated (Nehuen, 2015).

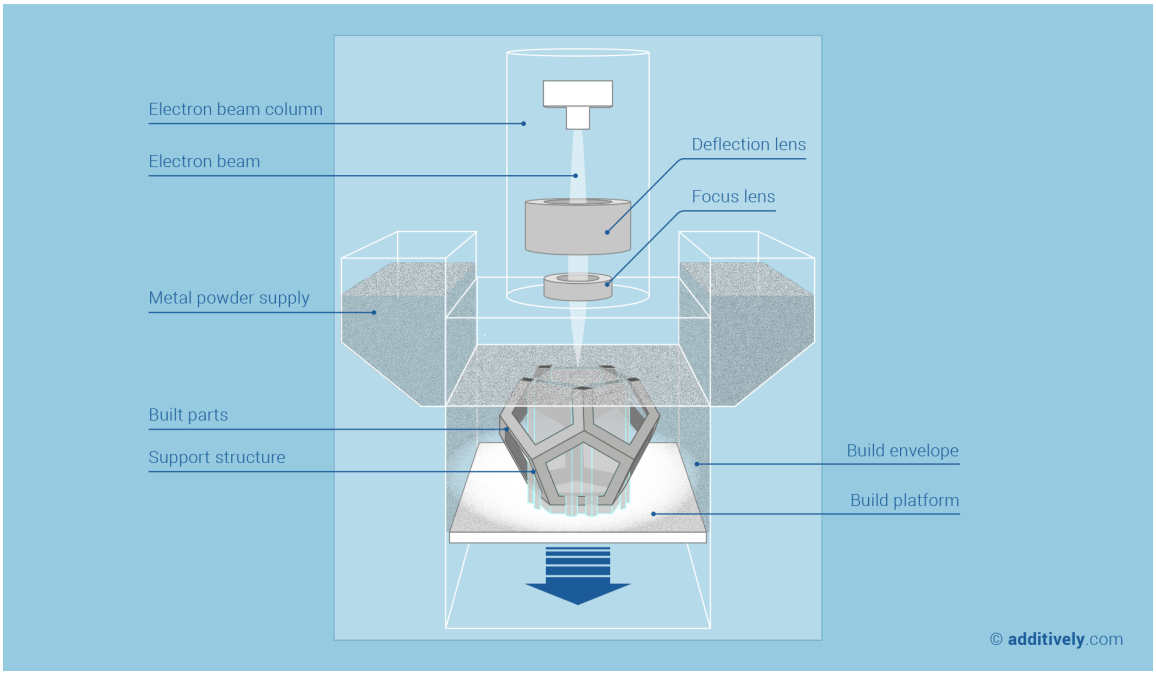

Figure B-8: The metal powder is melted layer by layer using an electron beam under vacuum. Between each cycle a layer of material is added to the build envelope (Additively, n.d.).

B.3 The Load Scenarios

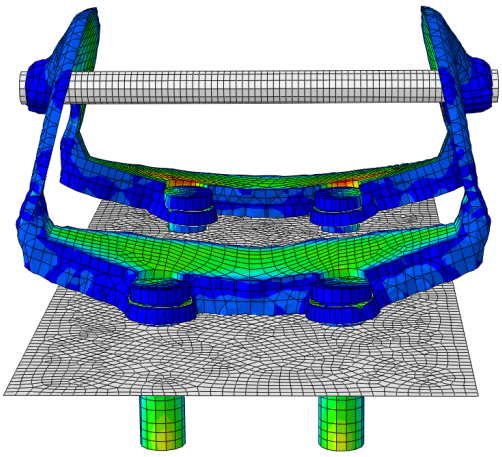

Figure B-9: Topology optimization with one load case: Fy applied to centre of the shoe-pin.

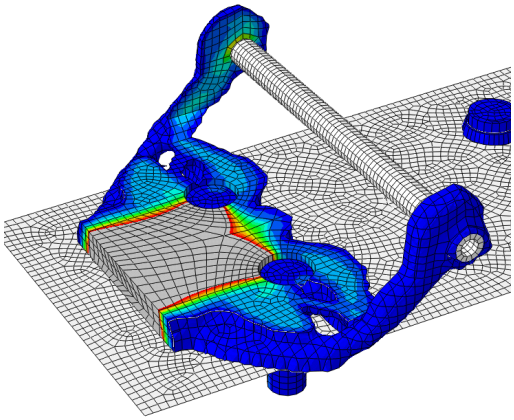

Figure B-10: Topology optimization with one load case: Fy applied to the centre of the shoe-pin and an evenly distributed pressure to the 'flex area'.

Figure B-11: Finding the angle in the Mx load case.

Figure B-12: First test with a load cell using aluminium plates.

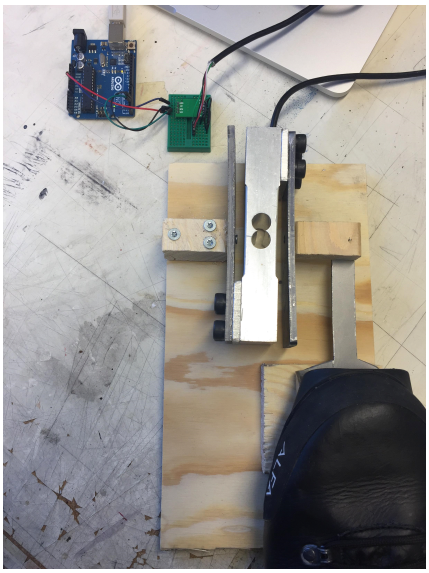

Figure B-13: Testing My.

Figure B-14: A heel piece for a cross country ski binding. When a person is standing on the skis, the shoe will 'lock' into the heel piece since the shape of the shoe fits in the heel piece, this will support against any twisting motion of the shoe.

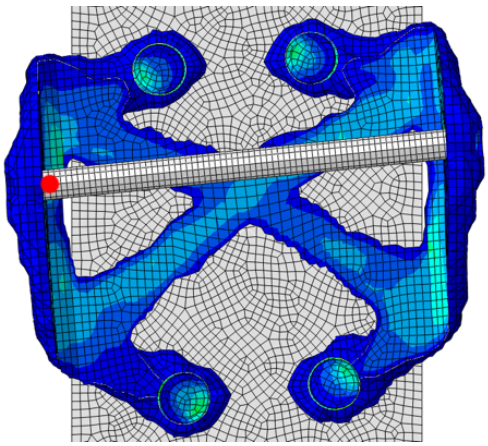

Figure B-15: Optimized result. Torque = 50 Nm applied to centre of the shoe-pin, pre-tension = 0 N, friction coefficient = 0.3 between the binding and the ski. Displacement at the red point = 0.0680226 mm.

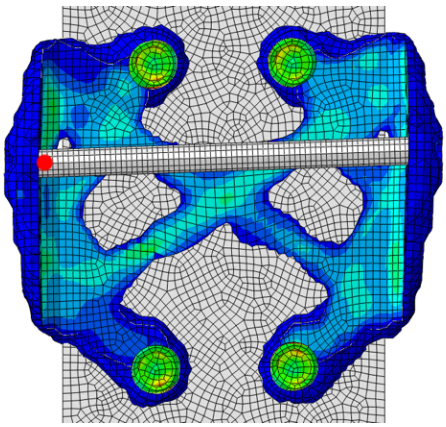

Figure B-16: Optimized result. Torque = 50 Nm applied to centre of the shoe-pin, pre-tension = 1 500 N, friction coefficient = 0.3 between the binding and the ski. Displacement at the red point = 0.0227543 mm.

B.4 Design Variables - Glue

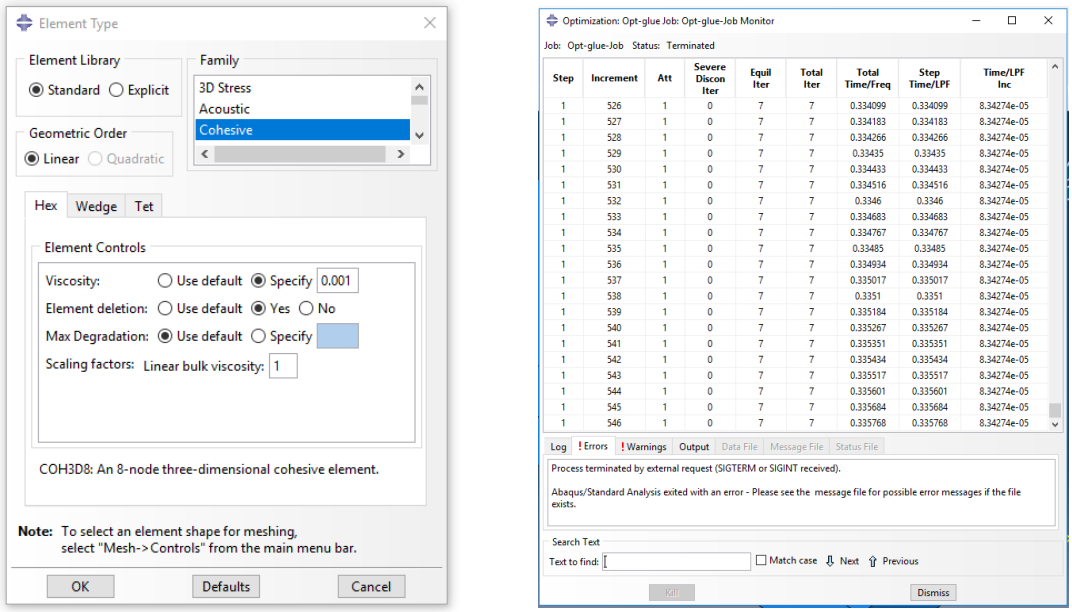

Figure B-17: Testing out adhesive elements in Abaqus. The increment size was here reduced to 0.000083427 by the software because of the complexity of the analysis, which means the algorithm will need a huge number of increments to reach 1, which is one step.

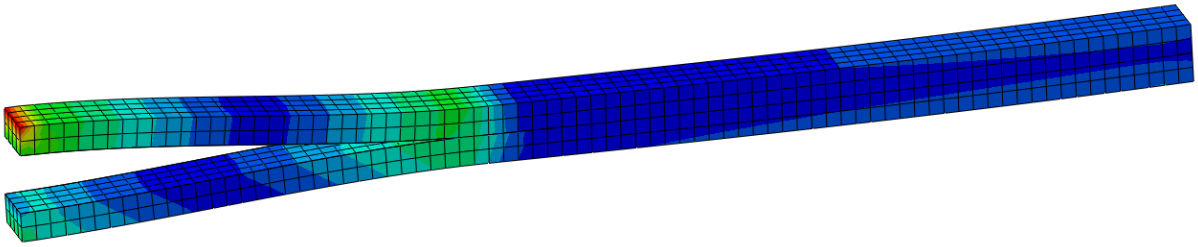

Figure B-18: FEA test of the model used to test out adhesive elements. Adhesive elements were added between the two plates, then a force was applied to the left, separating the plates. The part was fixed at the right end.

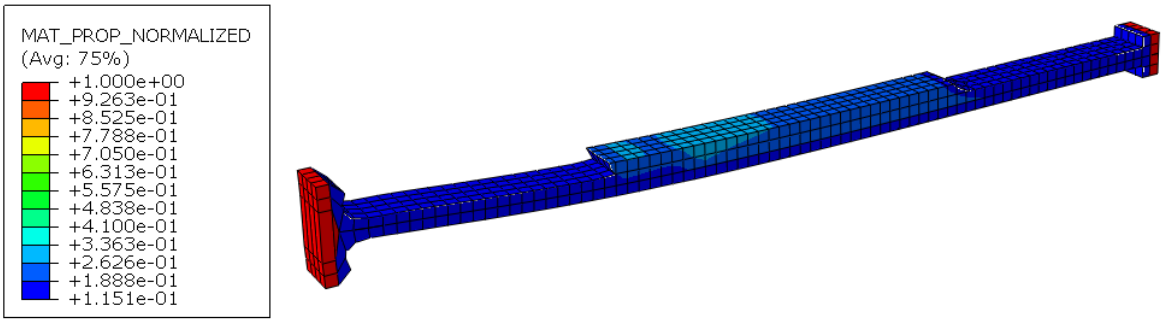

Figure B-19: The topology optimized result after 3 cycles, the optimization was aborted by the user due to too low increment size. Something that can happen when there are large displacements. The long red elements on the left is the adhesive elements.

Variable	Restricted by:	Direction	Size [mm]
Height of the holes	Defined by Rottefella	y	12
Max. width of screws	ISO-standards	x	26
Flex area	Computational capacity and time	y * x	9 * 26
Placement of flex area	Computational capacity and time	y	12
Placement of front screws	Existing bindings, computational capacity and time	y	6
Shoe pin hole	Defined by Rottefella	diameter	5
Screw hole dimension	ISO-standards, Rottefella	diameter	6.3

Table B-2: The fixed variables.

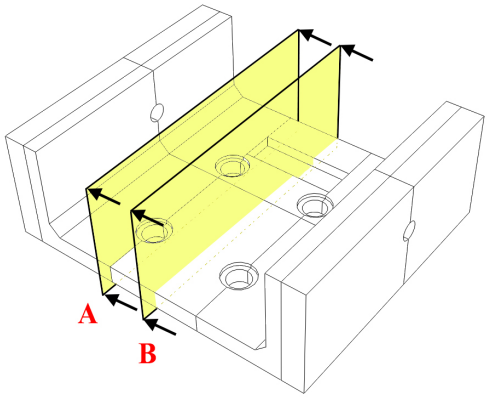

Figure B-20: Cutting planes A and B.

B.5 Counteract My

The theory is based on 'Loading of screw connections / Belastning av en skrueforbindelse' in the book *Dimensjonering av maskindeler* (Härkegård, 2014, pp. 155-156).

If the pre-tension force of a screw is F_p and the friction coefficient between the surfaces is μ, then the shear force must be $F_{shear} < \mu F_p$ to avoid gliding.

If a torsion moment M_t is applied to the centre of the binding in Figure B-21, the following equation must be fulfilled to avoid gliding: $M_t = 4 F_{shear} r < 4 \mu F_p r$.

Thus, by increasing the distance r for the same moment M_t, F_{shear} will decrease. This means a higher moment can be applied before the binding will glide. So, increasing the distance r will help to counteract the moment M_t.

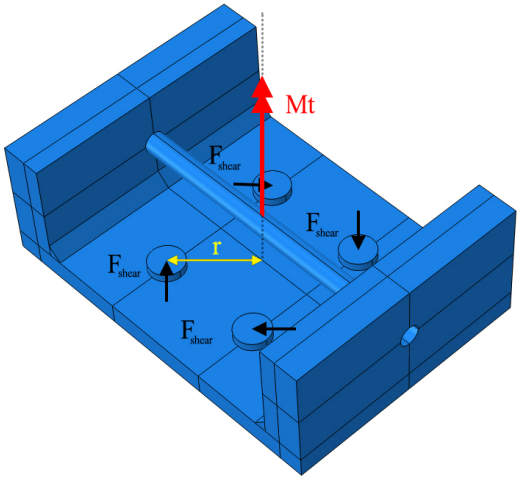

Figure B-21: Moment M_t applied to a ski binding. r is the distance to the centre of rotation.

B.6 Counteract Mx

When the skier is falling forwards, he / she will generate a moment Mx on the ski binding, because the flex is compressed at the same time as the shoe is rotated, trying to lift the binding of the ski. To keep the binding from rotating ($\sum M = 0$) the distance to the rear screw holes (d) in Figure B-22 can be increased, as a result a lower force F is needed, since $Mx = 2\ d\ F$.

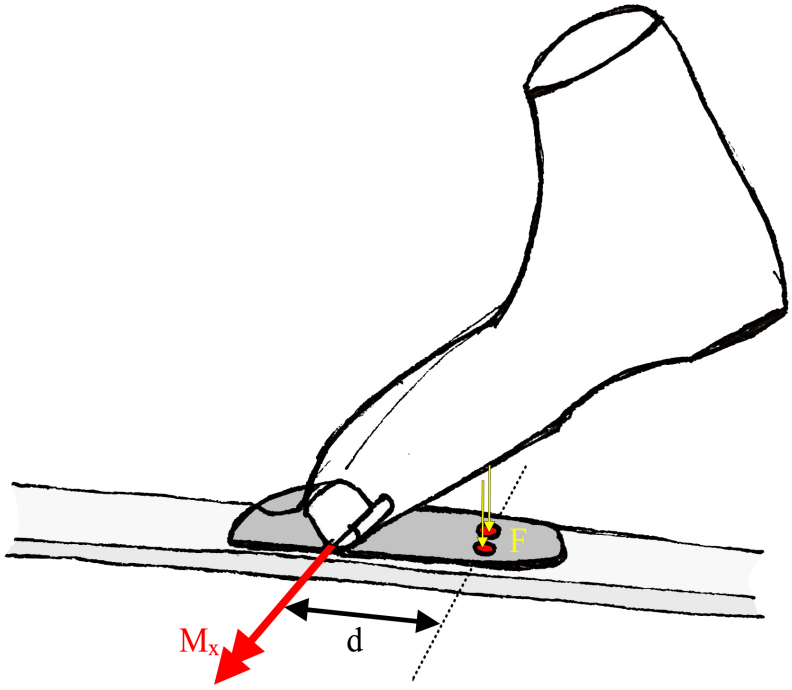

Figure B-22: Moment Mx generated when the skier is falling forwards.

C Optimization Cycle and FEA

C.1 FE Model

Mesh

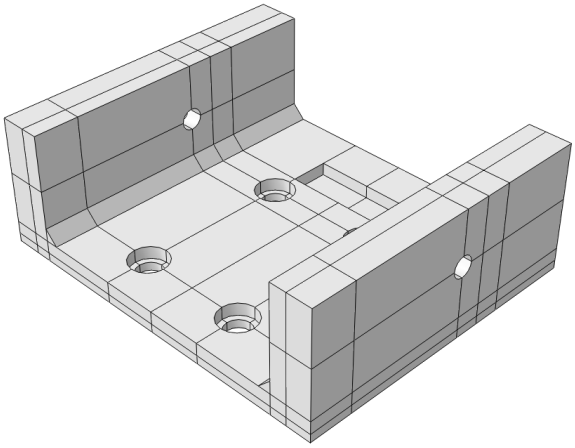

Figure C-1: Model partitioned (15 partitions).

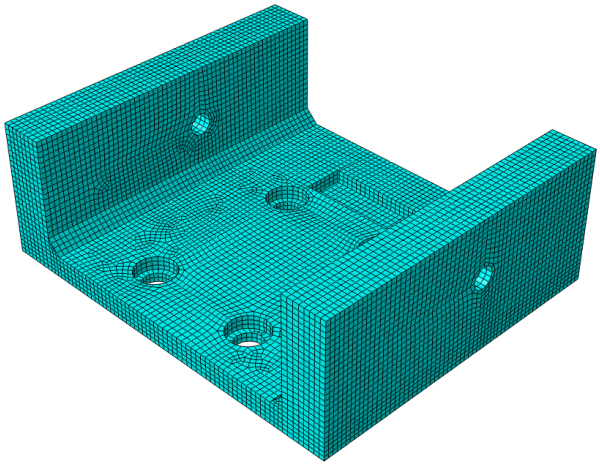

Figure C-2: Bracket (43 250 C3D8R-elements, seed = 1.2).

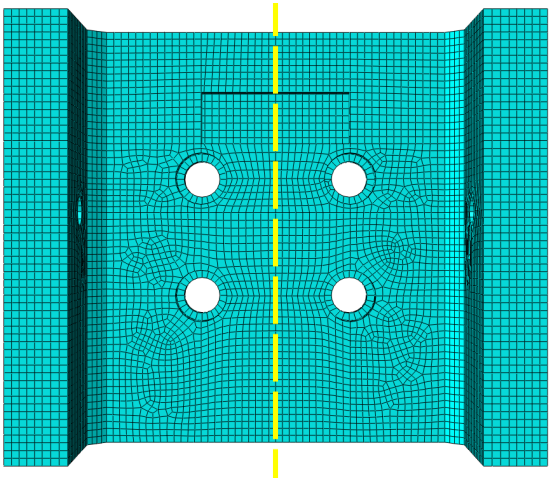

Figure C-3: Mesh when the bracket was partitioned using a centre-plane (yellow line).

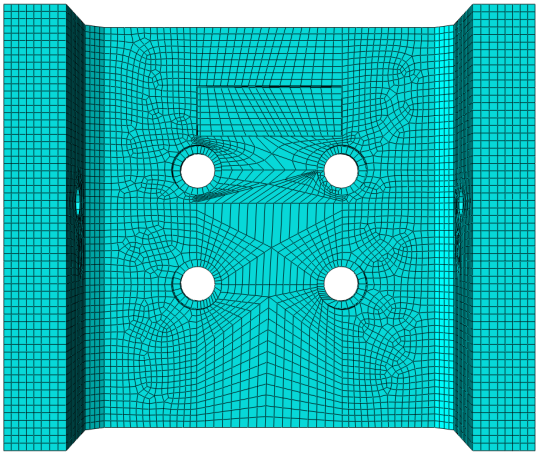

Figure C-4: Mesh without partitioning with a centre-plane.

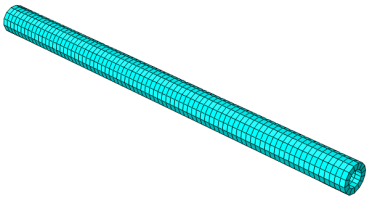

Figure C-5: Shoe-pin (2212 R3D4-elements and 2 R3D3 elements, seed = 1.2).

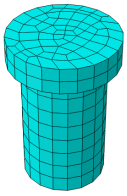

Figure C-6: Screw (456 C3D8R elements, seed = 1.2).

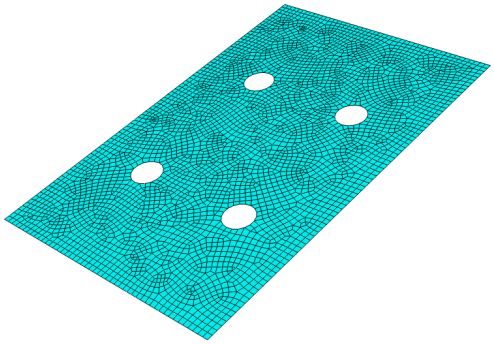

Figure C-7: Ski (3918 R3D4-elements and 135 R3D3 elements, seed = 1.2).

The Optimization Cycle

Variable	Direction	Step increment [mm]	Min [mm]	Max [mm]
Height of the binding (h)	y-direction	1	2	6
Support to screws (sh)	y-direction	1	2	5
Support to flex (fh)	y-direction	1	2	5
Screw placement (d)	z-direction	5	10.5	40.5

Table C-1: The adjustable variables.

C.2 FEA

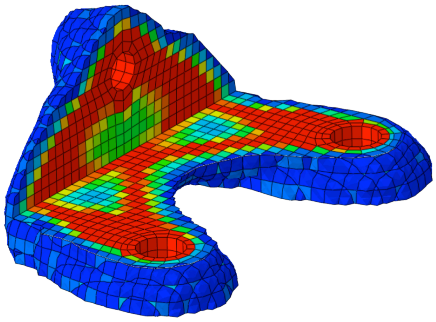

Figure C-8: Many intermediate elements; yellow, orange and green.

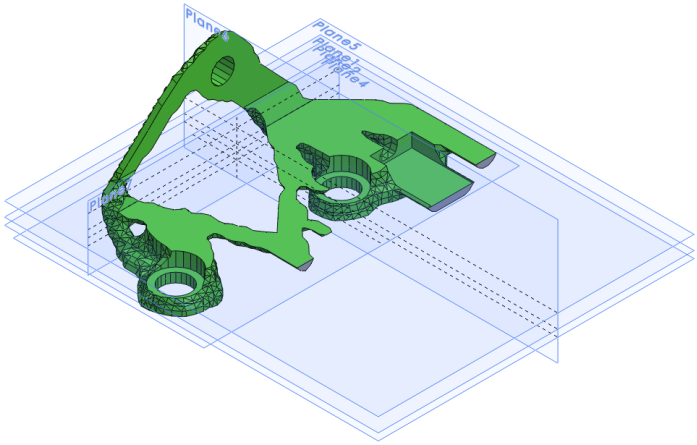

Figure C-9: Datum planes placed where the topology changed.

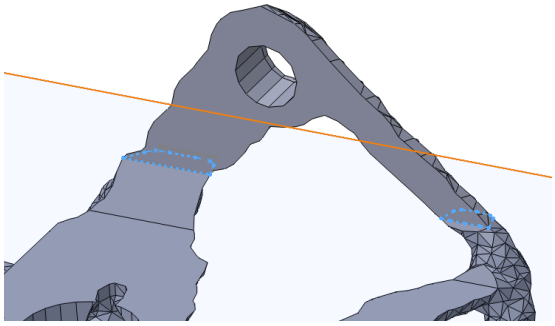

Figure C-10: Intersection-curves between reference model and datum-plane.

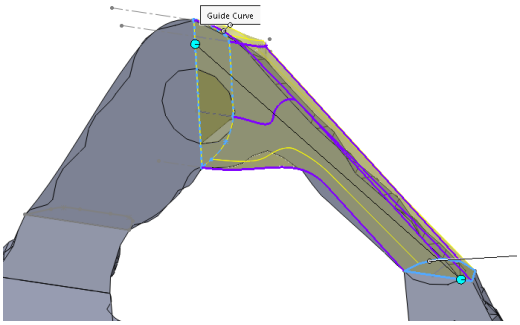

Figure C-11: Lofted section.

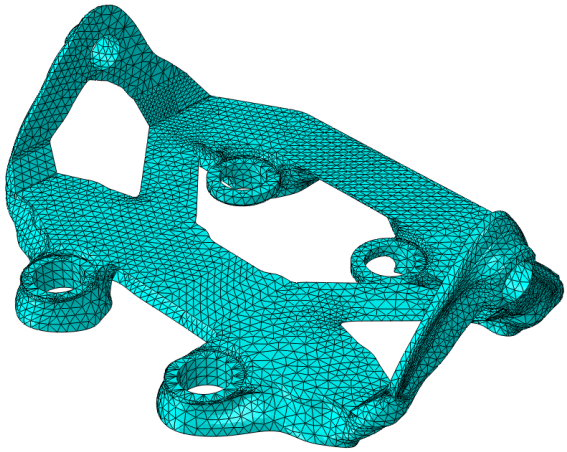

Figure C-12: Tetrahedral mesh.

C.3 Fatigue

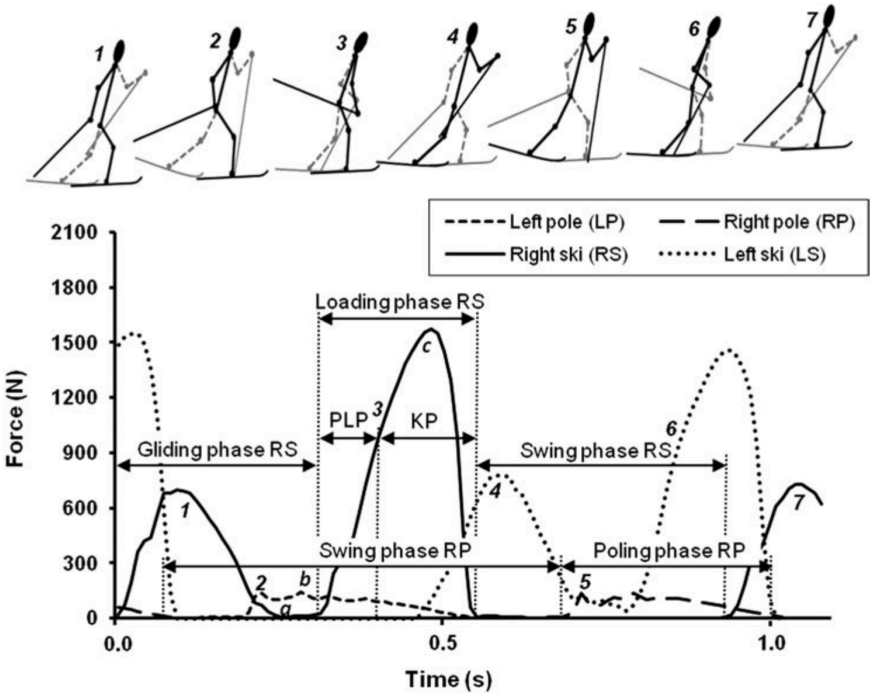

Figure C-13: Diagonally striding (Andersson, Pellegrini, Sandbakk, Stöggl, & Holmberg, 2014).

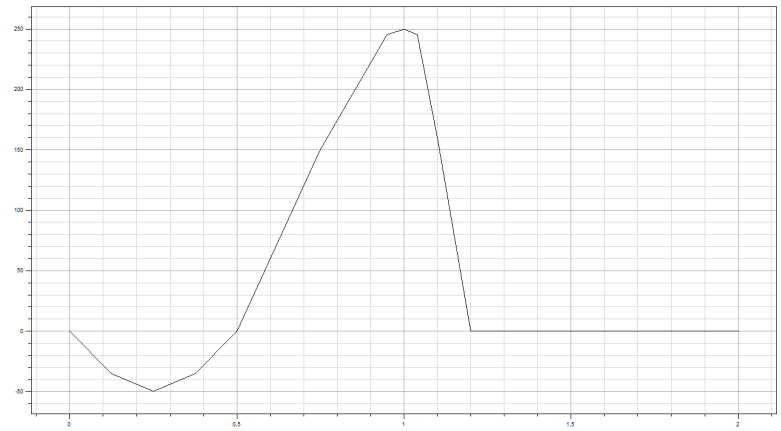

Figure C-14: Function 1: describing Fy.
Force [N] on the y-axis, time [s] on the x-axis.

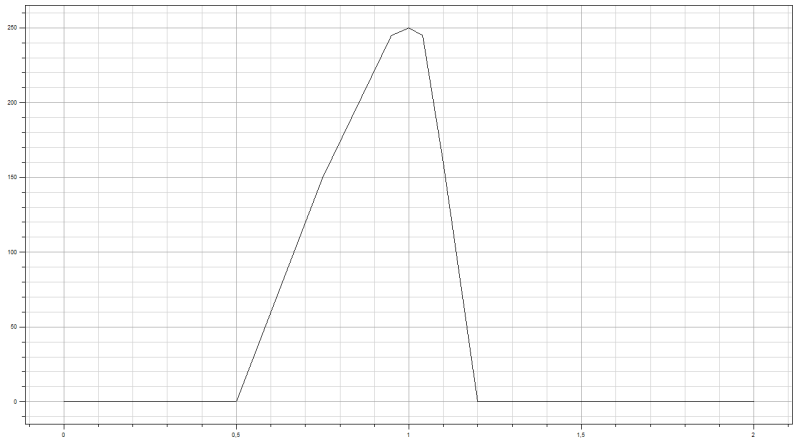

Figure C-15: Function 2: describing the force which goes into the flex.
Force [N] on the y-axis, time [s] on the x-axis.

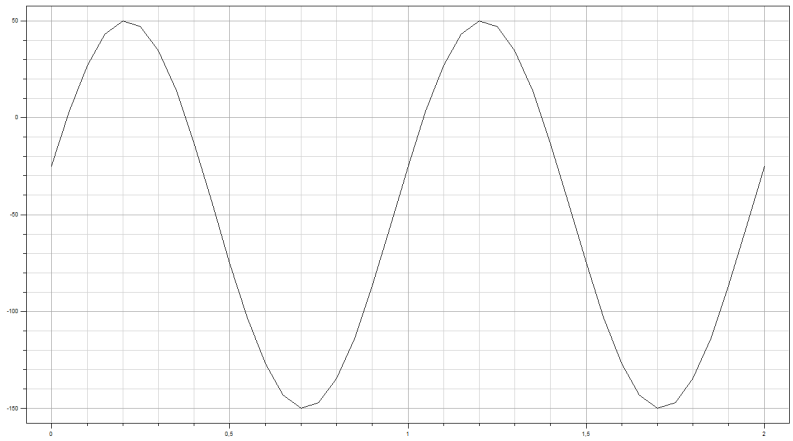

Figure C-16: Function 3: simulating skiing down an ice slope.
Force [N] on the y-axis, time [s] on the x-axis.

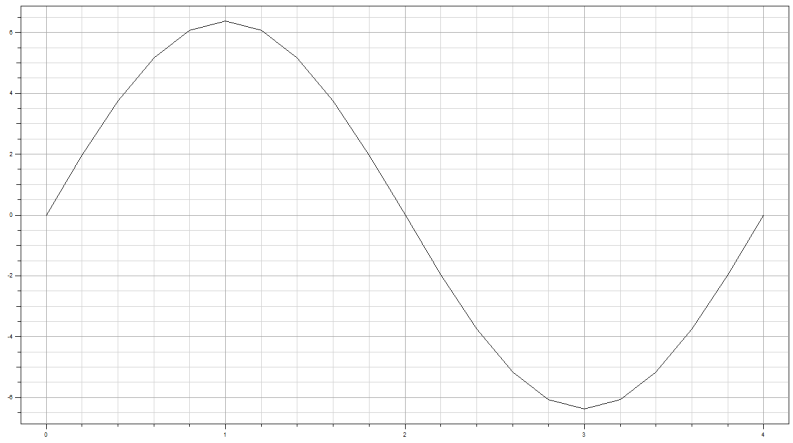

Figure C-17: Function 4: describing Mz.
Moment [Nm] on the y-axis, time [s] on the x-axis.

C.4 Gate 2

An estimate on how many cycles the binding should withstand before it fails, see Table C-2. This is for the striding load case, since this is believed to occur most frequently.

Walking per day	8 hours
Skiing / year	14 days
Skiing downhill	50 %
On each leg	50 %
Length of each step	2 seconds
Steps / year	50 400

Table C-2: Skiing / year.

If the binding should have a service life of 20 years it must withstand 50 400 cycles * 20 = 1 008 000 cycles before failure.

C.5 Functional Testing

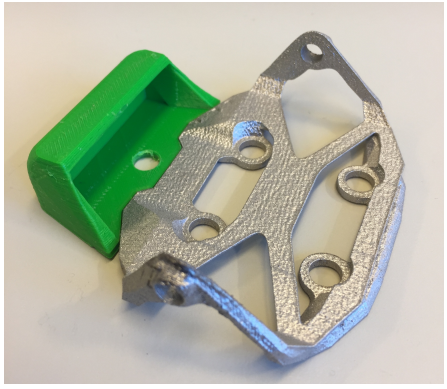

Figure C-18: The first prototype for fastening the flex. This was too high and the shoe touched it when the shoe rotated.

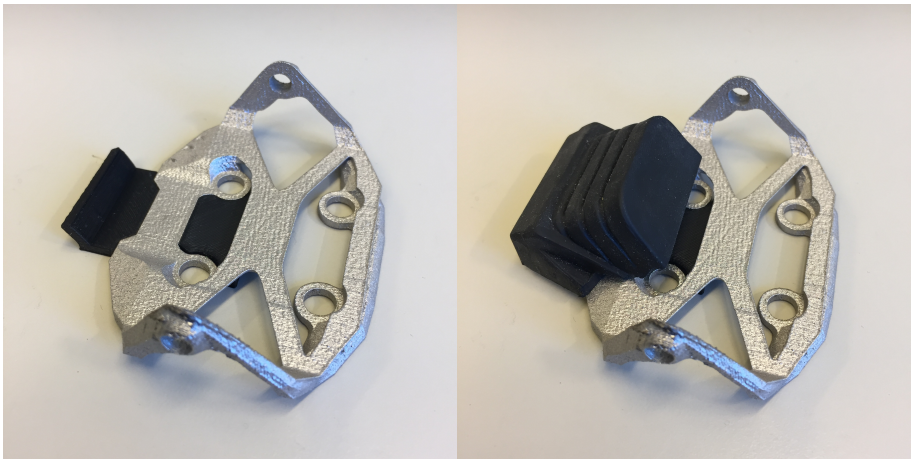

Figure C-19: The second prototype. Here the flex was too loose.

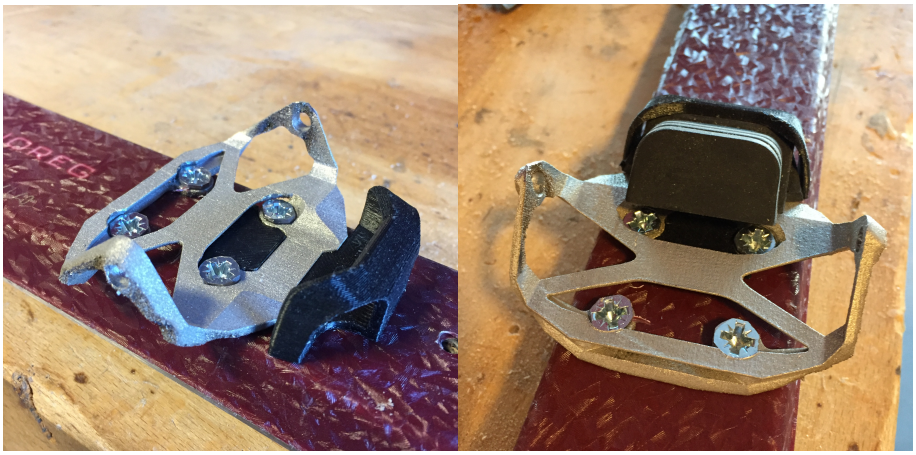

Figure C-20: The third prototype. This worked fine and was used in the field-tests.

C.6 Mechanical Testing

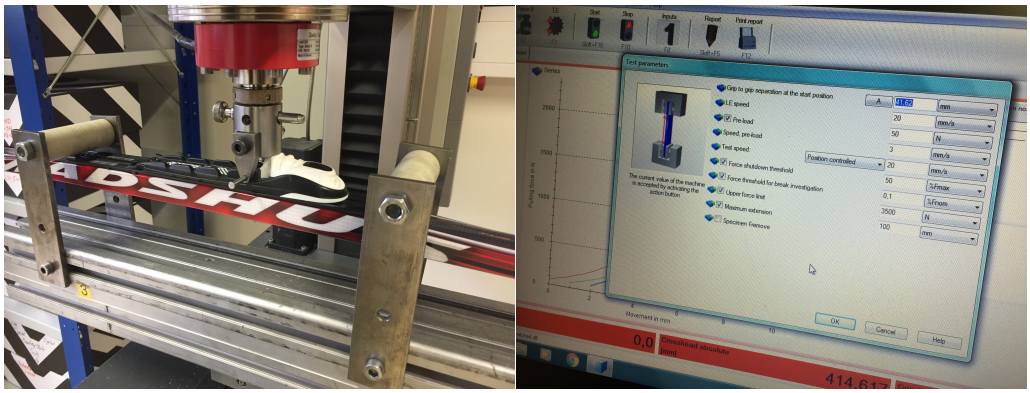

Figure C-21: The tensile testing machine at Rottefella.

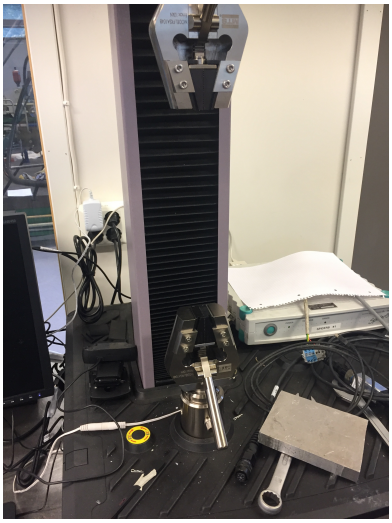

Figure C-22: The tensile testing machine at IPM.

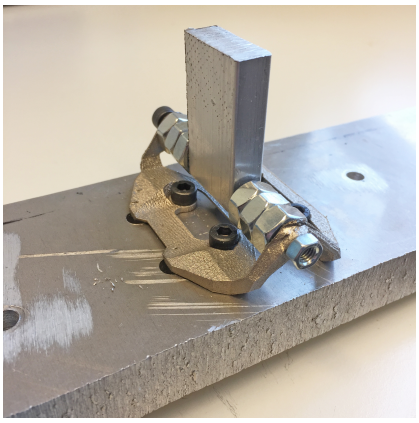

Figure C-23: Because the screws might have been ripped out of a ski before the binding would be destroyed, an aluminium profile was made instead of testing a ski.

Figure C-24: For fastening the aluminium profile. Two rollers were constructed to make sure that only a vertical force was transferred through the binding.

D The Results of the Optimization Cycle

D.1 Initial Testing

Figure D-1, Figure D-2 and Figure D-3 show tests that were done to define the setup. Figure D-1 display tests where several distances between the screw holes were tested out; the four best were then selected to be tested further. Figure D-2 shows tests that were done to see how low volume constraint that could be requested, before the models had too high von Mises stress. In Figure D-3 different heights (the thickness of the binding) were tested.

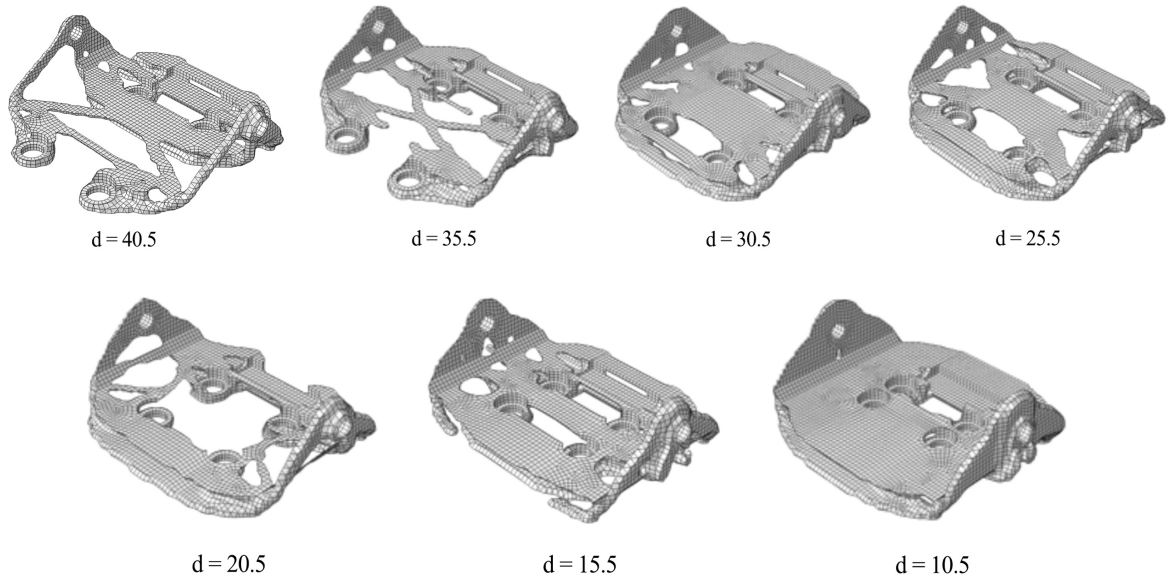

Figure D-1: Testing high and low values for the distance d.

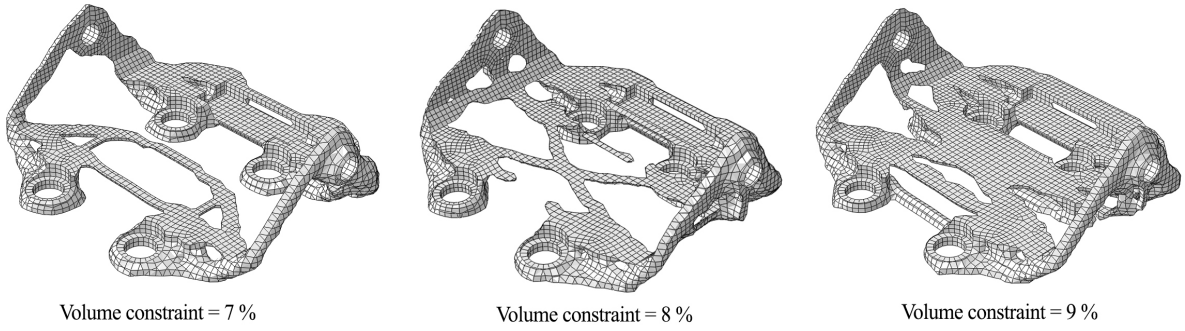

Figure D-2: Testing different volume constraints.

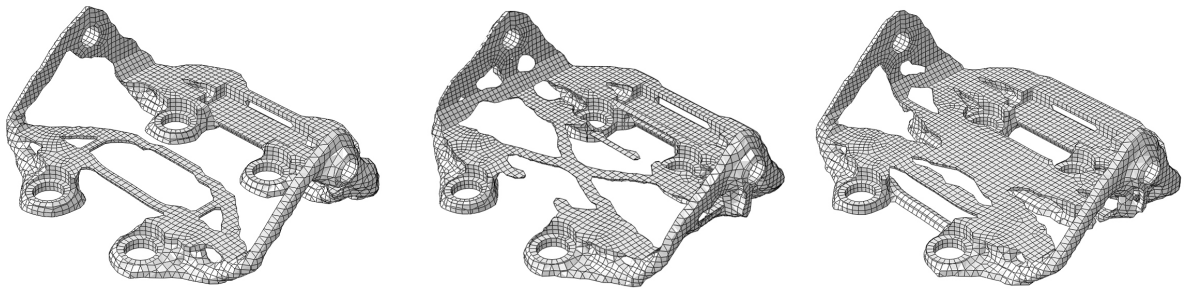

Figure D-3: Testing different binding heights (h).

D.2 Testing the Adjustable Variables

Test 1

h [mm]	sh [mm]	fh [mm]	d [mm]
5	2	2	20.5 → 35.5

Table D-1: The adjustable variables. Four different values for d were tested.

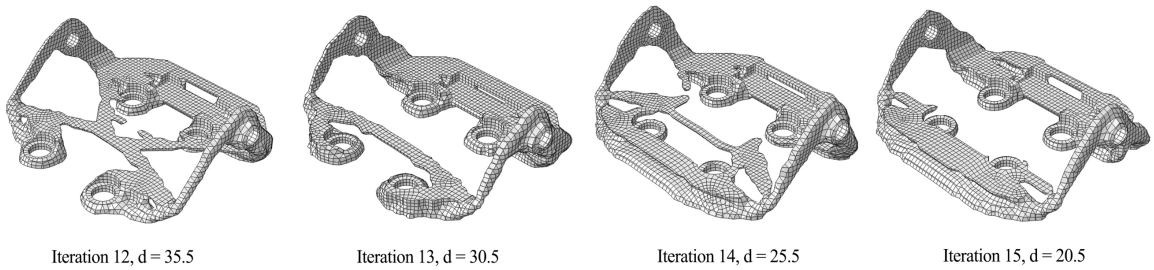

Figure D-4: Iteration 13 (d = 35.5) was the best, strain energy = 485 mJ.

Test 2

h [mm]	sh [mm]	fh [mm]	d [mm]
5	2	5	20.5 → 35.5

Table D-2: The adjustable variables. fh was changed to 5 mm, then four different values for d were tested.

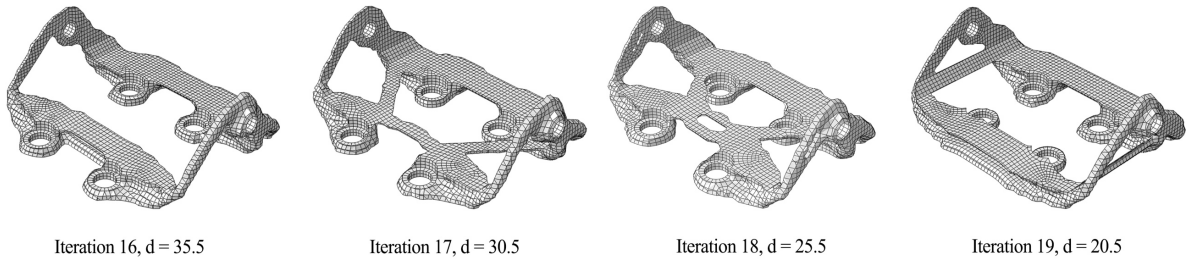

Figure D-5: Iteration 17 (d = 30.5) was here the best, strain energy = 369 mJ.

From these two tests Iteration 17 (fh = 5 mm, d = 30.5 mm) was selected.

Test 3

h [mm]	sh [mm]	fh [mm]	d [mm]
2 → 5	2	h	30.5

Table D-3: The adjustable variables. Different values for h was tested.

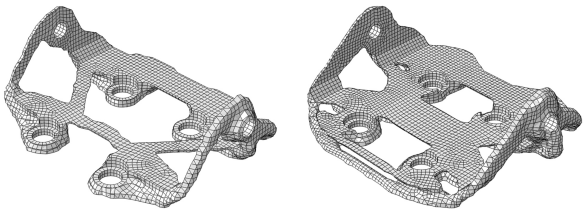

Figure D-6: Iteration 17 was still favourable.

Iteration 17 was selected; the tests were not completed if changing the variable led to a worse result. E.g. if decreasing the height from 5 mm to 4 mm increased the strain energy, then a height of 3 mm was not tested.

Test 4

h [mm]	sh [mm]	fh [mm]	d [mm]
5	2 → 5	2	30.5

Table D-4: The adjustable variables. Different values for sh tested.

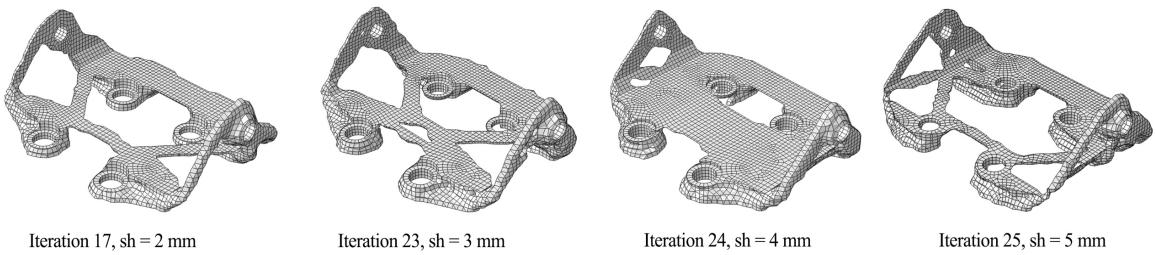

Figure D-7: Here iteration 24 was the best, strain energy = 320 mJ.

Test 5

h [mm]	sh [mm]	fh [mm]	d [mm]
2 → 5	h - 1	h	30.5

Table D-5: The adjustable variables. Different values for h tested again on the new model.

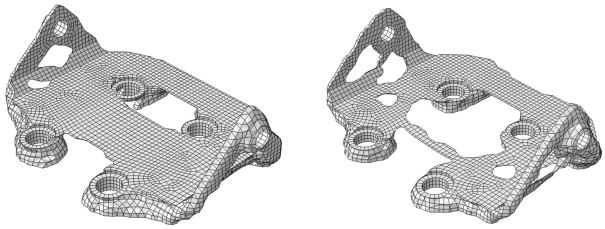

Iteration 24, h = 5 mm Iteration 26, h = 4 mm

Figure D-8: Iteration 24 was still the best.

Test 6

h [mm]	sh [mm]	fh [mm]	d [mm]
5	4	5	30.5

Table D-6: The adjustable variables were locked during these tests.

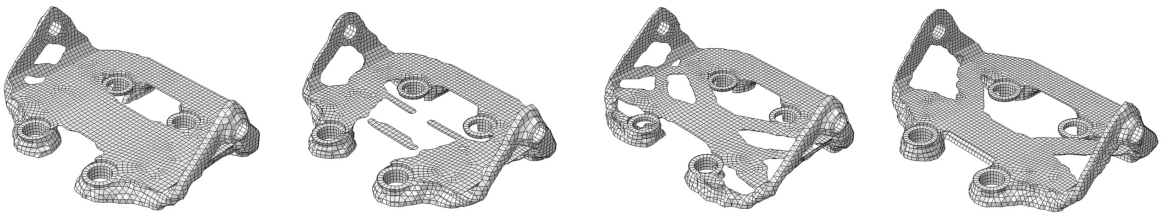

Iteration 24, mesh = 1.2 Iteration 27, VC = 7 % Iteration 28, 44 cycles Iteration 29, mesh = 1

Figure D-9: Iteration 29 was selected; it had a little higher strain energy (346 mJ), but was lighter than iteration 24.

Iteration	Description		SE	end VF	DS V	end V
1	Testing distance d	d = 35.5	710	7,387 %	64710,9	4780,2
2		d = 30.5	774	8,287 %	64710,9	5362,6
3		d = 25.5	862	7,414 %	64710,9	4797,7
4		d = 20.5	368	11,360 %	64710,9	7351,2
5		d = 15.5	214	17,951 %	64710,9	11616,3
6		d = 10.5	270	15,100 %	64710,9	9771,3
7		d = 40.5	594	9,373 %	64710,9	6065,4
8	Volume constraint	vc = 0.09	384	10,295 %	64710,9	6662,0
9		vc = 0.07	594	8,320 %	64710,9	5383,9
10	Height (h)	h = 4 mm	567	10,060 %	59118,47	5947,3
11		h = 6 mm	523	8,680 %	70303,34	6102,3
12	Test 1, fh = 2	d = 35.5	485	9,300 %	64710,9	6018,1
13		d = 30.5	500	9,300 %	64710,9	6018,1
14		d = 25.5	505	9,295 %	64710,9	6014,9
15		d = 20.5	508	9,300 %	64710,9	6018,1
16	Test 2, fh = 5	d = 35.5	397	9,310 %	65412,9	6090,1
17		d = 30.5	369	9,298 %	65412,9	6082,3
18		d = 25.5	375	9,306 %	64710,9	6021,9
19		d = 20.5	424	9,302 %	65412,9	6084,4
20	Iterating on vc and d	d = 30.5, 0.07	465	8,312 %	65412,9	5437,4
21		d = 30.5, seed 1	348	9,291 %	65412,9	6077,6
22	Test 3, heith	h = 4 mm	270	15,07 %	51366,37	7740,9
23	Test 4, screw holes	sh = 3 mm	370	9,198 %	65542,68	6028,5
24		sh = 4 mm	320	9,186 %	65672,42	6032,9
25		sh = 5mm	349	9,177 %	65802,24	6038,9
26	Test 5, heigth	h = 4 mm	408	13,20 %	43276	5712,4
27	Test 6	inital low vc	378	8,198 %	65672,42	5383,9
28		44 cycles	442	8,227 %	65672,46	5402,9
29		mesh = 1	346	8,192 %	65672,46	5379,7

Table D-7: Summary of the 29 iterations. SE: strain energy, end VF: volume fraction when the model was optimized, DS V: Design space volume, end V: volume of the result.

D.3 FEA

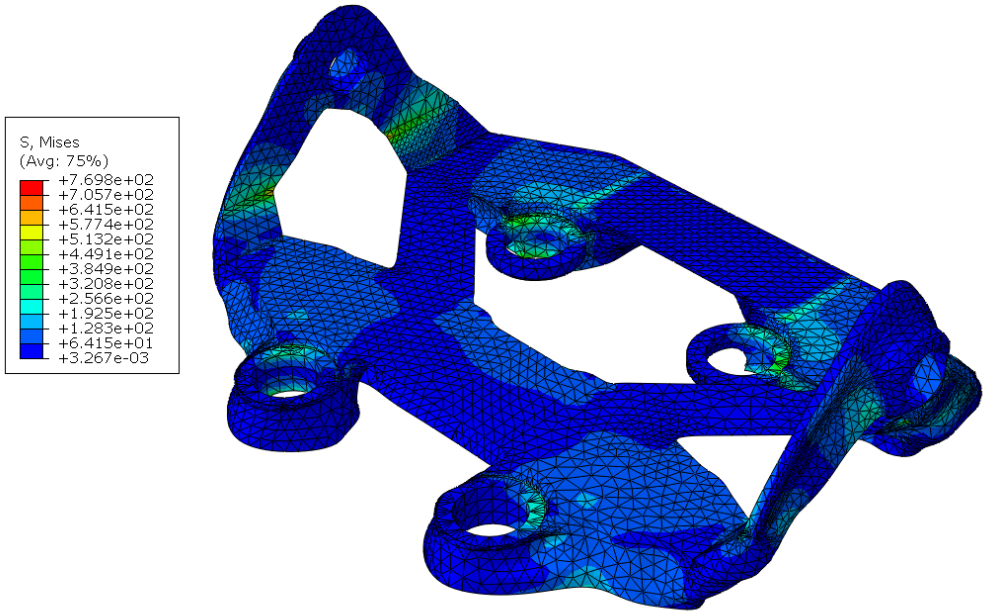

Figure D-10: Load case Mx.

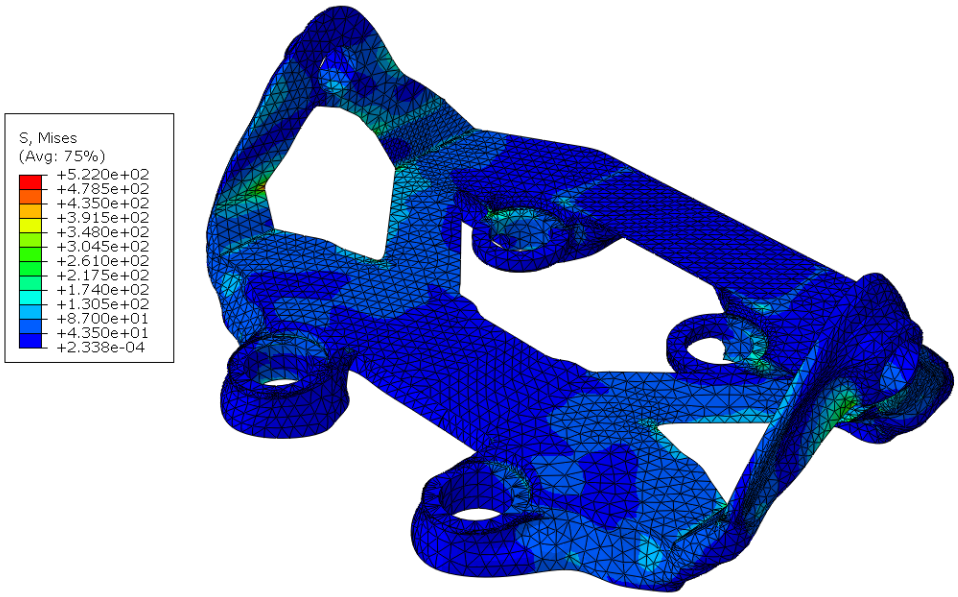

Figure D-11: Load case My.

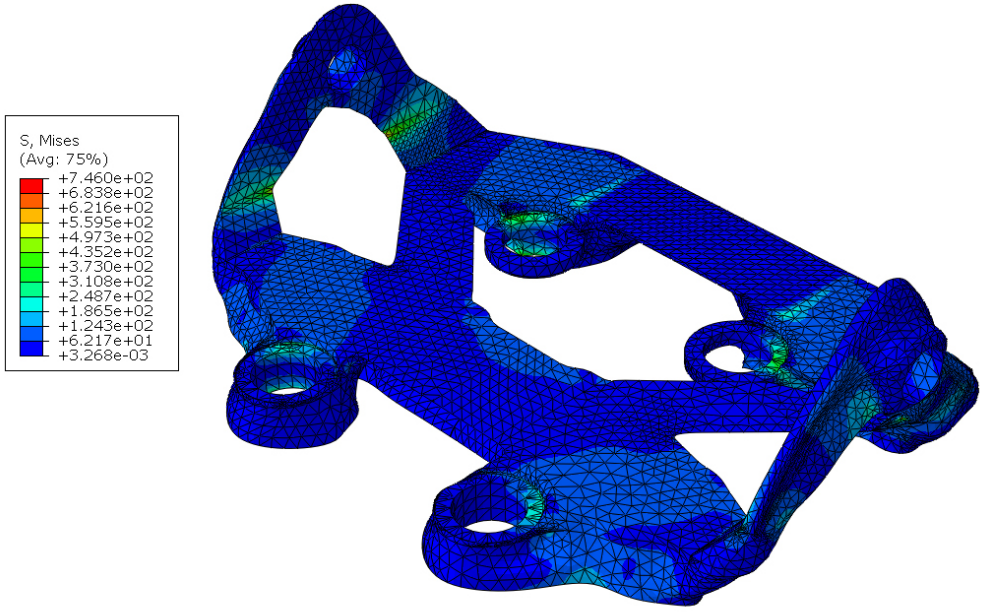

Figure D-12: Load case Fy.

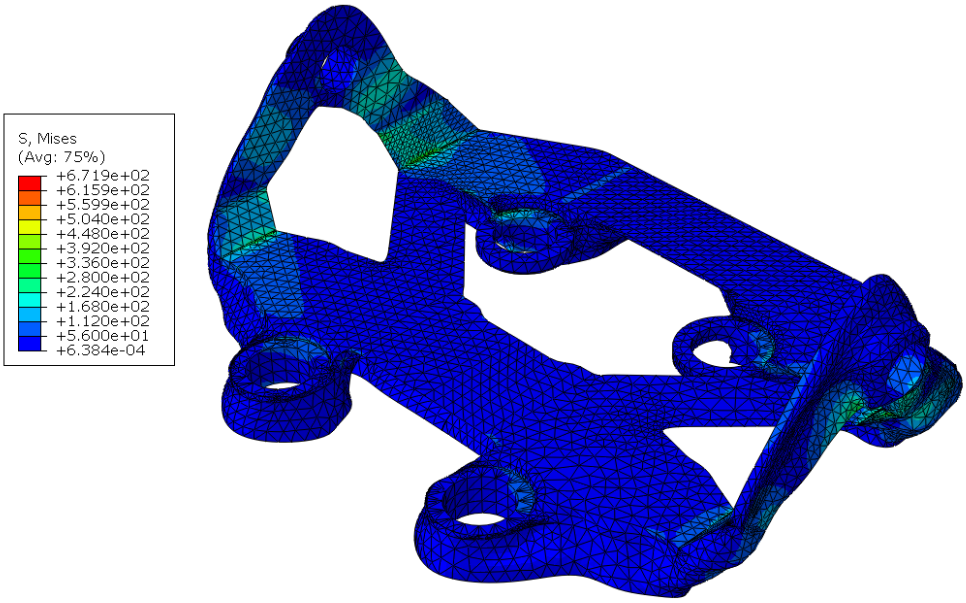

Figure D-13: Load case Fx.

D.4 Fatigue

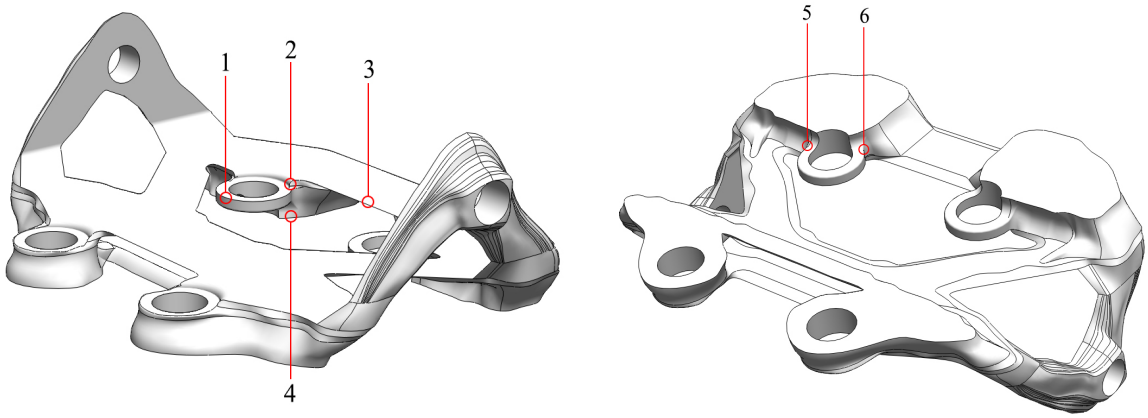

Figure D-14: Overview over where the strain rosettes were placed.

Test	Rosette number	Load case	Fatigue life	Rosette number	Load case	Fatigue life
1	3	Mx	916 933	2	Mx	103 560
2	6	Mx	187 445	5	Mx	86 400
3	6	Mx	281 102	1	Mx	1 339 200
4	2	Mz	1 043 954	1	Mx	980 375
5	1	Mx	950 400	4	Mx	2 340 243
6	1	Mx	1 328 720	4	Mx	1 414 774

Table D-8: Summary of the fatigue analysis. The table shows the fatigue life (cycles to failure) for two rosettes per test.

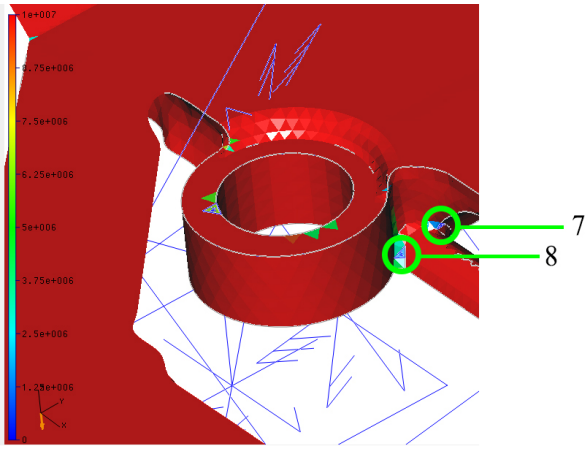

Figure D-15: Front left screw hole.

Test	Rosette number	Load case	Fatigue life	Rosette number	Load case	Fatigue life
7	7	Mx	1 194 048	8	Mx	4 427 266

Table D-9: Checking the last redesign (Model E).

D.5 Mechanical Testing

Material	E $[GPa]$	Density $[g/cm^3]$	Tensile strength $[MPa]$
Ti-6Al-4V	1.7	0.93	58

Table D-10: Material properties of PA 2200.

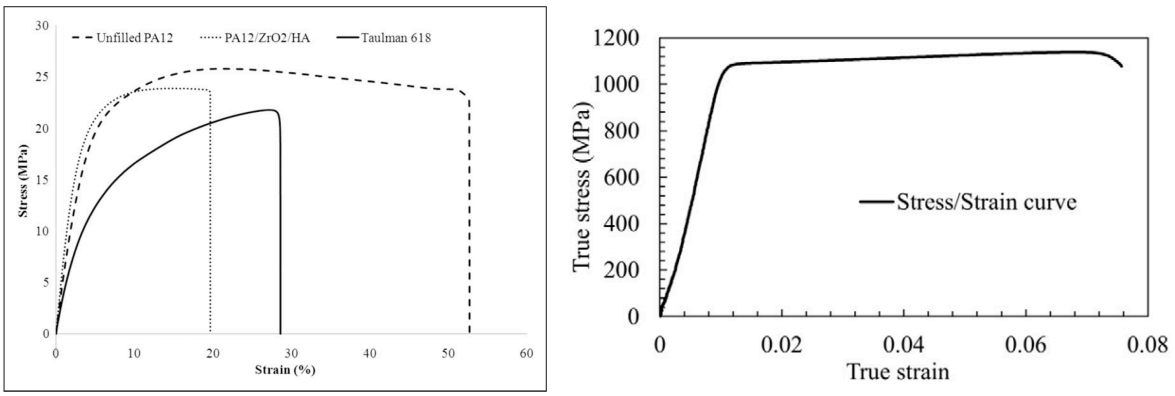

Figure D-16: On the left side is a stress-strain curve for PA12 / PA2200 (Tuan Rahim, Abdullah, Md Akil, Mohamad, & Rajion, 2015), and on the right side is the stress-strain curve for Ti6Al4V (Fadida, Rittel, & Shirizly, 2015). As seen, titanium behaves more linear than PA 2200 in the elastic region (before the material yields). This means the linear analyses in Abaqus predicts the behaviour of titanium much more accurately than PA 2200 in the elastic region.

Figure D-17: Force vs. displacement for test 1 (blue graph) and test 2 (orange graph).

E Future Research Needs

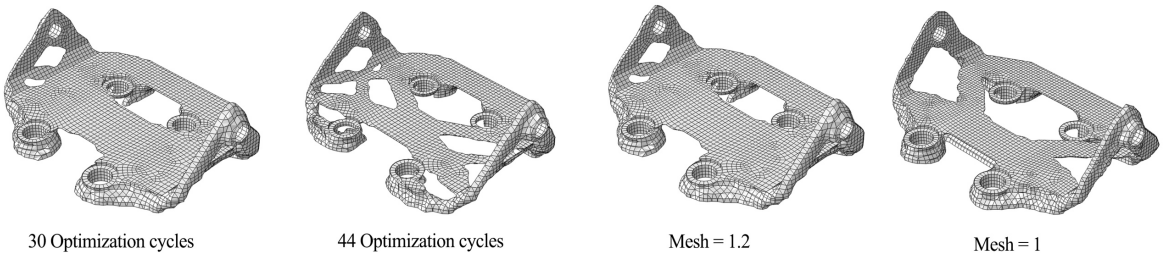

Figure E-1: Different number of optimization cycles and mesh seeds for the same loads and design variables.

F The Paper: *State of the Art of Generative Design and Topology Optimization and Potential Research Needs*

NordDesign 2018
August 14 – 17, 2018
Linköping, Sweden

State of the art of generative design and topology optimization and potential research needs

Evangelos Tyflopoulos[1], David Tollnes Flem[2], Martin Steinert [3], Anna Olsen [4]

[1] *Department of Mechanical and Industrial Engineering, NTNU*
evangelos.tyflopoulos@ntnu.no
[2] *Department of Mechanical and Industrial Engineering, NTNU*
davidtoflem@gmail.com
[3] *Department of Mechanical and Industrial Engineering, NTNU*
martin.steinert@ntnu.no
[4] *Department of Mechanical and Industrial Engineering, NTNU*
anna.olsen@ntnu.no

Abstract
Additive manufacturing allows us to build almost anything; traditional CAD however restricts us to known geometries and encourages the re-usage of previously designed objects, resulting in robust but nowhere near optimum designs. Generative design and topology optimization promise to close this chasm by introducing evolutionary algorithms and optimization on various target dimensions. The design is optimized using either 'gradient-based' programming techniques, for example the optimality criteria algorithm and the method of moving asymptotes, or 'non gradient-based' such as genetic algorithms SIMP and BESO. Topology optimization contributes in solving the basic engineering problem by finding the limited used material. The common bottlenecks of this technology, address different aspects of the structural design problem.

This paper gives an overview over the current principles and approaches of topology optimization. We argue that the identification of the evolutionary probing of the design boundaries is the key missing element of current technologies. Additionally, we discuss the key limitation, i.e. its sensitivity to the spatial placement of the involved components and the configuration of their supporting structure. A case study of a ski binding, is presented in order to support the theory and tie the academic text to a realistic application of topology optimization**.**

Keywords: topology optimization, product development, design, finite element analysis

1. Introduction

The ideal linkage between the additive manufacturing (AM) and the structural optimization (SO) is the key element in product development these days. On the one hand, models are produced by the addition of thousands of layers with the use of additive manufacturing (AM). That offers to designers a huge geometrical flexibility, with no additional cost, compared to traditional manufacturing. AM encompasses many technologies such as 3D printing, rapid prototyping and direct digital manufacturing (DDM). On the other hand, structural optimization reduces the material usage, shortens the design cycle and enhances the product quality. SO can be implemented according to size, shape, and topology (see Figure 1). Topology optimization is usually referred to as general shape optimization (Bendsøe, 1989). Most of the techniques optimize either the topology or both the size and the shape. There are only few examples that have tried to confront the problem in a holistic way (M. Zhou, Pagaldipti, Thomas, & Shyy, 2004).

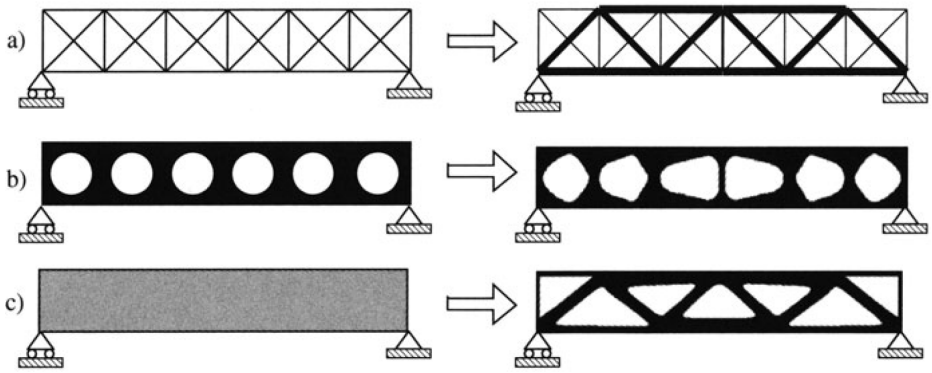

Figure 1: Illustration of a truss model and its different categories of structural optimization by: a) size, b) shape and c) topology (Bendsøe & Sigmund, 2003).

The current state of the art of topology optimization (TO) is most oriented in the conceptual design phase. The general idea is to find the optimal material distribution of a structure with respect to its design and boundary constraints. However, the main challenge of TO is to provide a design parameterization that leads to a physically optimal design too (Sigmund & Petersson, 1998).

The first article about topology optimization was published in 1904 by the insightful Australian mechanical engineer Michell (1904). Michell's article addressed the problem of least-volume topology of trusses with a single condition and a stress constraint. His contribution to topology optimization was the introduction of essential elements the so-called now, after a century, layout optimization, continuum-type optimally criteria, adjoin strain field and ground structure (Rozvany, 2009). After approximately 70 years it was Rozvany (1972) who extended Michell's theory from trusses to beam systems and introduced the first general theoretical background of topology optimization termed 'optimal layout theory' (Rozvany, 1977). The scientific revolution in this field had begun and it has been mainly carried out the last 30 years with many interesting articles. There are three main approaches which deal with the topology optimization problem: element-based solution approaches (density, topological derivatives, level set, phase field, etc.), discrete approaches (evolutionary based algorithms) and combined approaches (Sigmund & Maute, 2013). The most known methods of topology optimization are: the solid isotropic material with penalization (SIMP) and the evolutionary structural optimization (ESO) or the bi-directional evolutionary structural optimization (BESO).

In the same direction, either gradient-based (optimality criteria algorithm, convex linearization, method of moving asymptotes, etc.) or non-gradient algorithms (genetic algorithms) were developed to support the theory of topology optimization.

Optimality criteria algorithm (OC) is the most fundamental gradient-based mathematical method. In this method, there is a proportional dependency between the design variables and the values of the objective function (Prager, 1968). The 99-line MATLAB by Sigmund (2001), which tackles the compliance problem for the Messerschmitt-Bölkow-Blohm (MBB) beam, is based on OC and nested analysis and design formulation (NAND). Convex linearization (CONLIN) is a linear mathematical programming method for structural optimization with mixed variables and respect to the problem's characteristics. This method was introduced by Fleury and Braidbant (1986). Svanberg (1987) presented the method of moving asymptotes (MMA) which is a more aggressive version of CONLIN that is expanded by moving limits. The MMA creates an enormous sequence of improved feasible solutions of the examined problem. In addition to that, it can handle general non-linear problems and simultaneously take into account both constrains, design variables and characteristics of the structural optimization problem (cost, robustness, etc.). That was the foundation of the homogenization method (isotropic material) which was conducted the next year by Bendsøe and Kikuchi (1988) and a predecessor of the density-based approach of solid isotropic material with penalization (SIMP) (Bendsøe, 1989; M. Zhou & Rozvany, 1991)

The most notable non-gradient algorithms are the successive linear programming (SLP) and the successive quadratic programming (SQP). Both these methods transform the non-linear problem to a linear at a design point and optimize it within a limited region by movable boundary limits (Dantzig, 1963).

The aim of this paper is to give an overview over the different topology optimization approaches and practices. In addition, we run a case study of a ski binding using different practices of design optimization in order to implement the approaches and identify their needs. Of particular interest is the problem of the a priori fixed boundary and the real nearby limits to the potential designs and solutions.

2. Topology optimization (TO) and Finite Element Analysis (FEA)

Topology optimization is an iterative procedure adapted to the computer-added design (CAD). The main goal of this method is the best structural performance through the identification of the optimum material distribution inside the available volume of a structure with respect to its loads, boundary conditions and constraints. If TO is integrated into the traditional finite element analysis, the procedure can be divided to 8 steps as it is shown in Figure 2. This figure illustrates the geometry shift of a structure from its original geometry to topology geometry. In the beginning, FEA is implemented. It is possible to be used geometric modifications in order to simplify the initial problem. This stage is challenging to be computerized because it involves applying experience and judgement in a qualitative manner. However, the most crucial step at FEA is the definition of the problem statement and its equivalent mathematical model with all the required parameters (material properties, loads and restraints). The optimum results occur through the discretization (meshing) of the model and with a repetitive convergence method. The topology optimization method offers a new optimized design geometry with a notable mass reduction (or increment) which can be used as a new starting point for the FEA. Finally, the new FEA results validate or evaluate the success of the TO approach.

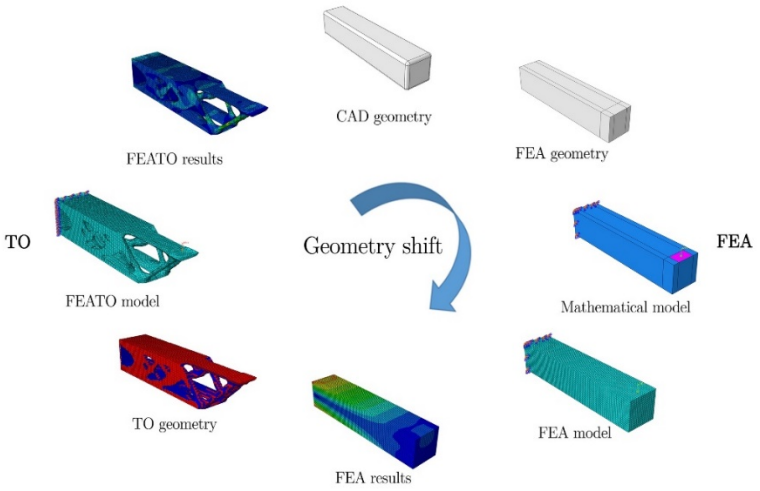

Figure 2: The geometry shift model of a cantilever beam with Abaqus based on the Kurowski FEA model (2017, pp. 10-11) and Simulia's ATOM lifecycle.

3. The general topology optimization problem

The general mathematical solution of a continuous element-based optimization problem seeks the minimum (top down) or maximum (bottom up) value of a function $f(x)$ and its related variable vector $x = (x_1, \dots, x_n) \epsilon IR^n$ which generates it, with respect to possible conditions and constrains. According to Hassani and Hinton (1999, p. 3), the f can be called the objective or cost function and respectively the quantities x_i, $i = 1, \dots, n$ design variables and n the number of design variables. The design variables are depended due to equalities among the constrains, so it can be assumed that the real design space is a sub-space of IR^n, where its dimension will be n minus the number of the independent equality constraints. Then the optimization problem can be expressed as:

$$\begin{aligned} & f(x) && \text{minimize this objective function} \\ & h_j(x) = 0, && j = 1, \dots, n_h \quad \text{equality constrains} \\ & g_k(x) \leq 0, && k = 1, \dots, n_g \quad \text{inequality constraints} \\ & x_i^l \leq x_i \leq x_i^u, && i = 1, \dots, n \quad \text{design variables} \end{aligned} \tag{1}$$

where
n_h: number of equality constraints
n_h: number of inequality constraints
n_h: number of design variables
x_i^l: lower bound of the design variable x_i
x_i^u: upper bound of the design variable x_i

The term feasible domain can be used for the set of design variables which satisfy all the equality constrains and respectively infeasible domain the set of them which outrage at least one. Hence, there are either linear optimization problems, where both equality and inequality constraints are

linear functions of the design variables or non-linear optimization problems (most of the structural optimization problems), where at least one of the constraints is a non-linear function of the design variables (Hassani & Hinton, 1999, pp. 3-4).

4. Topology Optimization approaches

Topology optimization approaches can be categorized into element-based, discrete and combined, depending on the different argorithms they use.

4.1 Element-based approaches

The traditional topology optimization approaches are element-based. The general approach of these methods is the discretization of the problem domain in a number of finite elements whose solution is known or can be approximated. The definition of CAD geometry, by a number of solid elements and their connection points (nodes), is a prerequisite in FEM. These nodes have known degrees of freedom (loads, temperature, displacement, etc.). All the discrete solid elements of the model are used in their turn, in the definition of the mathematical interactions of node's degrees of freedom and are combined to create the system's equations. Finally, the solutions of these equations expose useful information about the system's behavior (Thompson & Thompson, 2017, pp. 1-2).

As a consequence, topology optimization can extend the FEA-geometry of the model to the FEATO-geometry (combined FEA and TO geometry, see Figure 2). This iterative convergence method indicates either full material, partial material or lack of material to each solid element. The interpretation and verification of the TO's results is a demanding procedure, especially in the case of combined size and shape optimization (Harzheim & Graf, 2005). The main challenge is that the building models have to be as close as their FEATO-geometry. If the interpretation of the results is not done properly from the designer, the whole optimization process will lose its significance (Cazacu & Grama, 2014)

The most notable element-based approaches are the density-based (gradient-based), the topological derivatives, the level set and phase filed approach.

At the density-based approaches, the basic topology optimization problem is tackled by discretizing the design domain Ω (allowable volume within the design can exist) using either solid elements or nodes. One of the most implemented and mathematically well-defined interpolation methodologies is the solid isotropic microstructure with penalization (SIMP). Other notable density-based methods are the rational approximation of material properties (RAMP), the optimal microstructure with penalization (OMP), the non-optimal microstructures (NOM) and the dual discrete programming (DDP) (Luo, Chen, Yang, Zhang, & Abdel-Malek, 2005; Rozvany, 2001; Sigmund & Maute, 2013)

Eschenauer et al. (1994) initiated the approach of topological derivatives known also with the name 'bubble-method'. According to this approach, a microscopic hole (bubble with center x and radius ρ) is introduced at point x in or out of the design domain Ω in order to predict the influence (derivative) and trigger the creation of new holes. The bubble-method is a special case of homogenization, where the topological derivatives represent the limit of density going to 0 (void). These derivatives can indicate the ideal placing of a new hole or can be used either together with the level set approach or directly in element-based update schemes (Allaire, 1997; Burger, Hackl, & Ring, 2004; Eschenauer et al., 1994).

Level set models (Osher & Sethian, 1988) are characterized from their flexibility, dealing with demanding topological changes, due to implicit moving boundary (IMB) models (Jia, Beom, Wang, Lin, & Liu, 2011). These complex boundaries can form holes, split into multiple pieces, or merge with other boundaries to form a single surface. Hence, the adaptive design of the structure is carried out to solve the problem of structural topology optimization. At the traditional level set method (LSM), the boundary of structure is defined by the zero level (contour) of the level set function $\varphi(x)$. The zero level, in its turn, is derived by the objective function (such as energy of deformation, stress, etc.) and the optimal structure can be obtained through the movement and conjunction of its external boundary. The structure is defined by the domain Ω, where the level set function takes positive values (Sigmund & Maute, 2013).

Phase field methods correspond to density approaches with explicit penalization and regularization. The initial approach was implemented by Bourdin and Chambolle in order to carry out perimeter constrains and represent the surface dynamics of phase transition phenomena, such as solid-liquid transitions (2003). This approach works directly on the density variables and is based on a continuous density field Ω which eliminates the need for penalization of interfaces between elements (Wallin & Ristinmaa, 2014).

4.2 Discrete approaches

As it was mentioned at section 3, the basic topology optimization problem uses discrete variables. Hence, it is reasonable to deal with it by formulating it instantly in discrete variables. However, this mathematical solution (sensitivity analysis) can be very challenging. In addition, this approach has some limitations with respect to size of problems and structures (Mathias Stolpe & Bendsøe, 2011). Nevertheless, there are some notable discrete approaches, such as the evolutionary structural optimization (ESO), additive evolutionary structural optimization (AESO) and the bidirectional evolutionary structural optimization (BESO), which have considerable efficiency.

4.3 Combined approaches

As it is mentioned at section 1, the most of the topology optimization methods use, as optimizing parameter, either only the topology of the elements/nodes or both the size and shape of the structure. There are not many approaches which try to confront the problem in a holistic way. Some notable combined topology optimization approaches are the extended finite element method (xFEM) (Van Miegroet & Duysinx, 2007) and the deformable simplicial complex (DSC) (Misztal & Bærentzen, 2012). On the one hand, the purpose of the xFEM was an introduction of a generalized and adaptive finite element scheme which could allow us to work with meshes that can represent smooth and accurate boundaries. On the other hand, DSC scheme combines nonparametric shape optimization approaches with the ability to introduce and remove holes.

5. Comparison of the different Topology Optimization approaches

At this section, is presented a comparison between the main topology optimization approaches with respect to their procedure (top down/bottom up), characteristics, strengths and weaknesses. The comparison is based on both review and research papers about topology optimization and is shown in Table 1.

Table 1. Comparison of the Topology Optimization Approaches

Approach				Procedure/Description	Strengths	Weaknesses	Recom. papers
Category	Element-based	Density-based	Solid Isotropic Microstructures with Penalization (SIMP)	• Eulerian (fixed mesh) method • Discretization to solid isotropic elements • Remove material • Nested analysis and design approach (NAND) • Minimize the compliance subject to a volume constrain problem via an iterative converge method • 'Soft-kill' penalization method (white: void, gray: fractional material, black: material)	• Homogenization is not a prerequisite • Computational efficiency • Robustness • Adaptive to (almost) any design condition • Freely adjusted penalization • Conceptual simplicity (no higher mathematics required • Available for all combinations of designs constrains	• Intermediate densities • Mesh-dependent • Dependent on the degree of penalization • Nonconvex	(Bendsøe, 1989; Rozvany, 2001; M. Zhou & Rozvany, 1991)
			Rational Approximation of Material Properties (RAMP)	• Eulerian (fixed mesh) method • Based on SIMP • Nonzero sensitivity at zero density	• Convex	• Dependent on the degree of penalization • Numerical difficulties in low density	(Deaton & Grandhi, 2014; Luo et al., 2005; M. Stolpe & Svanberg, 2001)
			Optimal Microstructure with Penalization (OMP)	• Eulerian (fixed mesh) method • Based on SIMP • Discretization to optimal nonhomogeneous elements • 'Hard-kill' penalization method (white: void, black: material)	• More information about the isotropic-solid/empty/porous (ISEP) optimum	• Intermediate densities • More computational effort than SIMP • Nonrobust • Advanced mathematics • Nonconvex • Requires homogenization • Dependent on the degree of penalization • Available only for compliance	(Allaire, 1997; Rozvany, 2001)
			Non-Optimal Microstructures (NOM)	• Eulerian (fixed mesh) method • Based-on SIMP • Discretization to nonoptimal nonhomogeneous elements • No penalization	• Available for all combinations of designs constrains • Less variables/element than OMP	• More variables/element than SIMP • Fix and insufficient penalization • Nonconvex • Requires homogenization	(Bendsoe & Kikuchi, 1988; Rozvany, 2001)
			Dual Discrete Programming (DDP)	• Eulerian (fixed mesh) method • Discretization to solid isotropic elements • Remove material	• Penalization is not necessary	• Available only for compliance	(Beckers & Fleury, 1997; Rozvany, 2001)
		Topological derivatives ('The Bubble-method')		• Lagrangian (boundary following mesh) method • Special case of homogenization • Remove material • Combine shape and topology optimization • Introduce microscopic hole in order to predict the influence (derivative) and trigger the creation of new holes	• Indirectly include filtering by mapping between nodal and element (or subelement) based on design variables.	• Complex mathematics • It is yet unclear whether the computed derivatives are useful	(Allaire, 1997; Burger et al., 2004; Eschenauer et al., 1994)
		Level set		• Eulerian (fixed mesh) and Hybrid methods • Operate with boundaries instead of local density variables. • Implicit moving boundary (IMB) models	• Flexibility in topological changes • Can be mesh-independent • Can find shape variations for robust design	• Restricted geometry from existing boundaries • Inability to generate new holes at points surrounded by solid material (in 2D)	(Jia et al., 2011; Osher & Sethian, 1988)

			• Boundaries can form holes, split into multiple pieces, or merge with other boundaries to form a single surface • Boundary of structure = zero level (contour) • Modified density approach (uses shape derivatives for the development of the optimal topology) • Most use ersatz material and fixed meshes	• Formulate objectives and constraints on the interface and describe boundary conditions at the interface	• Starting guess results • Regularization, control of the spatial gradients of the level set function, and size control of geometric features • Must combined with topological derivatives in 2d	
		Phase field	• Eulerian (fixed mesh) method • Works directly on the density variables • Smooth the design field by adding the total density variation to the objective • Correspond to density approaches with explicit penalization and regularization	• Total density variation to the objective • Carry out perimeter constrains and represent the surface dynamics of phase transition phenomena such as solid-liquid transitions	• Very slow boundary translation and convergence solution	(Bourdin & Chambolle, 2003; Wallin & Ristinmaa, 2014)
	Discrete	Evolutionary Structural Optimization (ESO)	• Use of discrete variables • Remove material • 'Hard-kill' method (white: void, black: material) • The structure turns into an optimum by repetitively removing inefficient material • The elements with the lowest value of their criterion function are eliminated	• Small evolutionary ratio (ER) and fine mesh can produce a good solution	• Mesh and parameters dependent • Heuristic • Computationally rather inefficient • Methodologically lacking rationality • Tackle only simple 2D problems • Breaks down with rapidly changing sensitivity	(Yi Min Xie & Huang, 2010; Yi M Xie & Steven, 1993; M Zhou & Rozvany, 2001)
		Additive Evolutionary Structural Optimization (AESO)	• Based-on ESO • Use of discrete variables • Add material (to reduce the local high stresses) • Optimization starts from a core structure that is the minimum to carry the applied load	• Small evolutionary ratio (ER) and fine mesh can produce a good solution	• Mesh and parameters dependent • Heuristic • Computationally rather inefficient • Methodologically lacking rationality • Tackle only simple 2D problems • Breaks down with rapidly changing sensitivity	(Querin, Steven, & Xie, 1998, 2000; Querin, Young, Steven, & Xie, 2000)
		Bidirectional Evolutionary Structural Optimization (BESO)	• Mathematically combination of ESO and AESO • Use of discrete variables • Add and remove material where needed • 0: absence of element, 1: presence of element	• Mesh-independent • Reduction of computational time comparing to ESO • Adaptive shape • Using a small evolutionary ratio ER and a fine mesh can produce a good solution	• Can be dependent on mesh	(Huang & Xie, 2007; Querin, Young, et al., 2000)
	Combined	Extended Finite Element Method (xFEM)	• Generalized shape optimization • Introduction of a generalized and adaptive finite element scheme which work with meshes that can represent smooth and accurate boundaries • Based on level set.	• Overcome FEM discontinuities • No remeshing is required • Can study large 3D scale industrial problems	• Large errors in the stress estimation	(Van Miegroet & Duysinx, 2007)
		Deformable Simplicial Complex (DSC)	• Hybrid method • Combine nonparametric shape optimization and introduction/removal of holes	• Robust topological additivity • Topology control natural and simple • Allows for nonmanifold configurations in the surface mesh	• Numerical diffusion • Slower than the level set method • Insufficient mesh quality	(Misztal & Bærentzen, 2012)

6. Design optimization practices and examples

It is important to differentiate between a local optimum (a solution of a defined CAD model) and the optimal solution of a structural problem. A lot of design optimization practices have been developed the last years which try to combine both topology, shape and/or size optimization approaches in order to avoid the local optimum. Three main categories have been identified: a) predefined design space practice, b) maximum possible design space practice (with respect to boundary conditions) and c) integrated shape and topology optimization practice (IST). An overview of these practices is presented in Table 2.

Table 2. Overview of the design optimization practices

Practice	Examples	Strengths	Weaknesses	Recom. papers
Predefined design space	Upper carriage of a naval gun	Partially hold of the initial visual design	Restricted design space (fixed dimentions and boundary conditions)	(Wang & Ma, 2014)
Maximum possible design space	Laser-remote-scanner	Larger design space (less restrictions on the algorithm)	Restricted design space (fixed dimentions and boundary conditions)	(Emmelmann, Kirchhoff, & Beckmann, 2011)
	Compressor bracket			(Chang & Lee, 2008)
	Trailer chassis			(Ma, Wang, Kikuchi, Pierre, & Raju, 2006)
	Hanger			(McKee & Porter, 2017)
Integrated shape-and topology optimization practice	Automotive Design and Manufacturing	Optimization of boundary conditions	Computationally costly and time consuming	(Fiedler, Rolfe, & De Souza, 2017)

7. Case study of a ski binding

In order to present the limitations of the topology optimization approaches and design practices, an example of a minimum compliance design of a ski binding will be presented. The optimization problem is restricted due to time and computational limitations. We assume that the applied forces are given and the ski binding is fixed to the ground with four screws. Hence, the topology optimization of the structure is conducted in conjunction with the optimization of the positions of the screws. In this case, the model was built in Abaqus CAE 2017 and the optimization was conducted using the optimization software Tosca Structure, which is based on SIMP topology optimization approach. First the three main practices were tested in our case and finally a new practice is recommended based on the identified limitations of the existing practices.

7.1 Topology optimization of a ski binding

In Figure 3, both the predefined design space and maximum possible design space practices of the ski binding are presented.

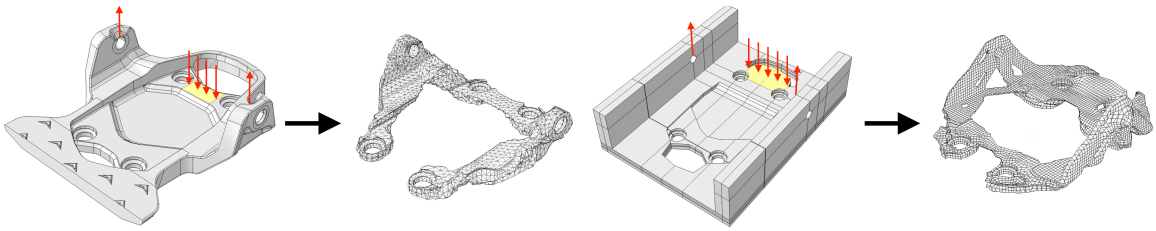

Figure 3: Ski binding optimization with use of a) the predefined design space (left) and b) the maximum possible design space practice (right)

As it is shown in Figure 3, the maximum possible design space practice resulted to an optimum with a larger design space.

In Figure 4, is illustrated the mathematical model in the IST practice which consists of the design envelope, a set of screws and a contact set with a ski. As dynamic design parameters are used the distance d between the pairs of the screws and the thickness t of the support structure under the yellow area.

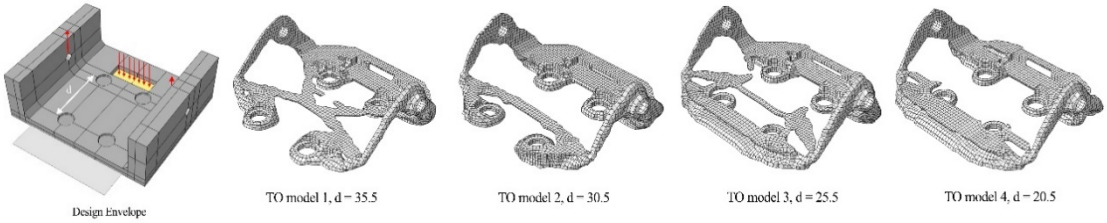

Figure 4: Topology optimization with IST practice of the ski binding with thickness of the support structure, $t = 2mm$ (yellow colour) and different distances between the pairs of screws (from left to right), $d = 35.5mm$, $d = 30.5mm$, $d = 25.5mm$ and $d = 20.5mm$.

Two different studies are executed in order to detect the optimal solution. In the first study, the chosen thickness of the support structure is $t = 2mm$, while the distance d between the pairs of screws are decreased by $5mm$ in each iteration in a range of $20.5 - 35.5mm$ (see Figure 4). In the second study, the same screw-hole patterns are re-tested but now with thickness of the support structure, $t = 5mm$ (see Figure 5).

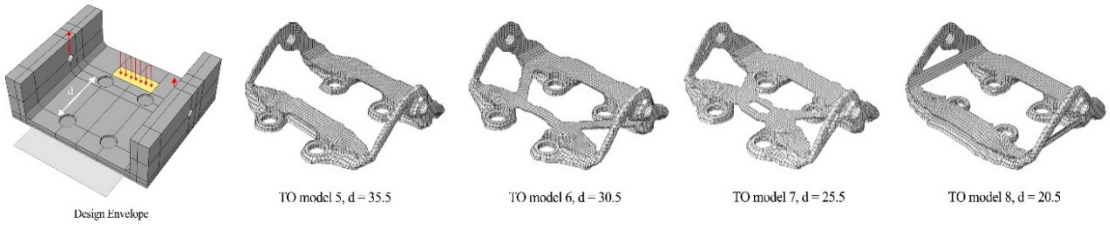

Figure 5: Topology optimization with Abaqus 2017 of the ski binding with thickness of the support structure, $t = 5mm$ (yellow colour) and different distances between the pairs of screws (from left to right), $d = 35.5mm$, $d = 30.5mm$, $d = 25.5mm$ and $d = 20.5mm$.

Comparing the results of the three practices, TO model 1 and TO model 6 from the IST practice are the solutions with the lowest strain energy (i.e. the stiffest result) and thus the local optimum in study one and two respectively.

7.2 Evaluation of the applied practices

It is clear that these practices led to a local optimum and not to the best optimized solution of the ski binding. It is crucial to understand that the optimum solution to a defined setup might not be the ideal solution to the problem. In other words, the optimum material distribution is influenced by the initial boundary conditions defined by the engineer. Therefore, it is not possible to find the real optimum of a structure, if its outer boundary conditions are not optimal and predefined. Then it is necessary to find first the optimum input (boundary conditions) for the topology optimization, and second the optimum material distribution.

In this case, the identification of the real optimum has been carried out by comparing the different optimized design models in the conducted practices. However, this methodology has several limitations such as the requirement of a huge amount of time and computer capacity due to the analysis of big data (different sizes and placements of screws, variation of the support structure for the loads and boundary conditions, etc.). This method also implies the need of all the setups to be defined by an engineer, making the final design more vulnerable to human error and his/her previous experience.

7.3 Suggestions about a new practice

The success of a topology optimization approach could be achieved through the identification of the evolutionary probing of the design boundaries. Hence, the topology optimization problem could be divided in two sub-problems (levels); the optimization of the outer boundary conditions, and the optimization for the inner optimum. The CAD-geometry of the structure could be replaced by a black box with the allowable design envelope (level 1). A topology optimization algorithm, based on NAND formulation, could be used for calculating the optimum adaptive (moving) boundaries of the structure with respect to outer design parameters (i.e. length, width, height, holes, etc.), constrains, loads and contact sets. The optimum boundary conditions could be used in their turn, as a starting point for a traditional topology optimization of the structure's interior (level 2). The geometry shift model and the principle flow chart of this approach are presented in Figures 5 & 6 respectively.

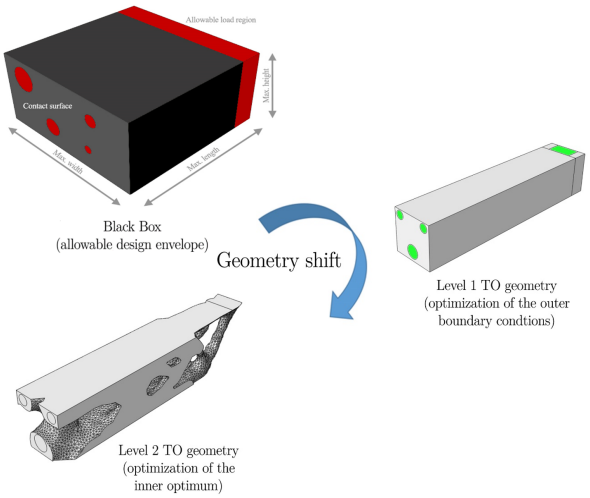

Figure 6: The geometry shift model of a cantilever beam based on the two-level topology optimization approach with Abaqus 2017

A comparison between the traditional (Figure 2) and the two-level (Figure 6) geometry shift shows that both CAD and FEA geometries have been replaced by a more 'generative design based' optimization approach. This can result in optimum and high applicable structural designs with minimized human error and reduced number of convergence iterations.

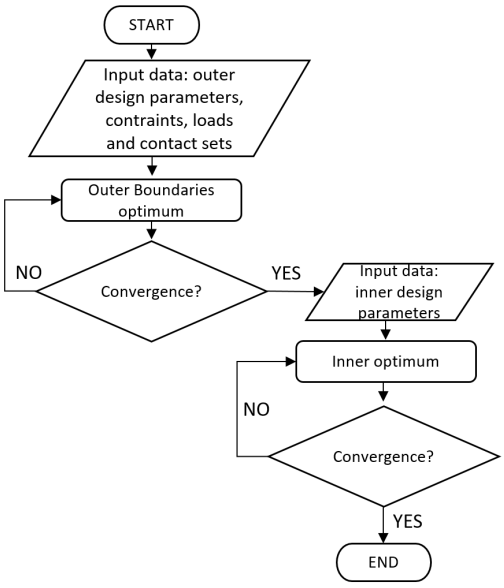

Figure 7: Principle flow chart for the two-level topology optimization approach

8. Conclusion and future research potentials

In this paper, in the first section, was presented the general topology optimization problem and the most implemented topology optimization approaches. The most used and commercial applied method is the SIMP. ESO is also a promising method with many potentials, but it is still missing the mathematical background for multiple constraints and loads. However, all the approaches have their advantages and limitations. Both SIMP and ESO are dependent on the design parameters (CAD), mesh and boundary conditions of the structures.

In the second section, some design optimization practices were used in the case of a ski binding. Through the applied optimization practices and their results we agreed on the following limitations:

- CAD is a limited design methodology due to its design parameters restrictions to known geometries.
- CAD encourages the re-usage of previously designed objects resulting in robust but nowhere near optimum designs.
- The main key limitation of the topology optimization is its sensitivity to the spatial placement of the involved components and the configuration of their supporting structure. For example, the local optimum of the ski binding will be completely different if we use three screws instead of four.
- Many topology optimization approaches are still dependent on starting guesses.
- All the existing topology optimization approaches and practices are time consuming and demand huge computational effort when they try to tackle big 3D construction models.

It is clear that there is a need of new practices which could overcome these limitations. Suggestions about a new practice were presented. The main goal of this approach is to implement a two level optimization, first the outer bounder conditions optimum and as a consequence the inner optimum which is based on the first one. A geometry shift model and a principle flow chart of this approach were presented. Further research, validation of the applicability of this practice and the development of its mathematical formulation are needed to be done.

References

Allaire, G. (1997). The Homogenization Method for Topology and Shape Optimization. In G. I. N. Rozvany (Ed.), *Topology Optimization in Structural Mechanics* (pp. 101-133). Vienna: Springer Vienna.

Beckers, M., & Fleury, C. (1997). *Topology optimization involving discrete variables.* Paper presented at the Proceedings of the second world congress of Structural and multidisciplinary optimization: May 26-30 1997, Zakopane, Poland.

Bendsøe, M. P. (1989). Optimal shape design as a material distribution problem. *Structural Optimization, 1*(4), 193-202.

Bendsoe, M. P., & Kikuchi, N. (1988). Generating Optimal Topologies in Structural Design Using a Homogenization Method. *Computer Methods in Applied Mechanics and Engineering, 71*(2), 197-224. doi:Doi 10.1016/0045-7825(88)90086-2

Bendsøe, M. P., & Sigmund, O. (2003). *Topology optimization : theory, methods, and applications*. Berlin ; New York: Springer.

Bourdin, B., & Chambolle, A. (2003). Design-dependent loads in topology optimization. *Esaim-Control Optimisation and Calculus of Variations, 9*(2), 19-48. doi:10.1051/cocv:2002070

Burger, M., Hackl, B., & Ring, W. (2004). Incorporating topological derivatives into level set methods. *Journal of Computational Physics, 194*(1), 344-362. doi:10.1016/j.jcp.2003.09.033

Cazacu, R., & Grama, L. (2014). Steel truss optimization using genetic algorithms and FEA. *7th International Conference Interdisciplinarity in Engineering (Inter-Eng 2013), 12*, 339-346. doi:10.1016/j.protcy.2013.12.496

Chang, J. W., & Lee, Y. S. (2008). Topology optimization of compressor bracket. *Journal of mechanical science and technology, 22*(9), 1668-1676.

Dantzig, G. B. (1963). Orgins of Linear-Programming. *Operations Research, 11*, B115-B115.

Deaton, J. D., & Grandhi, R. V. (2014). A survey of structural and multidisciplinary continuum topology optimization: post 2000. *Structural and Multidisciplinary Optimization, 49*(1), 1-38.

Emmelmann, C., Kirchhoff, M., & Beckmann, F. (2011). Systematic development of lightweight components for highly dynamic laser-remote-scanners using topology optimization. *Physics Procedia, 12*, 459-464.

Eschenauer, H. A., Kobelev, V. V., & Schumacher, A. (1994). Bubble Method for Topology and Shape Optimization of Structures. *Structural Optimization, 8*(1), 42-51. doi:Doi 10.1007/Bf01742933

Fiedler, K., Rolfe, B. F., & De Souza, T. (2017). Integrated Shape and Topology Optimization-Applications in Automotive Design and Manufacturing. *SAE International Journal of Materials and Manufacturing, 10*(2017-01-1344), 385-394.

Fleury, C., & Braibant, V. (1986). Structural Optimization - a New Dual Method Using Mixed Variables. *International Journal for Numerical Methods in Engineering, 23*(3), 409-428. doi:DOI 10.1002/nme.1620230307

Harzheim, L., & Graf, G. (2005). A review of optimization of cast parts using topology optimization - I - Topology optimization without manufacturing constraints. *Structural and Multidisciplinary Optimization, 30*(6), 491-497. doi:10.1007/s00158-005-0553-x

Hassani, B., & Hinton, E. (1999). *Homogenization and structural topology optimization : theory, practice, and software*. London ; New York: Springer.

Huang, X., & Xie, Y. (2007). Convergent and mesh-independent solutions for the bi-directional evolutionary structural optimization method. *Finite Elements in Analysis and Design, 43*(14), 1039-1049.

Jia, H. P., Beom, H. G., Wang, Y. X., Lin, S., & Liu, B. (2011). Evolutionary level set method for structural topology optimization. *Computers & Structures, 89*(5-6), 445-454. doi:10.1016/j.compstruc.2010.11.003

Kurowski, P. (2017). *Engineering Analysis with SOLIDWORKS Simulation 2017*: SDC Publications.

Luo, Z., Chen, L., Yang, J., Zhang, Y., & Abdel-Malek, K. (2005). Compliant mechanism design using multi-objective topology optimization scheme of continuum structures. *Structural and Multidisciplinary Optimization, 30*(2), 142-154.

Ma, Z.-D., Wang, H., Kikuchi, N., Pierre, C., & Raju, B. (2006). Experimental validation and prototyping of optimum designs obtained from topology optimization. *Structural and Multidisciplinary Optimization, 31*(5), 333-343. doi:10.1007/s00158-005-0530-4

McKee, H. J., & Porter, J. G. (2017). Lessons Learned in Part Design from Topology Optimization through Qualification.

Michell, A. G. M. (1904). LVIII. The limits of economy of material in frame-structures. *The London, Edinburgh, and Dublin Philosophical Magazine and Journal of Science, 8*(47), 589-597. doi:10.1080/14786440409463229

Misztal, M. K., & Bærentzen, J. A. (2012). Topology-adaptive interface tracking using the deformable simplicial complex. *ACM Transactions on Graphics (TOG), 31*(3), 24.

Osher, S., & Sethian, J. A. (1988). Fronts Propagating with Curvature-Dependent Speed - Algorithms Based on Hamilton-Jacobi Formulations. *Journal of Computational Physics, 79*(1), 12-49. doi:Doi 10.1016/0021-9991(88)90002-2

Prager, W. (1968). OPTIMALITY CRITERIA IN STRUCTURAL DESIGN. *Proceedings of the National Academy of Sciences, 61*(3), 794-796.

Querin, O., Steven, G., & Xie, Y. (1998). Evolutionary structural optimisation (ESO) using a bidirectional algorithm. *Engineering computations, 15*(8), 1031-1048.

Querin, O., Steven, G., & Xie, Y. (2000). Evolutionary structural optimisation using an additive algorithm. *Finite Elements in Analysis and Design, 34*(3-4), 291-308.

Querin, O., Young, V., Steven, G., & Xie, Y. (2000). Computational efficiency and validation of bi-directional evolutionary structural optimisation. *Computer Methods in Applied Mechanics and Engineering, 189*(2), 559-573.

Rozvany, G. I. N. (1972). Grillages of Maximum Strength and Maximum Stiffness. *International Journal of Mechanical Sciences, 14*(10), 651-&. doi:Doi 10.1016/0020-7403(72)90023-9

Rozvany, G. I. N. (1977). Optimum Choice of Determinate Trusses under Multiple Loads. *Journal of the Structural Division-Asce, 103*(12), 2432-2433.

Rozvany, G. I. N. (2001). Aims, scope, methods, history and unified terminology of computer-aided topology optimization in structural mechanics. *Structural and Multidisciplinary Optimization, 21*(2), 90-108. doi:DOI 10.1007/s001580050174

Rozvany, G. I. N. (2009). A critical review of established methods of structural topology optimization. *Structural and Multidisciplinary Optimization, 37*(3), 217-237. doi:10.1007/s00158-007-0217-0

Sigmund, O. (2001). A 99 line topology optimization code written in Matlab. *Structural and Multidisciplinary Optimization, 21*(2), 120-127. doi:DOI 10.1007/s001580050176

Sigmund, O., & Maute, K. (2013). Topology optimization approaches A comparative review. *Structural and Multidisciplinary Optimization, 48*(6), 1031-1055. doi:10.1007/s00158-013-0978-6

Sigmund, O., & Petersson, J. (1998). Numerical instabilities in topology optimization: A survey on procedures dealing with checkerboards, mesh-dependencies and local minima. *Structural Optimization, 16*(1), 68-75. doi:Doi 10.1007/Bf01214002

Stolpe, M., & Bendsøe, M. P. (2011). Global optima for the Zhou–Rozvany problem. *Structural and Multidisciplinary Optimization, 43*(2), 151-164.

Stolpe, M., & Svanberg, K. (2001). An alternative interpolation scheme for minimum compliance topology optimization. *Structural and Multidisciplinary Optimization, 22*(2), 116-124. doi:DOI 10.1007/s001580100129

Svanberg, K. (1987). The Method of Moving Asymptotes - a New Method for Structural Optimization. *International Journal for Numerical Methods in Engineering, 24*(2), 359-373. doi:DOI 10.1002/nme.1620240207

Thompson, M. K., & Thompson, J. M. (2017). *ANSYS mechanical APDL for finite element analysis*. Oxford, United Kingdom: Butterworth-Heinemann, an imprint of Elsevier.

Van Miegroet, L., & Duysinx, P. (2007). Stress concentration minimization of 2D filets using X-FEM and level set description. *Structural and Multidisciplinary Optimization, 33*(4-5), 425-438.

Wallin, M., & Ristinmaa, M. (2014). Boundary effects in a phase-field approach to topology optimization. *Computer Methods in Applied Mechanics and Engineering, 278*, 145-159. doi:10.1016/j.cma.2014.05.012

Wang, K., & Ma, D. W. (2014). *Multi-Objective Structure Optimization Design on the Upper Carriage of a Naval Gun.* Paper presented at the Applied Mechanics and Materials.

Xie, Y. M., & Huang, X. (2010). *Recent developments in evolutionary structural optimization (ESO) for continuum structures.* Paper presented at the IOP Conference Series: Materials Science and Engineering.

Xie, Y. M., & Steven, G. P. (1993). A simple evolutionary procedure for structural optimization. *Computers & Structures, 49*(5), 885-896.

Zhou, M., Pagaldipti, N., Thomas, H. L., & Shyy, Y. K. (2004). An integrated approach to topology, sizing, and shape optimization. *Structural and Multidisciplinary Optimization, 26*(5), 308-317. doi:10.1007/s00158-003-0351-2

Zhou, M., & Rozvany, G. (2001). On the validity of ESO type methods in topology optimization. *Structural and Multidisciplinary Optimization, 21*(1), 80-83.

Zhou, M., & Rozvany, G. I. N. (1991). The Coc Algorithm .2. Topological, Geometrical and Generalized Shape Optimization. *Computer Methods in Applied Mechanics and Engineering, 89*(1-3), 309-336. doi:Doi 10.1016/0045-7825(91)90046-9

G Risk Assessment

ID	27063	**Status**	**Dato**
Risikoområde	Risikovurdering: Helse, miljø og sikkerhet (HMS)	Opprettet	26.01.2018
Opprettet av	David Tollnes Flem	Vurdering startet	26.01.2018
Ansvarlig	David Tollnes Flem	Tiltak besluttet	26.01.2018
		Avsluttet	31.01.2018

Risikovurdering:

Risk Assessment - Master Thesis

Gyldig i perioden:
1/14/2018 - 6/11/2018

Sted:
NTNU Trondheim, IPM

Mål / hensikt
The main goal is to reduce the risk of injuries when performing work in the workshops and testing prototypes. It is also to avoid machines or equipment getting broken.

Bakgrunn
The assignment requires a lot of work in the workshops and labs. In these places there are different equipment which can be difficult to use for an untrained person.

Beskrivelse og avgrensninger
This risk assessment will focus on the work I, David Tollnes Flem, will do in the workshops at IPM. This means both the main workshop at the 1st floor, TrollLabs and the 3D-printer lab at the 2nd floor.

Forutsetninger, antakelser og forenklinger
The risk assessment is based on the tasks that I, at todays date, see as likely to do during this semester. If I see that I have to use other workshops and equipment, a new assessment will be conducted.

Vedlegg
[Ingen registreringer]

Referanser
[Ingen registreringer]

Oppsummering, resultat og endelig vurdering

I oppsummeringen presenteres en oversikt over farer og uønskede hendelser, samt resultat for det enkelte konsekvensområdet.

Farekilde: **Noise**

Uønsket hendelse: **Hearing damage / loss**

Konsekvensområde: Helse — Risiko før tiltak: Risiko etter tiltak:

Risikoreduserende tiltak	Ansvarlig	Registrert	Frist	Status
Appropriate safety equipment	David Tollnes Flem	20.09.2017	20.09.2017	Gjennomført

Farekilde: **Wrong use of the machines**

Uønsket hendelse: **Destroyed / damaged equipment**

Konsekvensområde: Materielle verdier — Risiko før tiltak: Risiko etter tiltak:

Risikoreduserende tiltak	Ansvarlig	Registrert	Frist	Status
Get appropriate training	David Tollnes Flem	20.09.2017	20.09.2017	Gjennomført

Uønsket hendelse: **Trapping, cutting or squeezing hands / fingers**

Konsekvensområde: Helse — Risiko før tiltak: Risiko etter tiltak:

Risikoreduserende tiltak	Ansvarlig	Registrert	Frist	Status
Get appropriate training	David Tollnes Flem	20.09.2017	20.09.2017	Gjennomført

Uønsket hendelse: **Getting pieces of clothing stuck in rotating machines**

Konsekvensområde: Helse — Risiko før tiltak: Risiko etter tiltak:
Materielle verdier — Risiko før tiltak: Risiko etter tiltak:

Risikoreduserende tiltak	Ansvarlig	Registrert	Frist	Status
Appropriate safety equipment	David Tollnes Flem	20.09.2017	20.09.2017	Gjennomført

Uønsket hendelse: **Getting steel shavings in the eyes / on clothing**

Konsekvensområde: Helse — Risiko før tiltak: Risiko etter tiltak:
Materielle verdier — Risiko før tiltak: Risiko etter tiltak:

Risikoreduserende tiltak	Ansvarlig	Registrert	Frist	Status
Appropriate safety equipment	David Tollnes Flem	20.09.2017	20.09.2017	Gjennomført

Endelig vurdering

This risk assessment is based on the information I have available at this date, if the thesis is changed and it is necessary to use other workshops, labs, equipment, etc., a new assessment will be conducted.

Involverte enheter og personer

En risikovurdering kan gjelde for en, eller flere enheter i organisasjonen. Denne oversikten presenterer involverte enheter og personell for gjeldende risikovurdering.

Enhet /-er risikovurderingen omfatter

- Institutt for maskinteknikk og produksjon

Deltakere

[Ingen registreringer]

Lesere

[Ingen registreringer]

Andre involverte/interessenter

Martin Steinert

Følgende akseptkriterier er besluttet for risikoområdet Risikovurdering: Helse, miljø og sikkerhet (HMS):

Helse	Materielle verdier	Omdømme	Ytre miljø
			

Oversikt over eksisterende, relevante tiltak som er hensyntatt i risikovurderingen

I tabellen under presenteres eksisterende tiltak som er hensyntatt ved vurdering av sannsynlighet og konsekvens for aktuelle uønskede hendelser.

Farekilde	Uønsket hendelse	Tiltak hensyntatt ved vurdering
Noise	Hearing damage / loss	Safety Equipment
	Hearing damage / loss	HMS course: main workshop (1st floor at IPM)
Wrong use of the machines	Destroyed / damaged equipment	Safety Equipment
	Destroyed / damaged equipment	HMS course: main workshop (1st floor at IPM)
	Destroyed / damaged equipment	User course: 3D-printer lab
	Destroyed / damaged equipment	User course: TrollLabs
	Trapping, cutting or squeezing hands / fingers	HMS course: main workshop (1st floor at IPM)
	Trapping, cutting or squeezing hands / fingers	User course: TrollLabs
	Getting pieces of clothing stuck in rotating machines	HMS course: main workshop (1st floor at IPM)
	Getting pieces of clothing stuck in rotating machines	User course: TrollLabs
	Getting steel shavings in the eyes / on clothing	Safety Equipment
	Getting steel shavings in the eyes / on clothing	HMS course: main workshop (1st floor at IPM)
	Getting steel shavings in the eyes / on clothing	User course: TrollLabs

Eksisterende og relevante tiltak med beskrivelse:

Safety Equipment

At all the workshops and labs there are necessary safety equipment.

HMS course: main workshop (1st floor at IPM)

I have an approved HMS course in the main workshop. Here necessary safety equipment, training for the different machines and workshop times were discussed.

User course: 3D-printer lab

I have an approved user course in the 3D-printer lab from the course 'Fuzzy Front End'.

User course: TrollLabs

I have gotten a user course in TrollLabs. Machines, equipment and which persons too contact for questions were explained.

Help

There are always (working time) workers present at the main workshop which know the machines. In both TrollLabs and the 3D-printer lab, contact information for the persons responsible for the different machines are listed.

Risikoanalyse med vurdering av sannsynlighet og konsekvens

I denne delen av rapporten presenteres detaljer dokumentasjon av de farer, uønskede hendelser og årsaker som er vurdert. Innledningsvis oppsummeres farer med tilhørende uønskede hendelser som er tatt med i vurderingen.

Følgende farer og uønskede hendelser er vurdert i denne risikovurderingen:

- **Noise**
  - Hearing damage / loss
- **Wrong use of the machines**
  - Destroyed / damaged equipment
  - Trapping, cutting or squeezing hands / fingers
  - Getting pieces of clothing stuck in rotating machines
  - Getting steel shavings in the eyes / on clothing

Detaljert oversikt over farekilder og uønskede hendelser:

Farekilde: Noise

Uønsket hendelse: Hearing damage / loss

Årsak: Loud machines in the workshops.

Sannsynlighet for hendelsen (felles for alle konsekvensområder): **Svært lite sannsynlig (1)**

Kommentar:
[Ingen registreringer]

Konsekvensområde: Helse

Vurdert konsekvens: **Middels (2)**

Kommentar: [Ingen registreringer]

Risiko:

Farekilde: Wrong use of the machines

Uønsket hendelse: Destroyed / damaged equipment

Årsak: Using the machines wrong

Sannsynlighet for hendelsen (felles for alle konsekvensområder): **Lite sannsynlig (2)**

Kommentar:
[Ingen registreringer]

Konsekvensområde: Materielle verdier

Vurdert konsekvens: **Liten (1)**

Kommentar: [Ingen registreringer]

Risiko:

Uønsket hendelse: Trapping, cutting or squeezing hands / fingers

Årsak: Reckless use of the machines

Årsak: Lack of focus on the task that is being done

Sannsynlighet for hendelsen (felles for alle konsekvensområder): **Lite sannsynlig (2)**

Kommentar:
[Ingen registreringer]

Konsekvensområde: Helse

Vurdert konsekvens: **Stor (3)**

Kommentar: [Ingen registreringer]

Risiko:

Uønsket hendelse: Getting pieces of clothing stuck in rotating machines

Årsak: Using unsuitable clothing, i.e. long sleeves

Sannsynlighet for hendelsen (felles for alle konsekvensområder): **Svært lite sannsynlig (1)**

Kommentar:
[Ingen registreringer]

Konsekvensområde: Helse

Vurdert konsekvens: **Middels (2)**

Kommentar: [Ingen registreringer]

Risiko:

Konsekvensområde: Materielle verdier

Vurdert konsekvens: **Middels (2)**

Kommentar: [Ingen registreringer]

Risiko:

Uønsket hendelse: Getting steel shavings in the eyes / on clothing

Årsak: Not using safety glasses

Årsak: Using unsuitable clothing

Sannsynlighet for hendelsen (felles for alle konsekvensområder): **Lite sannsynlig (2)**

Kommentar:
[Ingen registreringer]

Konsekvensområde: Helse

Vurdert konsekvens: **Middels (2)**

Kommentar: [Ingen registreringer]

Risiko:

Konsekvensområde: Materielle verdier

Vurdert konsekvens: **Liten (1)**

Kommentar: [Ingen registreringer]

Risiko:

Oversikt over besluttede risikoreduserende tiltak:

Under presenteres en oversikt over risikoreduserende tiltak som skal bidra til å reduseres sannsynlighet og/eller konsekvens for uønskede hendelser.

- Appropriate safety equipment
- Get appropriate training

Detaljert oversikt over besluttede risikoreduserende tiltak med beskrivelse:

Appropriate safety equipment

To use appropriate safety equipment; safety glasses, hearing protection, lab coat, safety gloves, etc, when needed.

Tiltak besluttet av:	David Tollnes Flem
Ansvarlig for gjennomføring:	David Tollnes Flem
Frist for gjennomføring:	9/20/2017

Get appropriate training

Get appropriate training on the machines which are relevant to use. Ask people at the workshops for help if I have a question.

Tiltak besluttet av:	David Tollnes Flem
Ansvarlig for gjennomføring:	David Tollnes Flem
Frist for gjennomføring:	9/20/2017

Detaljert oversikt over vurdert risiko for hver farekilde/uønsket hendelse før og etter besluttede tiltak

Farekilde: **Noise**

Uønsket hendelse: **Hearing damage / loss**

Sannsynlighetsvurderinger (felles for alle konsekvensområder):

Opprinnelig sannsynlighet: Svært lite sannsynlig (1)

Begrunnelse:

Sannsynlighet etter tiltak: Svært lite sannsynlig (1)

Begrunnelse:

Konsekvensvurderinger:

Konsekvensområde: **Helse**

Risiko:

Opprinnelig konsekvens: Middels (2)

Begrunnelse:

Konsekvens etter tiltak: Liten (1)

Begrunnelse:

Farekilde: **Wrong use of the machines**

Uønsket hendelse: **Destroyed / damaged equipment**

Sannsynlighetsvurderinger (felles for alle konsekvensområder):

Opprinnelig sannsynlighet: Lite sannsynlig (2)

Begrunnelse:

Sannsynlighet etter tiltak: Lite sannsynlig (2)

Begrunnelse:

Konsekvensvurderinger:

Konsekvensområde: **Materielle verdier**

Risiko:

Opprinnelig konsekvens: Liten (1)

Begrunnelse:

Konsekvens etter tiltak: Liten (1)

Begrunnelse:

Uønsket hendelse: **Trapping, cutting or squeezing hands / fingers**

Sannsynlighetsvurderinger (felles for alle konsekvensområder):

Opprinnelig sannsynlighet: Lite sannsynlig (2)

Begrunnelse:

Sannsynlighet etter tiltak: Svært lite sannsynlig (1)

Begrunnelse:

Konsekvensvurderinger:

Konsekvensområde: **Helse**

Risiko:

Opprinnelig konsekvens: Stor (3)

Begrunnelse:

Konsekvens etter tiltak: Middels (2)

Begrunnelse:

Uønsket hendelse: **Getting pieces of clothing stuck in rotating machines**

Sannsynlighetsvurderinger (felles for alle konsekvensområder):

Opprinnelig sannsynlighet: Svært lite sannsynlig (1)

Begrunnelse:

Sannsynlighet etter tiltak: Svært lite sannsynlig (1)

Begrunnelse:

Konsekvensvurderinger:

Konsekvensområde: **Helse**

Risiko:

Opprinnelig konsekvens: Middels (2)

Begrunnelse:

Konsekvens etter tiltak: Liten (1)

Begrunnelse:

Konsekvensområde: **Materielle verdier**

Risiko:

Opprinnelig konsekvens: Middels (2)

Begrunnelse:

Konsekvens etter tiltak: Liten (1)

Begrunnelse:

Uønsket hendelse: **Getting steel shavings in the eyes / on clothing**

Sannsynlighetsvurderinger (felles for alle konsekvensområder):

Opprinnelig sannsynlighet: Lite sannsynlig (2)

Begrunnelse:

Sannsynlighet etter tiltak: Svært lite sannsynlig (1)

Begrunnelse:

Konsekvensvurderinger:

Konsekvensområde: **Helse** ***Risiko:***

Opprinnelig konsekvens: Middels (2)

Begrunnelse:

Konsekvens etter tiltak: Liten (1)

Begrunnelse:

Konsekvensområde: **Materielle verdier** ***Risiko:***

Opprinnelig konsekvens: Liten (1)

Begrunnelse:

Konsekvens etter tiltak: Liten (1)

Begrunnelse: